EVALUATION OF THE PARAMETERS OF SIMPLE ELASTOPLASTIC CONSTITUTIVE MODELS FOR DHAKA CLAY

MUHAMMAD ABDUR RAHMAN

(BSc Engg., KUET)

A thesis Submitted to the Department of Civil Engineering, Military Institute of Science and Technology in Partial Fulfillment of the Requirements for the Degree of Masters of Science in Civil Engineering

DEPARTMENT OF CIVIL ENGINEERING

MILITARY INSTITUTE OF SCIENCE AND TECHNOLOGY (MIST)

2018

The thesis titled "Evaluation of the Parameters of Simple Elastoplastic Constitutive Models for Dhaka Clay" Submitted by Muhammad Abdur Rahman Roll No: 1014110009 Session: 2014-15 has been accepted as satisfactory in partial fulfillment of the requirement for the degree of Masters of Science in Civil Engineering on 12 November, 2018.

BOARD OF EXAMINERS

1 Chairman (Supervisor)

_____

Dr Hossain Md. Shahin
Professor
Department of Civil and Environmental Engineering,
IUT, Gazipur.

2 Member

_____

Dr. Md. Zoynul Abedin
Professor
Department of Civil Engineering, MIST, Dhaka.

3 Member (Ex-Officio)

_____

Col Md Masudur Rahman
Head
Department of Civil Engineering, MIST, Dhaka.

4 Member (External)

_____

Dr. Mohammad Shariful Islam
Professor
Department of Civil Engineering, BUET, Dhaka.

DECLARATION

I hereby declare that this thesis is my original work and it has been written by me in its entirety. I have duly acknowledged all the sources of information which have been used in the thesis.

This thesis has also not been submitted for any degree in any university previously.

_____

Muhammad Abdur Rahman

12 November 2018

ACKNOWLEDGEMENT

At the very outset the author expresses his deepest gratitude and profound indebtedness to his supervisor, Dr. Hossain Md. Shahin, Professor, Department of Civil and Environmental Engineering, Islamic University of Technology, Gazipur for his continuous guidance, valuable suggestions and encouragement throughout the research work. His sincere help and valuable advice at every stage made this research work possible.

The author is thankful to Brig Gen (LPR) Shah Md Muniruzzaman, PhD for his continuous support and encouragement. The support provided by Col Md Masudur Rahman, Head of the Civil Engineering Department is also duly acknowledged.

The author is grateful to Dr. Md. Zoynul Abedin, Professor, Department of Civil Engineering, Military Institute of Science and Technology for his guidance and support. Also, profound thanks goes to Dr. Mohammad Shariful Islam, Professor, Department of Civil Engineering, Bangladesh University of Engineering and Technology for his cooperation and support. Sincere gratitude goes to Capt Sampa Akter for his continues administrative supports.

All the laboratory tests of the study were conducted in Terzaghi Laboratory (Geotech Lab), MIST. I am indebted to all the members of the laboratory. The help provided by Mr. Ruman Akond, Lab Assistant, Geotechnical Engineering Laboratory, MIST during sample collection and laboratory testing is duly acknowledged.

ABSTRACT

Geotechnical engineering problems are usually solved by considering soil as an elastic or rigid plastic material where stress-dilatancy characteristics are not taken into considerations. As actual soil is an elastoplastic material most of the designs are either over designed or under designed for not taking proper considerations of constitutive model, i.e., stress – strain relation. On the contrary, most of the constitutive models are not able to simulate total behavior of the soil or very complex in nature where parameter determination requires sophisticated tests.

Dhaka city and its adjacent Gazipur and Savar is placed on the southern part of Madhupur tract the oldest sediment deposit. As a rapid expanding city, it often require to solve complex geotechnical problems where geotechnical engineers have to deal with the Dhaka soil. In this research work two well-known constitutive models, i.e., Subloading t_{ij} model and Cam-clay model were considered to apply them on Dhaka clay and observe their performance on capturing the soil behavior.

This study focuses on collecting, testing and modelling of soil at undisturbed condition to get the best usability and application. Total six undisturbed soil samples were collected from various depth of Dhaka, Savar and Gazipur. Consolidated drained and undrained tests were performed under constant confining pressure to observe the stress-strain characteristics of Dhaka clay at various OCR. To evaluate the model parameters one dimensional consolidation tests were conducted for each locations.

From the test results of one dimensional consolidation test, the compression index were found in the range of 0.057 to 0.07 and swelling index is found in the range of 0.01 to 0.015. From triaxial compression test the principal critical stress ratio were found in the range of 2.5 to 3.3 for various locations. From the simulations the density parameter were found in the range of 300 to 480 and bonding parameters in the range of 10 to 15 for drained condition and 30 to 45 for undrained condition respectively.

To observe the performance of the models considered, the simulated results using the above parameters were plotted with the test results. It was found that for all the stress conditions and stress paths, Subloading t_{ij} model can capture the Dhaka clay behavior accurately at drained and undrained conditions. On the other hand Cam-clay and

Modified Cam-clay model have failed to capture the Dhaka clay behavior at undained condition. At drained condition Modified Cam-clay model can capture the soil strength behavior satisfactorily at normally consolidated condition. At all stress conditions, the volumetric strain simulated by both Cam-clay and Modified Cam-clay model were found to overestimate the observed test results.

DEDICATED

TO

MY FATHER, MOTHER AND WIFE

TABLE OF CONTENTS

Page No.

DECLARATION i

ACKNOWLEDGEMENT ii

ABSTRACT iii

TABLE OF CONTENTS vi

LIST OF TABLES x

LIST OF FIGURES xi

ABBREVIATIONS xix

Chapter One INTRODUCTION 1

1.1 General 1

1.2 Problem Statement 3

1.3 Objectives and Scopes of the Study 6

1.4 Organization of the Thesis 8

Chapter Two LITERATURE REVIEW 9

2.1 General 9

2.2 Development and Selection of Constitutive Models 9

2.3 Problem Solving Using Constitutive Models 10

2.4 Components of Elasto-Plastic Constitutive Models 12

2.5 Fundamentals of Constitutive Modelling 12

2.5.1 One-dimensional behavior of soil 12

2.5.2 Definition of Yield Function and Yield Surface 14

2.5.3 Definition of Plastic Flow Rule 14

2.6 Conventional One-dimensional Modelling of Soil 16

2.6.1 Modelling of Normally Consolidated Soil 16

2.6.2 Modelling of Over-consolidated Soil 18

2.6.3 Modelling of Structured Soil....21
2.7 Outline of Cam-clay Model....24
2.8 Applicability of Cam-clay Model....34
2.9 Modeling of Soil Behavior Based on the t_{ij} Concept....36
2.9.1 Definition of stress and strain invariants....36
2.9.2 Modelling of Normally Consolidated Soil....41
2.9.3 Modelling of Over-consolidated Soil....44
2.9.4 Modelling of Structured Soil....44
2.10 Other Constitutive Models and Their Features....45
2.10.1 The Mohr-Coulomb model (MC)....45
2.10.2 Drucker-Prager (MC)....47
2.10.3 Hyperbolic Model....47
2.11 Geological Aspects of Dhaka Clay....49
2.12 Studies on Modelling of Dhaka Clay....49
2.13 Conclusions....50
Chapter Three RESEARCH METHODOLOGY....51
3.1 General....51
3.2 Study Area....51
3.3 Research Scheme....54
3.4 Sample Collection....55
3.5 Preservation and Preparation of Sample....55
3.6 Laboratory Test....55
3.7 Physical Properties Test....55
3.8 Mechanical Properties Test....56
3.8.1 Preparation of Sample....56
3.8.1.1 Sample Extrusion....56
3.8.1.2 Specimen Preparation....56

3.8.2 Triaxial Compression Test 56
3.8.3 One-dimensional Consolidation Test 57
3.8.4 Data Collection and Calculation 58
3.9 Simulation Steps 58
Chapter Four RESULTS AND DISCUSSIONS 60
4.1 General 60
4.2 Index Properties 60
4.3 Model Parameters Obtained at Drained Condition 60
4.3.1 One-dimensional Consolidation Properties 61
4.3.2 Consolidated Drained Triaxial Properties 63
4.3.3 Simulations of the Test Results 69
4.3.3.1 Subloading t_{ij} model 69
4.3.3.2 Cam clay model 71
4.3.3.3 Simulations at different Initial OCR 74
4.3.3.4 Simulation of stress path test 76
4.3.3.5 Stress-dilatancy relation 77
4.3.3.6 Observed and simulated results of other locations 79
4.4 Model Parameters Obtained at Undrained Condition 89
4.4.1 One-dimensional Consolidation Properties 89
4.4.2 Consolidated Undrained Triaxial Properties 91
4.4.3 Simulations of the Test Results 94
4.4.3.1 Subloading t_{ij} model 94
4.4.3.2 Cam-clay model 97
4.4.3.3 Simulations at Extension Condition 101
4.4.3.4 Simulations of other locations 102
4.5 Influence of Various Parameters of Subloading t_{ij} model 108
4.5.1 Influence of Density and Bonding Parameters 108

4.5.2 Influence of Shape Function, β 113
4.6 Summary of the Parameters 115
Chapter Five CONCLUSIONS AND RECOMMENDATIONS FOR FUTURE STUDY 117
5.1 General 117
5.2 Summary of Findings 117
5.3 Conclusions 119
5.4 Recommendations for Future Studies 120
REFERENCES 121

LIST OF TABLES

Table 2.1 Comparison between the original and modified Cam-clay model (Hicher and Shaao 2002) 34

Table 2.2 Comparison between tensors and scalars related to stress and strain in the ordinary concept and the t_{ij} concept. 40

Table 2.3 Some Constitutive Models, Their Attributes and Their Capabilities (Lade, 2005) 48

Table 2.4 Parameters of Subloading t_{ij} model for Dhaka clay (Islam et al. 2013) 49

Table 3.1 Soil investigation locations 51

Table 3.2 Physical property tests 55

Table 3.3 Input parameters for numerical simulation 59

Table 4.1 Consolidation Specimen Description 61

Table 4.2 Triaxial Specimen Description 64

Table 4.3 Material parameters at drained condition 69

Table 4.4 Consolidation Specimen Details 89

Table 4.5 Triaxial Specimen Description 91

Table 4.6 Material parameters at undrained condition 94

Table 4.7 Summary of parameters obtained from simulation of Subloading t_{ij} model for Dhaka clay. 116

LIST OF FIGURES

Figure 1.1 Challenges of geotechnical engineers during excavation in the ground subjected to high lateral earth pressure from adjacent high rise building. 4

Figure 1.2 Examples of damaged caused by the geotechnical failure inside the Dhaka city. 5

Figure 1.3 Map showing the total area covered by the Madhupur tract. 7

Figure 2.1 Simple and advanced procedures for predicting the behavior of prototype structures (Lade, 2005). 10

Figure 2.2 Retaining wall problems subjected to deformation (Lade, 2005). 11

Figure 2.3 Examples of complex geotechnical engineering problems. 11

Figure 2.4 Typical one-dimensional stress-strain behaviors of solid materials (Nakai, 2013). 13

Figure 2.5 Yield surface and aassociated flow rule in principal stress space (Nakai, 2013). 14

Figure 2.6 Non-aassociated flow rule: failure surface and the plastic potential (Puzrin, 2012). 15

Figure 2.7 e-lnσ relationship of a normally consolidated soil (Nakai et al, 2011). 17

Figure 2.8 Evolution of F and H in a normally consolidated soil (Nakai et al. 2011)....17

Figure 2.9 e-ln σ relationship of an over consolidated soil (Nakai et al. 2011).....18

Figure 2.10 Evolution of F and H in an over consolidated soil (Nakai et al. 2011).....19

Figure 2.11 (a) and (b) effect of power of the variable ρ (c) effect of different values of ρ0 (Nakai, 2013).....20

Figure 2.12 One dimensional compression: (a) structureless soil, (b) weakly structured soil with abrupt de-structuring and (c) strongly structured soil with gradual de-structuring (e.g. Belokas & Kavvadas, 2010). 21
Figure 2.13 Typical stress-strain behavior of soil in undrained triaxial compression; ((a) structureless soil, (b) weakly structured soil and (c) strongly structured soil (e.g. Belokas & Kavvadas, 2010). 21
Figure 2.14 e-lnσ relationship of a structured clay showing its various zones (e.g. Nakai 2013). 22
Figure 2.15 e-ln σ relationship of structured soil (Naka et al. 2011). 23
Figure 2.16 Evolution of F and H in an over consolidated soil (Nakai et al. 2011) 23
Figure 2.17 $G\rho\ and\ Q\omega$ given by linear function ρ and ω respectively (Nakai et al. 2011). 24
Figure 2.18 Definitions of p and q 24
Figure 2.19 Definitions of $d\varepsilon v$ and $d\varepsilon d$. 25
Figure 2.20 Explanation of equivoid ratio lines by Henkel (1960). 27
Figure 2.21 (a) Triaxial compression test of a NC soil under different constant mean principal stresses (b) e-lnp relation of a normally consolidated soil (Nakai, 2013). 28
Figure 2.22 Stress ratio (η) versus deviatoric strain (εd) versus volumetric strain (εv) 29
Figure 2.23 Relation between volumetric strain, εv and stress ratio, η for normally consolidated soils under constant mean principal stresses. 29
Figure 2.24 Relationship between void ratio and effective pressure in a normally consolidated (NC) soil. 30
Figure 2.25 Initial and current yield surface in the p-q plane and direction of plastic flow in the Cam-clay model (Nakai 2013). 32

Figure 2.26 Shape of Yield surface of Cam-clay model on *p*-*q* plane (Nakai, 2013). .32
Figure 2.27 Stress-dilatancy relation of Cam-clay model (Nakai 2013). 33
Figure 2.28 Stress-dilatancy relation of modified Cam-clay model (Nakai 2013).....33
Figure 2.29 Observed stress-starin relation of a NC Fujinomori clay under extension and compression (Nakai 2013). 35
Figure 2.30 Observed stress-dilatancy relation of a NC Fujinomori clay under extension and compression (Nakai et al 2013). 35
Figure 2.31 Stress-dilatancy relation of a NC Dhaka clay under extension and compression (Rahman et al. 2018). 36
Figure 2.32 Spatially mobilized plane the three-dimensional space (Nakai, 2013). 36
Figure 2.33 Plane of maximum mobilization at different principal stresses (Nakai, 2013). 37
Figure 2.34 Definitions of tN and tS (Nakai, 2013). 39
Figure 2.35 Definitions of $d\varepsilon N*, d\varepsilon S*$ (Nakai, 2013).....39
Figure 2.36 Definitions of $d\varepsilon N*, d\varepsilon S*$ (Nakai 213). Shape of Matsuoka–Nakai SMP criterion, (extended) von Mises criterion, and Mohr–Coulomb criterion on the octahedral plane in three principal stresses space. (a) Stress quantities used in the ordinary concept; (b) stress quantities used in the t_{ij} concept.....40
Figure 2.37 Initial and current yield surfaces in the t_N–t_S plane and direction of plastic flow for the model based on the t_{ij} concept (Nakai 2011).....41
Figure 2.38 Stress-dilatancy relation of subloading t_{ij} model.....42
Figure 2.39 Observed stress-dilatancy relation of drained triaxial compression and extension test on Fujinomori clay (Nakai et al. 2011).....43
Figure 2.40 Stress-starin relation of a NC Dhaka clay under extension and compression (Rahman et al. 2018).....43

Figure 2.41 $e - lntN$ relation of an OC soil (Nakai 2013).....44

Figure 2.42 Function $G(\rho)$ and $Q(\omega)$ for evolution rule of ρ (Nakai, 2013). 45

Figure 2.43 Elastic-perfectly plastic Mohr-Coulomb model compared with typical soil under drained triaxial compression test (Wood & Gajo, 2005).....46

Figure 2.44 Mohr-Coulomb criterion on the octahedral plane in three principal stresses (Brinkgreve, 2005).....46

Figure 2.45 Drucker-Prager yield criteria (Islam, M. R. 2014).....47

Figure 2.46 Hyperbolic model perdition of a drained triaxial test (Wood & Gazo, 2005). 47

Figure 3.1 Map showing the area covered by the Madhupur track inside the Dhaka city. 52

Figure 3.2 Map showing the locations of soil sample collection inside the Dhaka city. 53

Figure 3.3 triaxial test in progress. 57

Figure 3.4 Consolidation test in progress. 58

Figure 4.1 Observed $e - lnp$ relationship of the Sample of (a) Gazipur 61

Figure 4.2 Observed (a) stress-deviator strain-volumetric strain relationship, (b) effective stress path of Gazipur Sample in CD triaxial compression test.....65

Figure 4.3 Observed (a) stress-deviator strain-volumetric strain relationship, (b) effective stress path of Mirpur DOHS Sample in CD triaxial compression test 66

Figure 4.4 Observed (a) stress-deviator strain-volumetric strain relationship, (b) effective stress path of Rokeya Sarani Sample in CD triaxial compression test 67

Figure 4.5 Observed (a) stress-deviator strain-volumetric strain relationship, (b) effective stress path of Savar Sample in CD triaxial compression test 68

Figure 4.6 Observed and Predicted $e - lnp$ relationship of Gazipur sample.....70

Figure 4.7 Observed and predicted stress-strain relation of Gazipur soil at drained condition. 70
Figure 4.8 Observed and predicted effective stress path in CD triaxial compression test 71
Figure 4.9 Observed and predicted stress-strain relation of Gazipur soil under CD triaxial test....72
Figure 4.10 Observed and predicted stress-strain relation of Gazipur soil under CD triaxial test....72
Figure 4.11 Observed and Predicted $e - lnp$ relationship of Gazipur sample (a) Cam-clay model (b) Modified Cam-clay model.....73
Figure 4.12 Predicted results at initial OCR 6.0 and OCR 1.0 in CD Triaxial test. 74
Figure 4.13 Predicted results at Initial OCR 6.0 and OCR 1.0 in CD Triaxial test using (a) Cam-clay model (b) Modified Cam-clay model. 75
Figure 4.14 Simulated results at constant mean effective stresses, p for different OCR. 76
Figure 4.15 Simulated results at constant mean effective stresses, $\sigma 3$ for different OCR. 77
Figure 4.16 Observed and Predicted Stress-dilatancy relation of (a) Subloading t_{ij} (b) Cam-clay model....78
Figure 4.17 Observed and Predicted $e - lnp$ relationship of Mirpur DOHS sample. ...80
Figure 4.18 Observed and predicted stress-strain relation of Mirpur DOHS soil. 80
Figure 4.19 Observed and predicted stress-strain relation of Mirpur DOHS soil (a) Cam-clay (b) Modified Cam-clay model.....81
Figure 4.20 Observed and Predicted $e - lnp$ relationship of Mirpur DOHS sample (a) Cam-clay model (b) Modified Cam-clay model.....82

Figure 4.21 Observed and Predicted $e - lnp$ relationship of Rokeya Sarani sample. ...83
Figure 4.22 Observed and predicted stress-strain relation of Rokeya Sarani soil. 83
Figure 4.23 Observed and predicted stress-strain relation of Rokeya Sarani soil (a) Cam-clay (b) Modified Cam-clay model. 84
Figure 4.24 Observed and Predicted $e - lnp$ relationship of Rokeya Sarani sample (a) Original Cam-clay model (b) Modified Cam-clay model. 85
Figure 4.25 Observed and Predicted $e - lnp$ relationship of Savar sample. 86
Figure 4.26 Observed and predicted stress-strain relation of Savar soil under CD triaxial compression test. 86
Figure 4.27 Observed and predicted stress-strain relation of Savar soil 87
Figure 4.28 Observed and Predicted $e - lnp$ relationship of Savar sample (a) Original Cam-clay model (b) Modified Cam-clay model. 88
Figure 4.29 Observed $e - lnp$ relationship of (a) Shagufta (b) Baridhara sample. 90
Figure 4.30 Observed (a) stress-deviator strain-volumetric strain relationship, (b) effective stress path of Shagufta Sample 92
Figure 4.31 Observed (a) stress-deviator strain-volumetric strain relationship, (b) effective stress path of Baridhara sample 93
Figure 4.32 Observed and Predicted $e - lnp$ relationship of Shagufta sample. 95
Figure 4.33 Observed and predicted stress-strain relation of Shagufta sample. 96
Figure 4.34 Observed and predicted effective stress path of Shagufta sample. 96
Figure 4.35 Observed and predicted stress-strain relation of Shagufta sample. 97
Figure 4.36 Observed and predicted effective stress path in CU triaxial test. 98
Figure 4.37 Observed and predicted stress-strain relation at undrained condition. 99
Figure 4.38 Observed and predicted effective stress path in CU triaxial compression test. 99

Figure 4.39 Observed and Predicted $e - lnp$ relationship of Shagufta sample (a) Cam-clay model (b) Modified Cam-clay model. 100
Figure 4.40 Predicted results at extension condition in CU Triaxial simulation. 101
Figure 4.41 Observed and predicted effective stress path in CU triaxial compression and extension test 102
Figure 4.42 Observed and Predicted $e - lnp$ relationship of Baridhara sample. 103
Figure 4.43 Observed and predicted stress-strain relation of Baridhara soil under CU triaxial compression test. 103
Figure 4.44 Observed and predicted effective stress path in CU triaxial compression test. 104
Figure 4.45 Observed and predicted stress-strain relation of Baridhara soil under CD triaxial test 105
Figure 4.46 Observed and predicted effective stress path in CU triaxial compression test. 105
Figure 4.47 Observed and predicted stress-strain relation at undrained condition. 106
Figure 4.48 Observed and predicted effective stress path at undrained condition. 106
Figure 4.49 Observed and Predicted $e - lnp$ relationship of Baridhara sample (a) Original Cam-clay model (b) Modified Cam-clay model. 107
Figure 4.50 Observed and Predicted $e - lnp$ relationship with varying a. 108
Figure 4.51 Figure Observed and Predicted $e - lnp$ relationship with varying ω. 109
Figure 4.52 Observed and Predicted $e - lnp$ relationship with varying b. 110
Figure 4.53 Observed and predicted stress-strain relation at undrained condition with varying ω. 111
Figure 4.54 Observed and predicted effective stress path in CU triaxial compression test with varying ω. 111

Figure 4.55 Observed and predicted stress-strain relation under CD triaxial test with varying ω. 112
Figure 4.56 Observed and predicted stress-strain relation under CD triaxial test with varying β. 113
Figure 4.57 Observed and predicted stress-strain relation at undrained condition with varying β. 114
Figure 4.58 Observed and predicted effective stress path in CU triaxial compression test with varying β. 115

ABBREVIATIONS

a	Material parameter to describe the influence of density and/or confining pressure
a_1, a_2, and a_3	Principal values of a_{ij} (i.e., direction cosines of normal to the spatially mobilized plane, SMP)
a_{ij}	Symmetric tensor whose principal values are given by a_1, a_2, and a_3
b	Material parameter to describe the influence of bonding
$d\varepsilon_N$*	Strain increment invariant in t_{ij} concept (i.e., normal component of $d\varepsilon_{ij}$ with respect to the SMP (= $d\varepsilon_{ij}a_{ij}$)
$d\varepsilon_S$*	Strain increment invariant in t_{ij} concept (i.e., in-plane component of $d\varepsilon_{ij}$ witth respect to the SMP
$d\varepsilon_{ij}$	Deviatoric strain increment tensor based on *tij* concept
e_N	Void ratio on the normal consolidation line (NCL)
h_p	Plastic modulus
β	Material parameter to determine the shape of the yield surface
δ_{ij}	Unit tensor (Kronecker's delta)
ε_1, ε_2, and ε_3	Three principal strains
ε_{ij}	Strain tensor
ε_d	Deviatoric strain
ε_v	Volumetric strain
ϕ_{moij}	Mobilized angle between two principal stresses (σ_i and σ_j)
η	Stress ratio (= q/p)
η_{ij}	Stress ratio tensor by Sekiguchi and Ohta (= s_{ij}/p)
φ_1 and φ_2	Principal values of the fabric tensor
κ	Swelling index
λ	Compression index
ν_e	Poisson's ratio of elastic component
Superscript e	Elastic component
Superscript p	Plastic component
Subscript CS	value at critical state
Subscript NC	value at normally consolidated state

Chapter One
INTRODUCTION

1.1 General

Dhaka the capital city of Bangladesh is expanding rapidly with significant development. Rapid urbanization is going also on surrounding areas of Dhaka like Savar, Gazipur and Narayanganj. In a city like Dhaka, geotechnical engineers have to deal mainly with the problems related to foundations of buildings or bridges, roadside slopes etc. In near future, engineers will have to deal with the design of sophisticated structures like tunnel, buried pipelines etc. which are of great challenge in a densely populated area.

At present, most of this practical designs are done based on the framework of classical soil mechanics which is established mainly by Karl Terzaghi (e.g., Terzaghi, 1943) and two famous book, Terzaghi and Peck, 1948 and Taylor, 1948. In the classical soil mechanics the similar soils are assumed to have different properties when solving different problems, such as-

(i) Porous rigid material in seepage problems.
(ii) Nonlinear elastoplastic material in settlement problems.
(iii) Porous linear elastic material in consolidation problems.
(iv) Rigid plastic material in earth pressure and stability problems.
(v) Linear elastic material in calculating stress in the ground.

The classical soil mechanics thus limits itself because of such empirical assumptions. Most of the cases of geotechnical engineering problems are solved by considering soil as an elastic or rigid plastic material where stress-dilatancy characteristics are not taken into considerations. As actual soil is an elastoplastic material most of the designs are either over designed or under designed for not taking proper considerations of a constitutive model. There is the necessity of a constitutive model which can simulate the soil behavior accurately. On the contrary, most of the constitutive models are not able to simulate total behavior of the soil and does not fit with all the soil types as well.

With the development of modern geotechnical engineering, application of numerical techniques like finite element or finite difference method has become essential to solve the complex geotechnical engineering problems. These methods considerably depend on

the stress-strain behaviour, i.e., constitutive relation of geomaterials.

Over the past 50 years, constitutive models of geomaterials have achieved substantial improvement to capture the actual soil behavior. Initially formulated models were simple in terms of parameters required but later much complex models were developed to predict real soil behavior. However, the models are always expected to be simple and sophisticated.

The first simple model which considered the soil as an elastoplastic material is the Cam-clay model (e.g., Schofield and Wroth, 1968). In this model positive dilatancy during strain hardening is not taken into consideration along with some other limitations (Nakai et al., 2011) stated as follows:

(i) Influence of intermediate principal stress on the deformation and strength of soil
(ii) Stress path dependency on the direction of plastic strain increments
(iii) Positive dilatancy during strain hardening
(iv) Behavior of soil under cyclic loading
(v) Soil anistropy
(vi) Influence of density and/or confining pressure on the deformation and strength
(vii) Behavior of structured soil
(viii) Soil anisotropy and non-coaxiality
(ix) Time effect and age effect
(x) Unsaturated soils

To overcome the limitations of Cam-clay model, modified Cam-clay model and few others were developed, many models are formulated later on, but most them are either complicated in practice or have limited use. Later, Subloading t_{ij} model (Nakai et al, 2011) was developed that used to provide a better performance, in use. Some of the features of the Subloading t_{ij} model are as follows:

(i) The influence of intermediate principal stress on the deformation and strength is considered (Nakai and Mihara, 1984).
(ii) The stress path dependency of plastic flow is considered with the introduction of the plastic strain increment division into two components: a plastic strain increment which satisfies an associated flow rule in the t_{ij}, space and an isotropic plastic strain increment due to increasing mean stress.

(iii) The behavior of structured soil such as naturally deposited clay can be described (Nakai, 2007, Nakai et al., 2009).

(iv) Positive dilatancy during strain hardening is considered in Subloading t_{ij}, model (Nakai and Hinokio, 2004).

(v) Influence of density and/or confining pressure on the deformation and strength are taken into consideration by introducing and revising the subloading surface concept (Hashiguchi and Ueno, 1977; Hashiguchi, 1980).

The parameters required for a constitutive model depends on the soil types and stress conditions. Therefore, soils of different types of different deposition needs to be calibrated to achieve the accurate results.

1.2 Problem Statement

Geologically Dhaka and surrounding Savar, Gazipur and Narayanganj are situated in the southern half of the Madhupur tract which is the oldest sediment exposed. The area covered by the Madhupur tract which stretches from just south of Jamalpur in the north, to Fatullah of Narayanganj, in the south.

The Dhaka city is extending very fast as a capital city of this developing country. Numerous development works are going on every day. Geotechnical engineers have to deal with the Dhaka clay frequently which extends to a shallow depth of 8 to 30 m. Sometimes, complex situations arrive in this densely populated city during constructions like impact of foundation excavation to adjacent buildings (Figure 1.1), ground subsidence during and after the construction, settlement issues for high rise buildings. Improper design and handling of these complex problems often causes serious economic damage and take human lives. Some of the recent incidents are shown in Figure 1.2 that occured in Dhaka city.

These complex analysis cannot be done accurately with the concepts of classical mechanics. Experts take help of FEM software to simulate the real ground conditions in such cases. These software are required to have sophisticated constitutive models for the soils under study.

Inside and surroundings this city, shallow to medium depth foundations are mainly laid on the Dhaka clay. So, it is important to describe the stress-strain behavior of the soil accurately while using FEM simulation software, e.g., Abaqus, Plaxis. Several constitutive models of soils are available now a days which are either complex or cannot describe the soil behavior completely.

In this study two simple constitutive models, i.e., Cam-clay model and Subloading t_{ij} model would be taken into considerations. The model parameters would be calibrated for the Dhaka-clay which would be a guideline for numerical simulations. Also, performance of these models to describe the stress-strain behavior would be evaluated in the study.

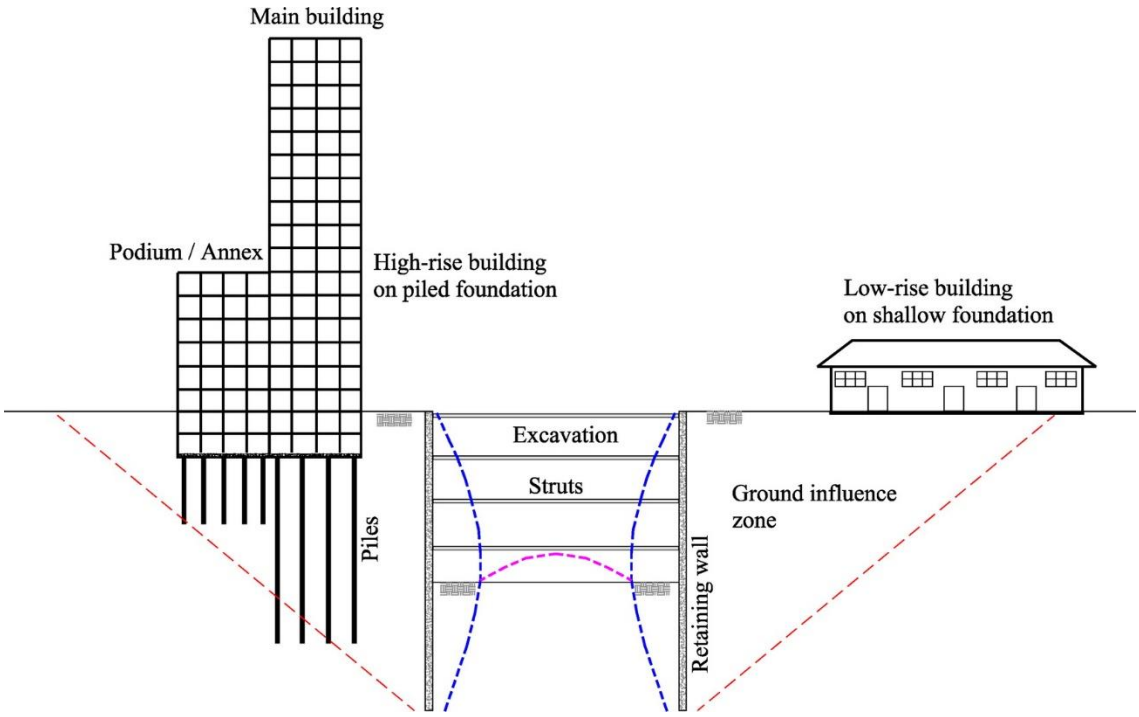

Figure 1.1 Challenges of geotechnical engineers during excavation in the ground subjected to high lateral earth pressure from adjacent high rise building.

(a) A six-storey building in capital Dhaka's Karwan Bazar has been evacuated after a street beside it suffered sudden subsidence.

(b) Rampura building collapse killing 12 person.

Figure 1.2 Examples of damaged caused by the geotechnical failure inside the Dhaka city.

1.3 Objectives and Scopes of the Study

The main objective of the study is to get a simple as well as sophisticated constitutive model for the Dhaka soil which will provide better results during numerical simulations. With this end in view, the objectives of the study are listed below:

(i) To determine the model parameters of simple constitutive models like Cam-clay and Subloading t_{ij} models for Dhaka clay.
(ii) To observe the stress-strain-dilatancy relationship of Dhaka clay using Cam-clay and Subloading t_{ij} models.
(iii) To evaluate the applicability of constitutive models like Cam-clay and Subloading t_{ij} model to describe the various properties i.e., stress, strain, settlement of the Dhaka clay.

The scope of the study is restricted to the determination of the soil property at in-situ condition. Hence undisturbed samples would be collected from selected locations of Dhaka. The parameters determined can also be applicable for the soil of Madhupur tract at various locations. Figure 1.3 shows the extent of the Madhupur tract. Most of the Dhaka city and surrounding Gazipur, Savar are situated on this tract.

Present study does not include the soil behavior of Dhaka-clay under dynamic loading. Required cyclic loading tests to determine the dynamic soil properties were not conducted. Hence the strain-strain characteristics of Dhaka-clay during earthquake cannot be described by this study and beyond the scope of the research. Also, soil behavior in unsaturated condition is not included in the study. Only soils under fully saturated condition is tested and analyzed.

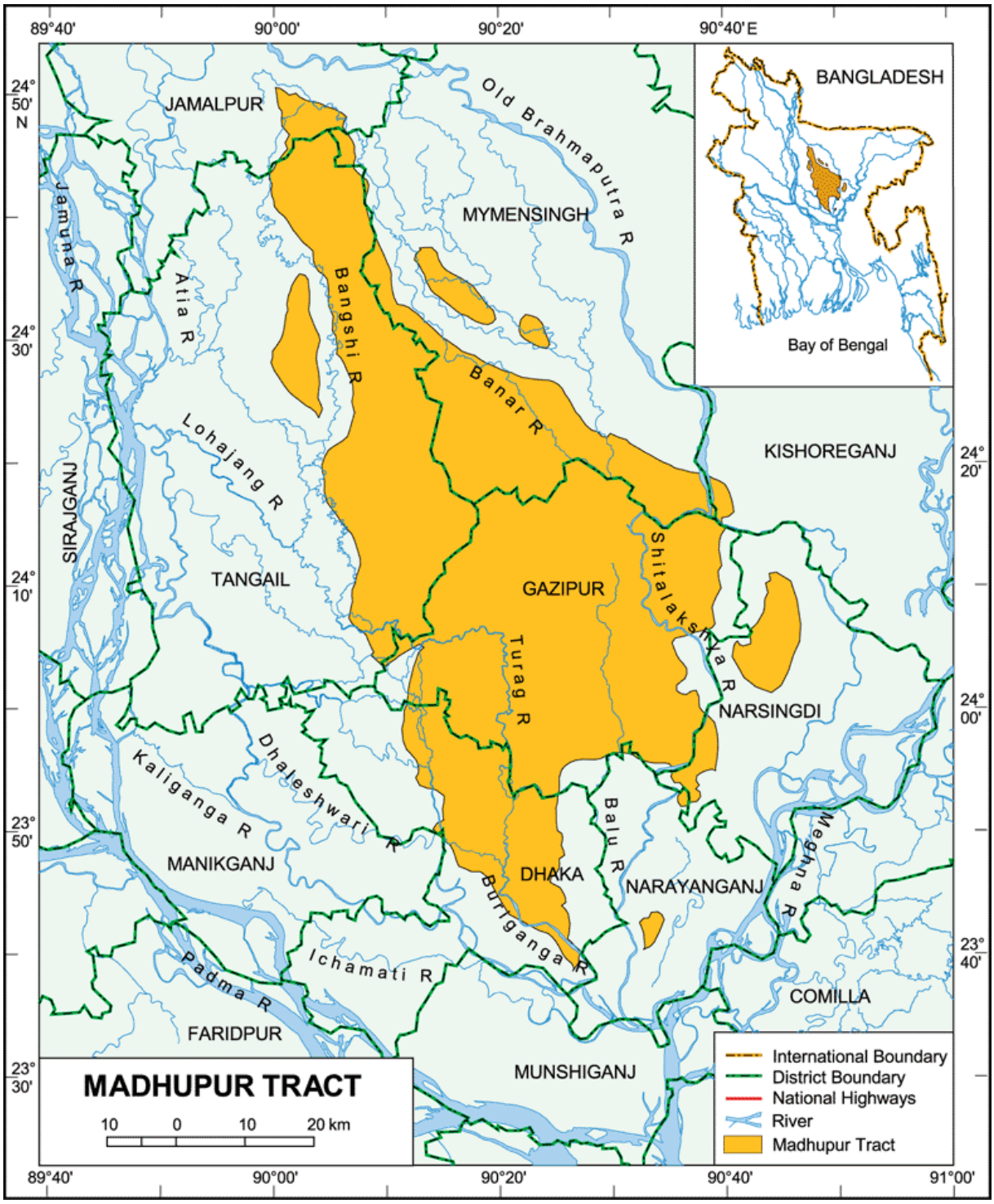

Figure 1.3 Map showing the total area covered by the Madhupur tract.

1.4 Organization of the Thesis

The present study is furnished in this thesis consisting of five chapters.

Chapter One gives an introduction of the relevant research background, statement of problems as well as the objectives and scope of this research.

Chapter Two focuses on the review of the geology of Dhaka soil as well as the work done by the past researches related to the study. It also describes the basic concept of elasticity and plasticity as well as salient features of different constitutive models. Detailed discussion on Cam clay and Subloading t_{ij} model is presented in this chapter.

Chapter Three contains the details of the study areas for the research. It also includes the description of sample collection from the field. Details of the sample preparation and experimential program are also discussed in the chapter.

Details of the laboratory test results have been described in Chapter Four. This chapter also focuses on the simulation results based on the laboratory test parameters. Finally test results are compared with the simulation result is presented to get the most accurate model for the Dhaka clay.

In Chapter Five conclusions obtained from the study is presented. Also, recommendations for future research works related to the constitutive models of other soil types of the Bangladesh are suggested in this chapter

Chapter Two
LITERATURE REVIEW

2.1 General

In this chapter, the existing literatures related to the present study are presented. Development of constitutive models and their attributes with applicability is discussed for easy understanding. Discussions on basic concept of elasticity and plasticity as well as salient features of different constitutive models are done. Detailed theoretical concepts on the formulation of Cam-clay and Subloading t_{ij} model are also presented in this chapter. Thereafter geological aspects of Dhaka clay is discussed.

2.2 Development and Selection of Constitutive Models

Soils are considered as the complex heterogeneous materials which consist of solid skeleton, voids filled with air and/ or water. The behavior of soil is very complex which depends on a wide variety of factors among which void ratio and confining pressure are the most important. In 1923, Terzaghi described that soils deform as the changes in effective stress acting on the body. Hence a theoretically sound model is formulated using the effective stress invariants. The aspects of soil behavior depends on the stress level, stress path, strain level, time, density, permeability, over-consolidation ratio, etc. (Brinkgreve, 2005).

There are several sophisticated experiments are available now a days to observe the soil behavior under three dimensional condition such as torsion shear, directional shear, simple shear, resilient modulus and so on. But a constitutive model should be such that the parameters required are obtained from relatively simple manner like triaxial test and oedometer test.

Figure 2.1 shows a comparison between classical analysis and the advanced numerical analyses using a sophisticated constitutive model. The analysis of the classical methods should usually be verified by the prediction of a constitutive model or full scale tests of elements of the prototype structures. But in most of the cases a full scale test is not feasible due to time and economy. Therefore, a sophisticated constitutive model which can capture the real soil behavior may be the most economical and pertinent solution.

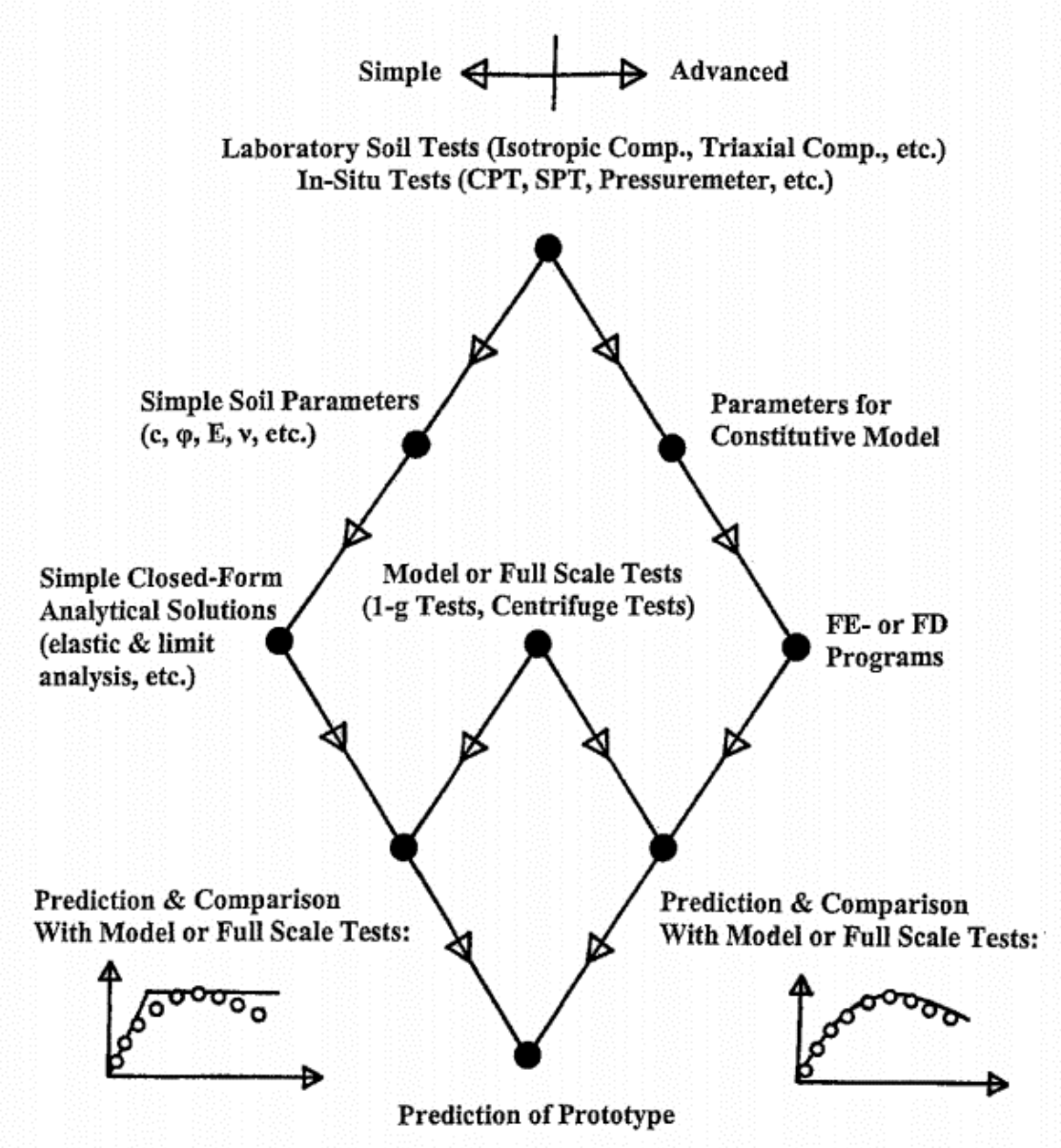

Figure 2.1 Simple and advanced procedures for predicting the behavior of prototype structures (Lade, 2005).

2.3 Problem Solving Using Constitutive Models

With the help of sophisticated constitutive models and numerical methods, different types of geotechnical problems can be solved accurately. Classical methods have limitations of considering appropriate soil-structure and soil-water-structure interactions, influence of nearby structures and so on. Numerical methods with a good constitutive model can analyze and predict the soil behavior in any complex conditions. For example, in case of a retaining wall as shown in Figure 2.2 the deformation cannot be predicted by classical

procedures. Figure 2.3 shows some other examples of applications of numerical methods for analysis apart from the conventional analytical methods (Lade, 2005).

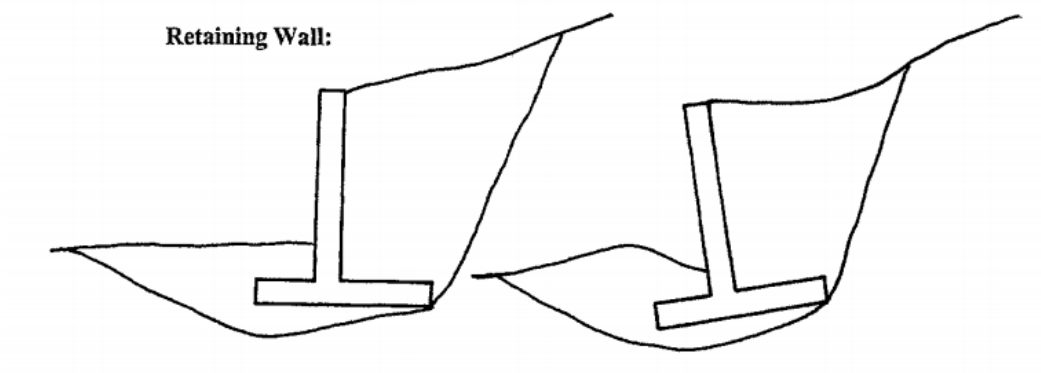

Figure 2.2 Retaining wall problems subjected to deformation (Lade, 2005).

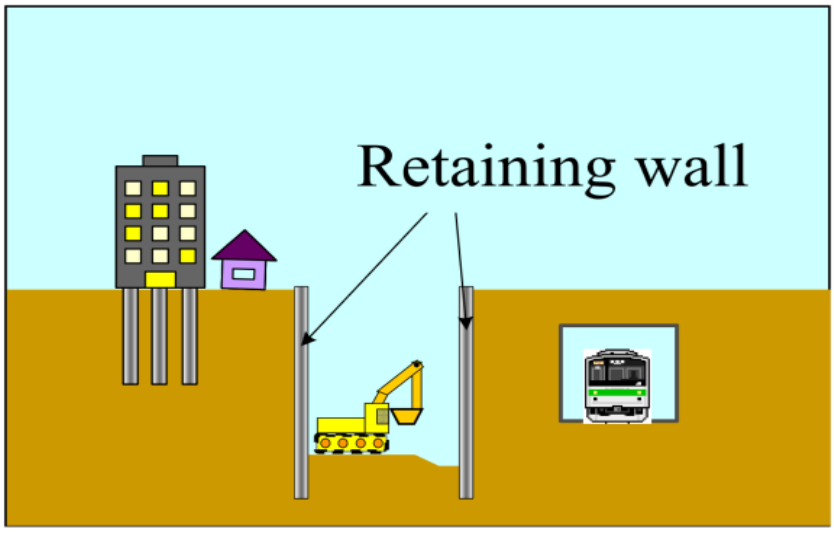

(a) Excavation problem

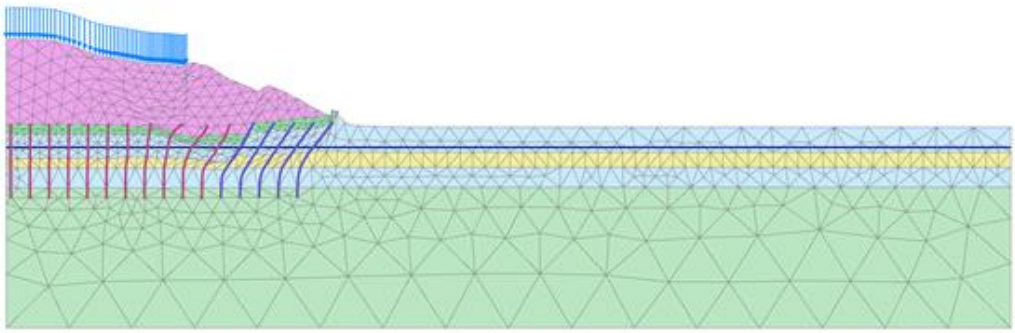

(b) Slope stability analysis

Figure 2.3 Examples of complex geotechnical engineering problems.

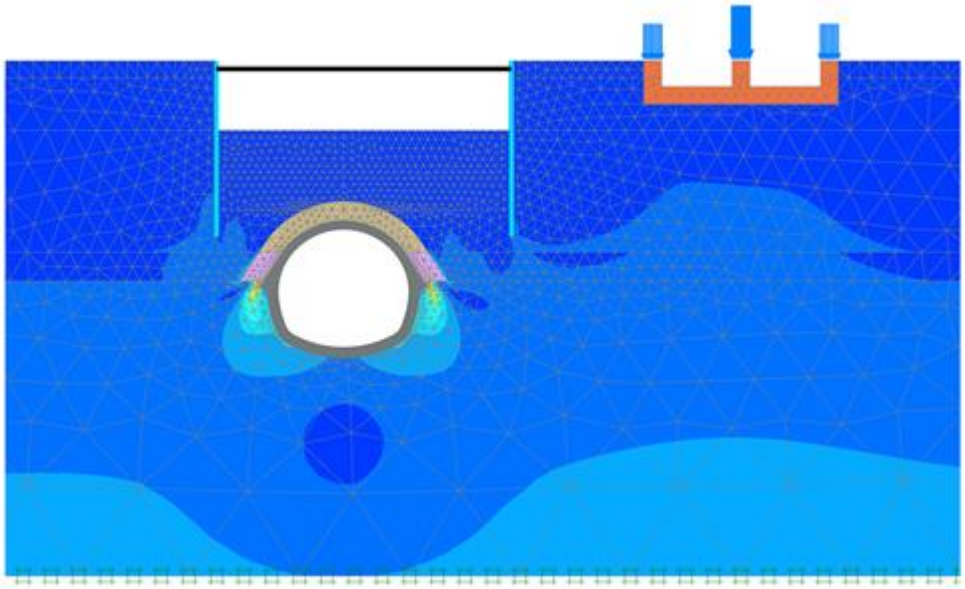

(c) Deformation analysis of Tunnels

Figure 2.3 (Contd.) Examples of complex geotechnical engineering problems.

2.4 Components of Elasto-Plastic Constitutive Models

The elastic behavior is expressed entirely by Hooke's Law where stress and strain varies proportionally. There are several components to describe the plastic behavior such as failure criterion, plastic potential function, yield criterion, hardening/softening relation. The failure criterion put limits on stress state that can be reached whereas, plastic potential function determines the magnitudes of plastic strain increments. Yield criterion determines when plastic strain increments occur and hardening and softening relation determines the magnitudes of plastic increments (Lade, 2005).

2.5 Fundamentals of Constitutive Modelling

2.5.1 One-dimensional behavior of soil

The stress-strain behavior of typical soil considered in different models are describe in five categories as shown in Figure 2.4. Figure 2.4 (a) shows the strain-stain relation based on the Hook's law of linear elasticity. Stress-strain relationship of a rigid- perfectly plastic model is expressed as shown in Figure 2.4 (b). Here it is assumed that no strain will occur until the stress reaches to the yield point and continues to infinity after the yield point.

In Figure 2.4 (c), it is shown that the material initially follows the Hook's law up to the proportional limit and then follows infinite plasticity. Such a model is called elastic perfectly-plastic model. Mohr-Coulomb model is an example of elastic perfectly-plastic model (Brinkgreve, 2005).

In Figure 2.4 (d), after crossing the elastic limit it is shown that in the plastic region, small amount of stress is developed as strain increases. Such a model is called strain-hardening elastoplactic model. Most of the elastoplastic models like Cam-clay model can be classified under this category. Again in some cases, stress decreases as the strain increases beyond the yield point as shown in Figure 2.4 (e). Such a model is called strain-softening elastoplastic model. Recent models like Subloading t_{ij} can be put under this category.

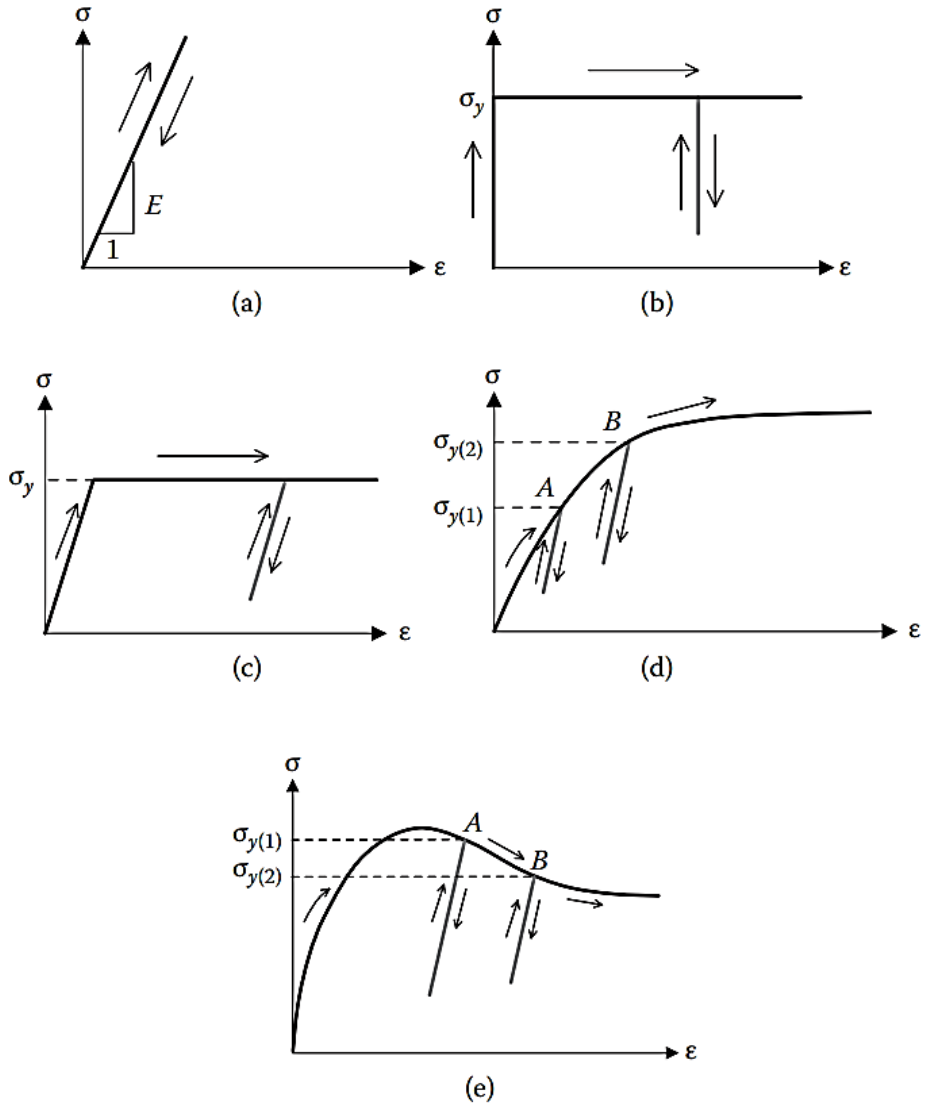

Figure 2.4 Typical one-dimensional stress-strain behaviors of solid materials (Nakai, 2013).

2.5.2 Definition of Yield Function and Yield Surface

Practically, the elastic domain is defined by a scalar function of the stress tensor which is called yield function. The yield function can be derived from the stress-strain relation as shown in Figure 2.5(a) and 2.5(b). In three-dimensional modelling the yield function is expressed as follows assuming an isotropic material (Nakai, 2013):

$$f = F(\sigma_{ij}) - H(\varepsilon_{ij}^{p}) = 0 \tag{2.1}$$

In terms of principal stress value

$$f = F(\sigma_1, \sigma_2, \sigma_3) - H(\varepsilon_1^{p}, \varepsilon_2^{p}, \varepsilon_3^{p}) = 0 \tag{2.2}$$

Where,

σ_{ij} is the stress tensor, ε_{ij}^{p} is the plastic strain tensor, $\sigma_1, \sigma_2, \sigma_3$are the principal stresses, $\varepsilon_1^{p}, \varepsilon_2^{p}, \varepsilon_3^{p}$ are the principal plastic strains.

The yield locus or yield surface is obtained by drawing yield function in 3D stress space. As in Figure 2.5 (a), the solid line indicates that there exists no plastic strain within it and when solid surface moves from point A to B, plastic strain occurs. Figure 2.5 (b) shows the direction of plastic stain increment in 3D stress-stain space.

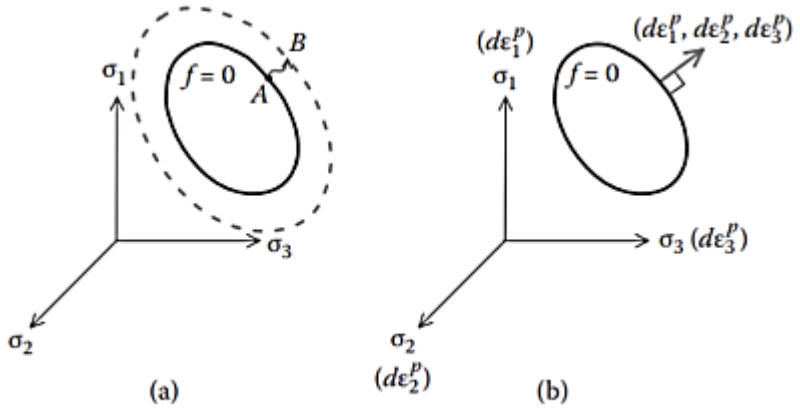

Figure 2.5 Yield surface and aassociated flow rule in principal stress space (Nakai, 2013).

2.5.3 Definition of Plastic Flow Rule

The plastic flow rule describes the evolution of the plastic strains. It provides an expression of the increment of plastic strain increment, $d\varepsilon_{ij}^{p}$ for a given state of stress.

Flow rule can be divided into two types namely associated flow rule and non-associated flow rule. As shown in Figure 2.6 (b), the associated flow rule implies that the axes of the three principal plastic stain increments coincide with those of the three principal stresses respectively, i.e., yield surface coincide with the plastic potential surface. The direction of plastic strain increments is outward and normal to the yield locus. The expression of associated flow rule assuming an isotropic material is expressed as follows (Nakai, 2013 & Hill 1950),

$$d\varepsilon_{ij}^{p} = \Lambda \frac{\partial F}{\partial \sigma_{ij}} \tag{2.3}$$

In terms of principal values,

$$d\varepsilon_{1}^{p} = \Lambda \frac{\partial F}{\partial \sigma_{1}} \quad d\varepsilon_{2}^{p} = \Lambda \frac{\partial F}{\partial \sigma_{2}} \quad d\varepsilon_{3}^{p} = \Lambda \frac{\partial F}{\partial \sigma_{3}} \tag{2.4}$$

Here, Λ is a positive scalar and known as the plastic multiplier.

The non-associated plastic flow rule states denies the normality condition (i.e., direction of plastic strain increment is normal to the yield surface). As shown in Figure 2.6 (a) and Figure 2.6 (b), the incremental plastic strain vector at this point is normal to the plastic potentical and not to the failure surface. The expression of the non-associated flow rule is given as follows,

$$d\varepsilon_{ij}^{p} = \Lambda \frac{\partial G}{\partial \sigma_{ij}} \tag{2.5}$$

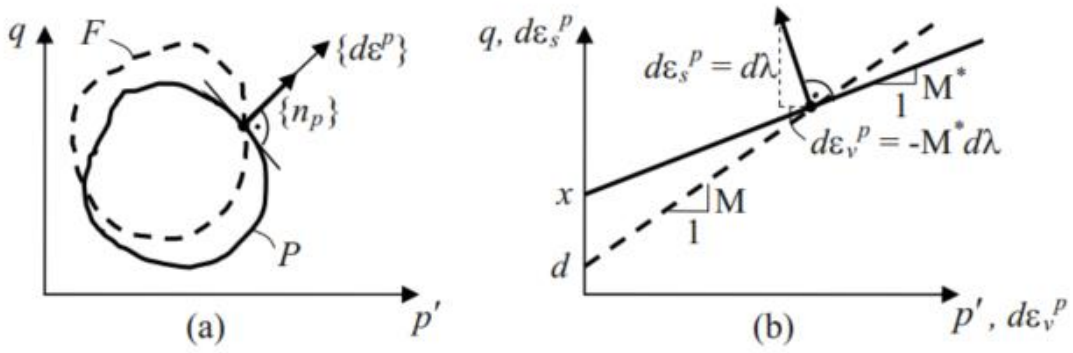

Figure 2.6 Non-aassociated flow rule: failure surface and the plastic potential (Puzrin, 2012).

It is of great advantage that, while using associated flow rule if provides both the yield and plastic potential surfaces by knowing either one of them. One of the major

disadvantages of the associated flow rule stated by Lade (2005) is that, the concept works well for solid metals. But too high rates of volume dilation are predicted if associated flow rule is used in case of frictional materials. Higher the frictional angle results the larger deviation between observed and predicted soil behavior. For clay, associated flow rule results satisfactorily. Most of the constitutive models like Cam-clay (Schofield and Wroth, 1968) and Subloading t_{ij} model (Nakai et al. 2011) use the associated flow rule. However, Hashiguchi (1989) presented some theoretical observations to the use of non-associated flow rules. Anandarajah (1994), developed a bounding surface model with associated flow rule and distorted ellipse yield surface (Soga and O'Sullivan, 2010).

The Cam-clay model (Schofield and Wroth, 1968; Roscoe and Burland, 1968) has been formulated using stress invariants (mean principal stress, p and deviatoric stress, q) and the strain increment invariants (volumetric strain increment, $d\varepsilon_v$ and deviatoric strain increment, $d\varepsilon_d$).

2.6 Conventional One-dimensional Modelling of Soil

The relation between the void ratio (e) and effective stress ($\ln\sigma$) obtained from a typical one-dimensional consolidation test is termed as conventional elastoplatic behavior of soil. In this section a simple one-dimensional model based on subloading surface concept (Hashiguchi, 1980) is presented.

2.6.1 Modelling of Normally Consolidated Soil

In Figure 2.7, typical e-ln$p$ relationship is shown for a normally consolidated soil. Where, I represents the initial stress and P represents the current stress. Therefore, change in the void ratio can be expressed as,

$$(-\Delta e) = e_0 - e = e_{N0} - e_N = \lambda \ln \frac{\sigma}{\sigma_0} \tag{2.6}$$

The elastic change in void ratio is expressed as follows:

$$(-\Delta e)^e = \kappa \ln \frac{\sigma}{\sigma_0} \tag{2.7}$$

Hence, the plastic change in the void ratio becomes,

$$(-\Delta e)^p = (-\Delta e) - (-\Delta e)^e = (\lambda - \kappa) \ln \frac{\sigma}{\sigma_0} \tag{2.8}$$

The yield function is then expressed as,

$$f = F(\sigma) - H((-\Delta e)^p) = 0 \tag{2.9}$$

Where,

$$F = (\lambda - \kappa)\ln \frac{\sigma}{\sigma_0} \tag{2.10}$$

$$H = (-\Delta e)^p \tag{2.11}$$

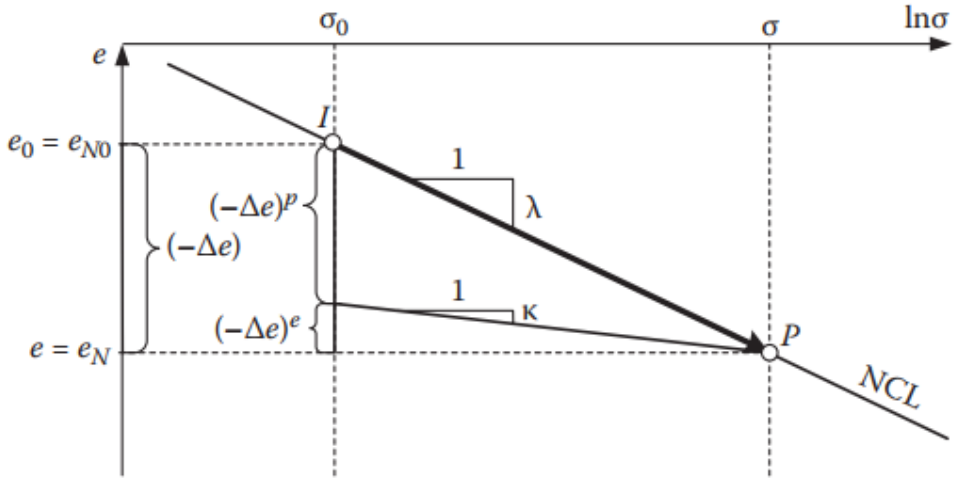

Figure 2.7 e-lnσ relationship of a normally consolidated soil (Nakai et al., 2011).

Evolution of the yield function with plastic change is known as the hardening rule. Equation 2.8 shows that the stress function F and plastic void ratio funtion H relates with unitary slope and thus the stress point is always on the yield surface.

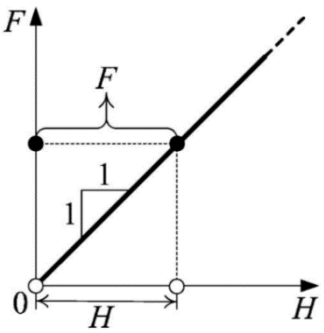

Figure 2.8 Evolution of F and H in a normally consolidated soil (Nakai et al., 2011)

From the consistency condition (*df*=0),

$$df = dF(\sigma) - dH((-\Delta e)^p) = 0 \tag{2.12}$$

$$d(-e)^p = (\lambda - \kappa) \ln \frac{d\sigma}{\sigma} \tag{2.13}$$

$$d(-e)^e = \kappa \ln \frac{d\sigma}{\sigma} \tag{2.14}$$

$$d(-e) = d(-e)^p + d(-e)^e = (\lambda - \kappa) \ln \frac{d\sigma}{\sigma} \tag{2.15}$$

2.6.2 Modelling of Over-consolidated Soil

In Figure 2.9 typical relationship between void ratio, e and effective stress, σ is presented for an over consolidated soil. Here, point I and P denotes the initial and current state of stress, respectively. Two virtual point I' and P' is taken on the normal consolidation line which corresponds to the initial and current state of stress respectively. A new variable ρ is introduced which denotes the difference in void ratio between the virtual point on the NCL and the actual void ratio. The variable ρ decreases as the void ratio approaches more to the NCL with the increase of effective pressure.

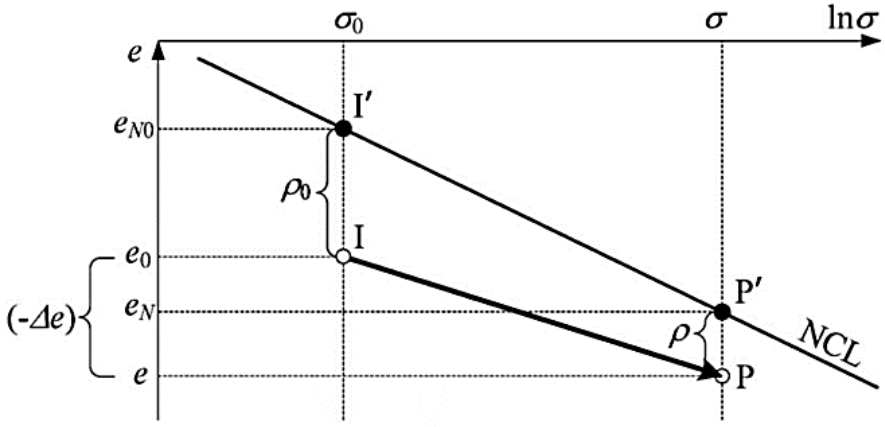

Figure 2.9 e-ln σ relationship of an over consolidated soil (Nakai et al., 2011).

Rewriting the equations (2.6) and (2.8) with the variable ρ gives,

$$(-\Delta e) = e_0 - e = (e_{N0} - \rho_0) - (e_N - \rho) = \lambda \ln \frac{\sigma}{\sigma_0} - (\rho_0 - \rho) \tag{2.16}$$

$$(-\Delta e)^p = (-\Delta e) - (-\Delta e)^e = (\lambda - \kappa) \ln \frac{\sigma}{\sigma_0} - (\rho_0 - \rho) \tag{2.17}$$

Yield function for over consolidated soil is expressed as follows,

$$f = F - \{H + (\rho_0 - \rho)\} = 0 \tag{2.18}$$

From consistency condition *(df=0)*,

$$df = dF - \{dH - d\rho\} = (\lambda - \kappa) \ln \frac{d\sigma}{\sigma} - \{d(-e)^p - dp\} = 0 \quad (2.19)$$

In Figure 2.10, solid line represents the relation between F and H for an over consolidated soil whereas the broken line is the virtual relation for a NC soil. It shows that with the development of plastic deformation, variable ρ decreases and the solid line approaches to the broken line of normally consolidated condition. Therefore,

$$d\rho \propto d(-e)^p$$

or

$$d\rho = -G(\rho).d(-e)^p \quad (2.20)$$

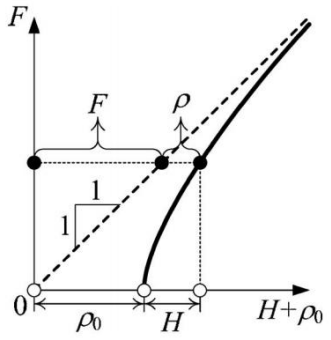

Figure 2.10 Evolution of F and H in an over consolidated soil (Nakai et al., 2011)

Then, the increment of total void ratio is expressed as follows,

$$d(-e) = d(-e)^p + d(-e)^e = \left\{\frac{(\lambda-\kappa)}{1+G(\rho)} + \kappa\right\}.\frac{d\sigma}{\sigma} \quad (2.21)$$

Here, $G(\rho)$ is the variable which represents the effect of stiffness of the soil. It varies with the variable ρ as shown in Figure 2.11 (a). In Figure 2.11 (b), the effect of power of ρ on the relationship between void ratio and effective stress is shown. Figure 2.11 (c) shows how the increasing value of variable ρ increase the stiffness of soil.

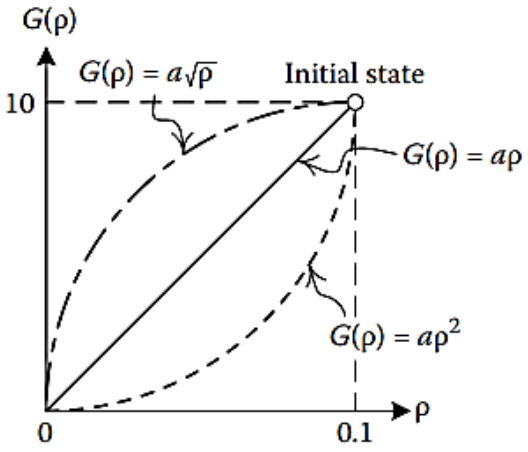

(a) Three kinds of function $G(\rho)$

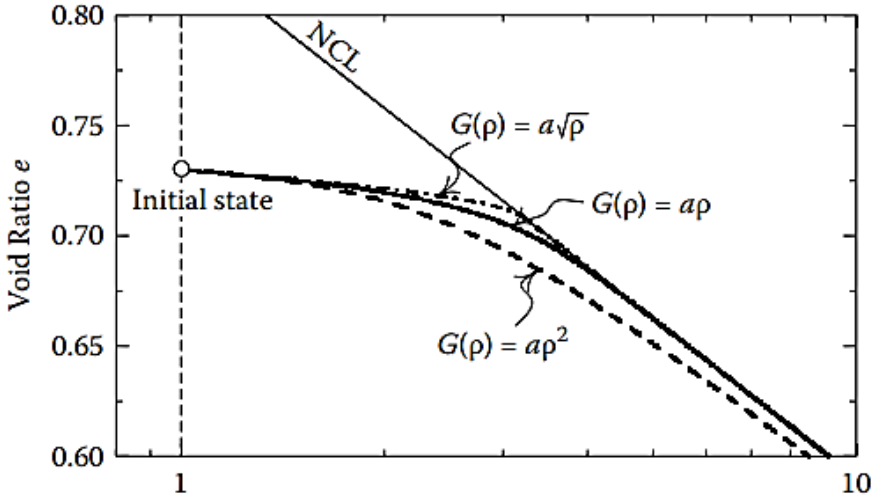

(b) Calculated e - logσrelation

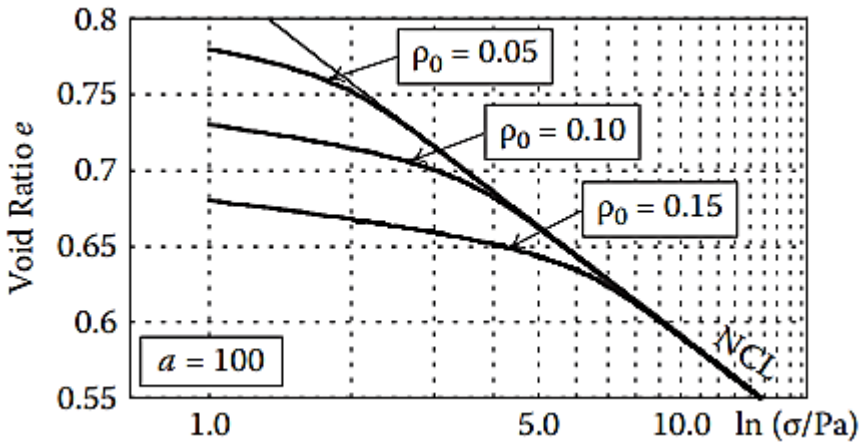

Figure 2.11 (a) and (b) effect of power of the variable ρ (c) effect of different values of ρ_0 (Nakai, 2013).

2.6.3 Modelling of Structured Soil

Usually naturally occurring sedimentary and residual soils have similar characteristics to those of porous weak rock due to bonded structure (e.g. Leroueil and Vaughan, 1990). The properties of reconstitute soil differ from the natural or intact condition because of soil structure, i.e. fabric and bonding (e.g. Mitchell, 1976; Burland, 1990). Figure 2.12 and Figure 2.13 show typical stress-strain behavior of structureless and structured soils due to 1-D compression and UU triaxial compression tests respectively.

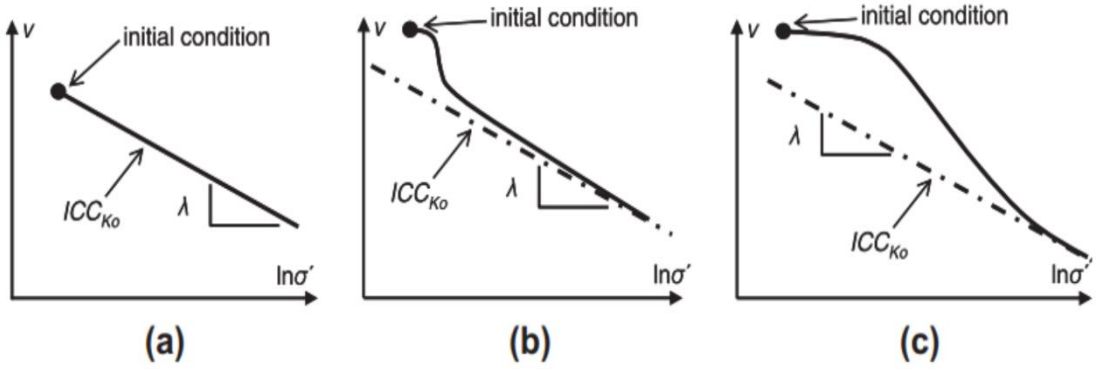

Figure 2.12 One dimensional compression: (a) structureless soil, (b) weakly structured soil with abrupt de-structuring and (c) strongly structured soil with gradual de-structuring (e.g. Belokas & Kavvadas, 2010).

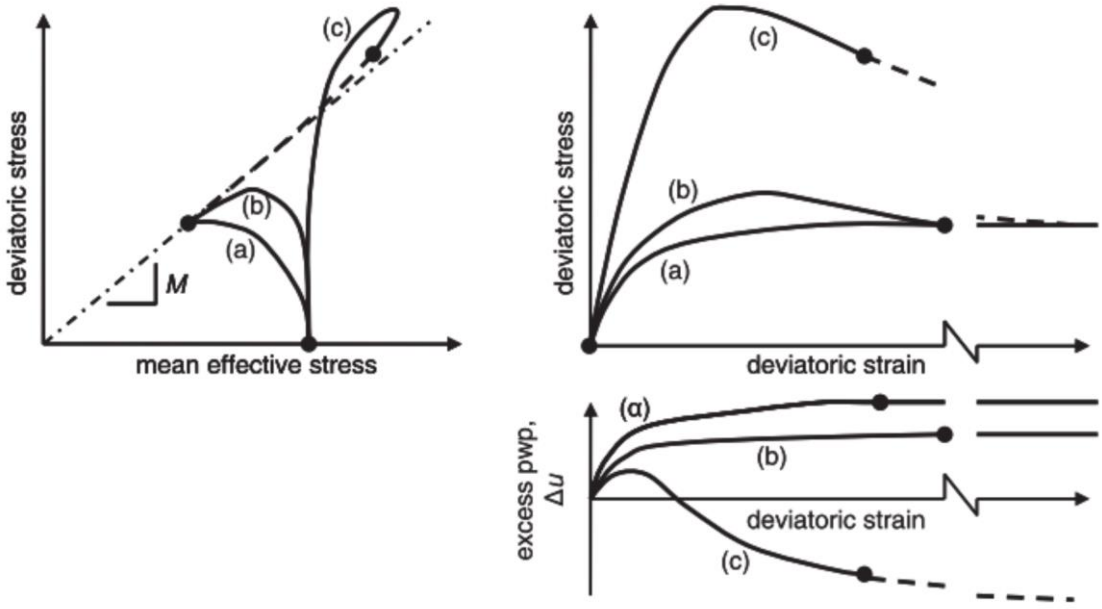

Figure 2.13 Typical stress-strain behavior of soil in undrained triaxial compression; ((a) structureless soil, (b) weakly structured soil and (c) strongly structured soil (e.g. Belokas & Kavvadas, 2010).

Structured soils show void ratio larger than that of structureless soil at a certain stress limit (as shown in Figure 2.14 from point J to point L) and yet the soil is stiffer due to natural bonding. Asaoka, Nakano, and Noda (2000a) and Asaoka (2003) developed a model to describe the behavior of structured soils by modifying the Cam-clay model. They introduced subloading and superloading surfaces and a factor related to the overconsolidation ratio introduced to increase the initial stiffness, and a factor related to the soil skeleton structure and to decrease the stiffness as the stress state approached the normally consolidated condition.

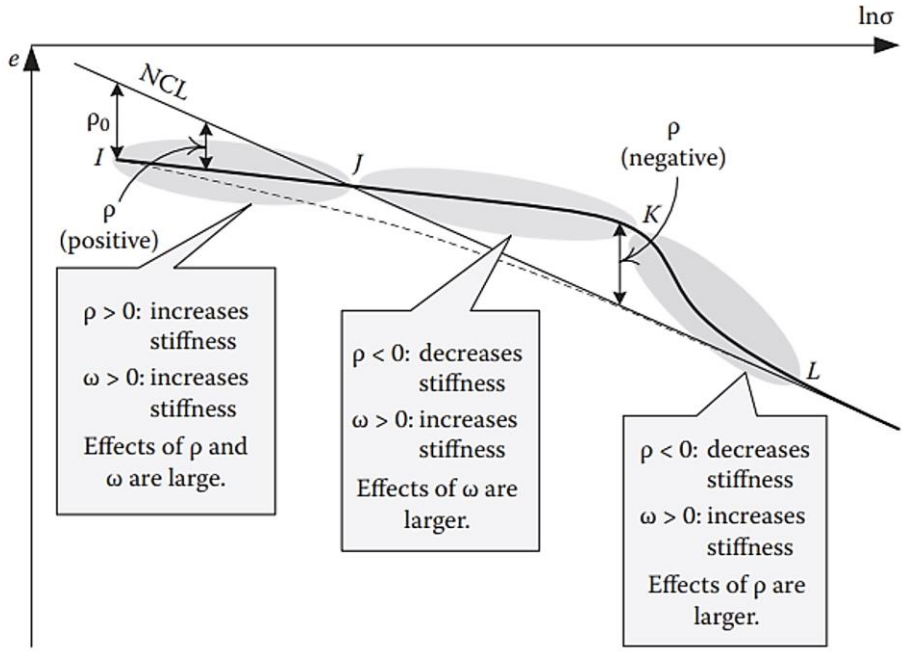

Figure 2.14 e-lnσ relationship of a structured clay showing its various zones (Nakai, 2013).

As shown in Figure 2.14, besides the density, a new factor ω is introduced to take the bonding effect into consideration. It shows the effects of factors ρ and ω on the shape of the e-ln σ curve. Figure 2.15 shows the magnified view of part of region I of Figure 2.14. The lower arrow in the broken line represents the similar change of void ratio as that for the overconsolidated unstructured soil. Now it can be understood that the structured soil is stiffer than a nonstructured overconsolidated soil, even if the initial state variable ρ_0 is the same. Then, the change in void ratio for the structured soil indicated by the arrow in

the solid line is smaller than that for a nonstructured overconsolidated soil (arrow in the broken line).

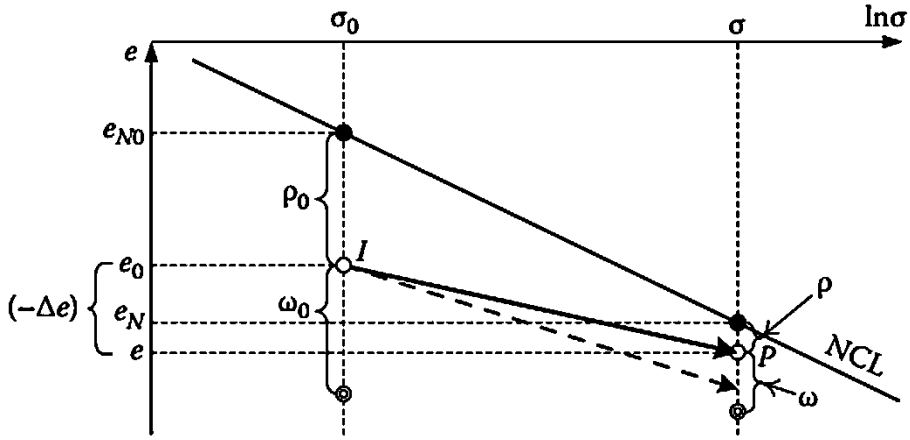

Figure 2.15 e-ln σ relationship of structured soil (Naka et al., 2011).

Figure 2.16 (a) shows that if the degradation of ω is faster, then the soil approaches to the broken line indicating NC condition, in the similar manner of an overconsolidated soil. For a slower degradation of ω, the solid line in Figure 2.16 (b) meets the broken line of NC condition before complete debonding and enter the region of ρ<0.

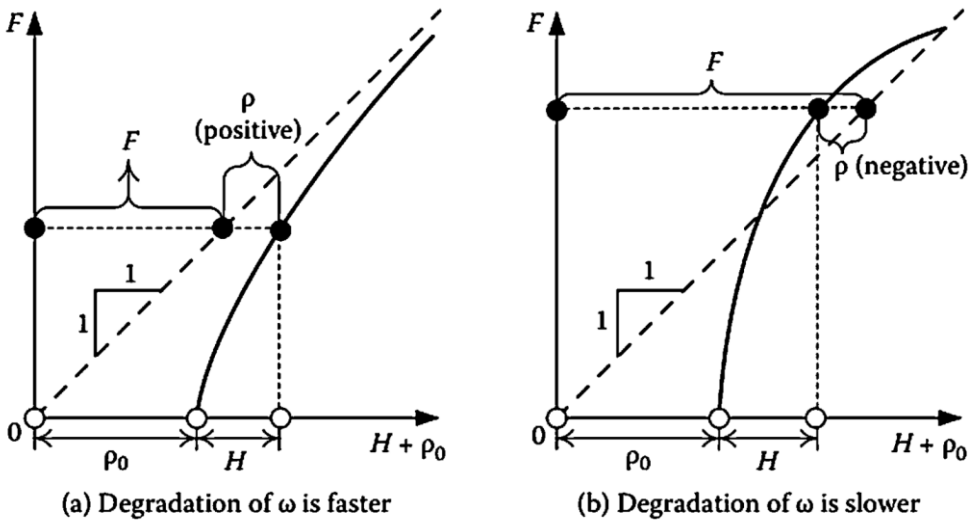

Figure 2.16 Evolution of F and H in an over consolidated soil (Nakai et al., 2011)

Introducing bonding variable ω in equation (2.20),

$$d\rho = -\{G(\rho) + Q(\omega)\}.d(-e)^p \tag{2.22}$$

Evolution of ω is as follows (Figure 2.17),

$$d\omega = -Q(\omega).d(-e)^p \tag{2.23}$$

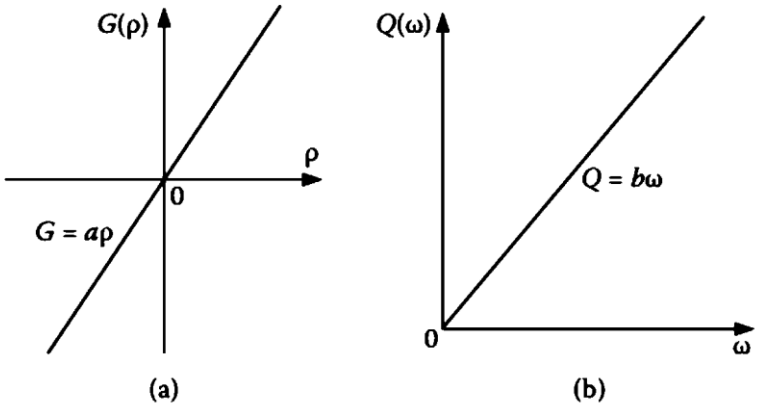

Figure 2.17 $G(\rho)$ *and* $Q(\omega)$ given by linear function ρ and ω respectively (Nakai et al., 2011).

The increment of total void ratio is expressed as follows,

$$d(-e) = d(-e)^p + d(-e)^e = \left\{\frac{(\lambda-\kappa)}{1+G(\rho)+Q(\omega)} + \kappa\right\}.\frac{d\sigma}{\sigma} \tag{2.24}$$

2.7 Outline of Cam-clay Model

The Cam-clay model (Schofield and Wroth 1968; Roscoe and Burland 1968) has been formulated using the mean principal stress (p) and the deviatoric stress (q), and the corresponding plastic strain increment invariants like the plastic volumetric strain (ε_v^p) and the plastic deviatoric strains (ε_d^p).

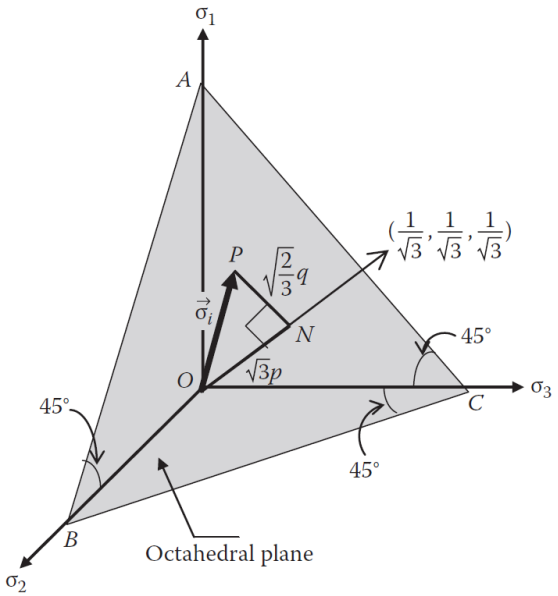

Figure 2.18 Definitions of p and q

Figure 2.18 shows the octahedral plane in principal stress space, where the current principal stress vector is represented by $\overline{\mathrm{OP}}$. Then, the mean stress p and the deviatoric stress q are defined by the normal and in-plane components of the stress with respect to the octahedral plane and by Eqs. (2.1) and (2.2) using three principal stresses – i.e., $\sigma_1, \sigma_2, \sigma_3$ or the stress-strain tensors – i.e., σ_{ij}, δ_{ij}.

$$p = \sqrt{\frac{1}{3}}\,\overline{\mathrm{OP}} = \frac{1}{3}\,(\sigma_1 + \sigma_2 + \sigma_3) = \frac{1}{3}\sigma_{ij}\delta_{ij} \tag{2.25}$$

$$q = \sqrt{\frac{2}{3}}\,\overline{\mathrm{NP}} = \frac{1}{\sqrt{2}}\,\sqrt{(\sigma_1 - \sigma_2)^2 + (\sigma_2 - \sigma_3)^2 + (\sigma_3 - \sigma_1)^2}$$

$$= \sqrt{\frac{3}{2}(\sigma_{ij} - p\delta_{ij})(\sigma_{ij} - p\delta_{ij})} \tag{2.26}$$

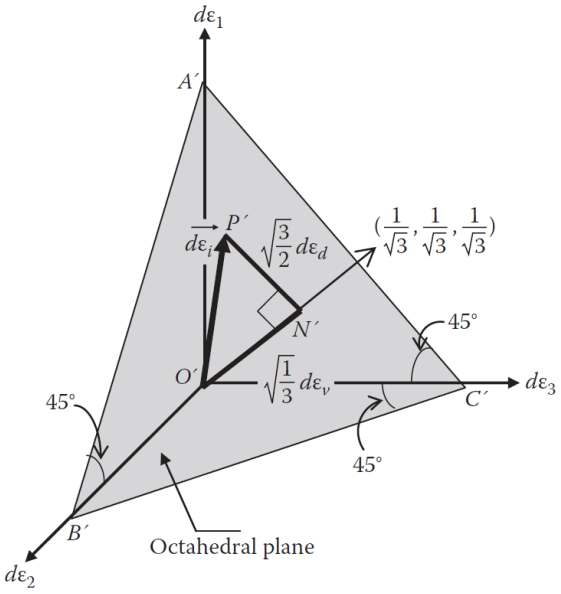

Figure 2.19 Definitions of $d\varepsilon_v$ and $d\varepsilon_d$.

Figure 2.19 shows the octahedral plane in principal strain space, where vector $\overline{\mathrm{O'N'}}$ represents the current principal strain. Then, volumetric strain increment $d\varepsilon_v$ and deviatoric strain increment $d\varepsilon_d$ are defined by the Eqs. (2.3) and (2.4).

$$d\varepsilon_v = \sqrt{3}\,\overline{\mathrm{O'N'}} = d\varepsilon_1 + d\varepsilon_2 + d\varepsilon_3 = d\varepsilon_{ij}\delta_{ij} \tag{2.27}$$

$$d\varepsilon_d = \sqrt{\frac{2}{3}(d\varepsilon_1 - d\varepsilon_2)^2 + (d\varepsilon_2 - d\varepsilon_3)^2 + d\varepsilon_3 - d\varepsilon_1)^2}$$

$$= \sqrt{\frac{2}{3}\left(d\varepsilon_{ij} - \frac{d\varepsilon_v}{3}\delta_{ij}\right)\left(d\varepsilon_{ij} - \frac{d\varepsilon_v}{3}\delta_{ij}\right)} \quad (2.28)$$

For a cylindrical shaped specimen under triaxial compression test condition, minor principal stress and intermediate principal stresses are equal .i.e., $\sigma_1 > \sigma_2 = \sigma_3$. Hence the stress and strain increment invariants are expressed as,

$$p = \frac{\sigma_1+\sigma_2+\sigma_3}{3} = \frac{\sigma_1+2\sigma_3}{3}, q = (\sigma_1 - \sigma_3) \quad (2.29)$$

$$d\varepsilon_v = d\varepsilon_1 + 2d\varepsilon_2,\ d\varepsilon_d = \frac{2}{3}(d\varepsilon_1 - d\varepsilon_3) \quad (2.30)$$

In case of triaxial tension, $\sigma_1 = \sigma_2 > \sigma_3$. Therefore, the stress and strain increment invariants are expressed as,

$$p = \frac{\sigma_1+\sigma_2+\sigma_3}{3} = \frac{2\sigma_1+\sigma_3}{3}, q = (\sigma_1 - \sigma_3) \quad (2.31)$$

$$d\varepsilon_v = 2d\varepsilon_1 + d\varepsilon_2,\ d\varepsilon_d = \frac{2}{3}(d\varepsilon_1 - d\varepsilon_3) \quad (2.32)$$

Similarly, the plastic volumetric strain (ε_v^p) and plastic deviatoric strain (ε_d^p) are also defined using the normal and in-plane components of the plastic strain with respect to the octahedral plane as follows,

$$\varepsilon_v^p = \varepsilon_1^p + \varepsilon_2^p + \varepsilon_3^p = \varepsilon_{ij}^p \delta_{ij} \quad (2.33)$$

$$\varepsilon_d^p = \frac{\sqrt{2}}{3}\sqrt{(\varepsilon_1^p - \varepsilon_2^p)^2 + (\varepsilon_2^p - \varepsilon_3^p)^2 + (\varepsilon_3^p - \varepsilon_1^p)^2}$$

$$= \sqrt{\frac{2}{3}\left(\varepsilon_{ij}{}^p - \frac{\varepsilon_v{}^p}{3}\delta_{ij}\right)\left(\varepsilon_{ij}{}^p - \frac{\varepsilon_v{}^p}{3}\delta_{ij}\right)} \quad (2.34)$$

Under triaxial compression (σ1 > σ2 = σ3), the expression of plastic strain invariants becomes,

$$\varepsilon_v^p = \varepsilon_1^p + 2\varepsilon_3^p,\ \varepsilon_d^p = \frac{2}{3}(\varepsilon_1^p - \varepsilon_3^p) \quad (2.35)$$

While in case of extension it becomes,

$$\varepsilon_v^p = 2\varepsilon_1^p + \varepsilon_3^p,\ \varepsilon_d^p = \frac{2}{3}(\varepsilon_1^p - \varepsilon_3^p) \tag{2.36}$$

The yield function for soils is fundamentally formulated using the mean principal stress, p and deviatoric stress, q and the plastic volumetric strain, ε_v^p and/or deviatoric strains, ε_d^p, i.e.,

$$f = F(p, q) - H(\varepsilon_v^p, \varepsilon_d^p) = 0$$

or

$$f = F(p, \eta = q/p) - H(\varepsilon_v^p, \varepsilon_d^p) = 0 \tag{2.37}$$

As the plastic deviatoric function, ε_d^p is not suitable for a hardening parameter as the elastic strain is independent of stress path. Rewriting the equation 2.37

$$f = F(p, \eta = q/p) - H(\varepsilon_v^p) = 0 \tag{2.38}$$

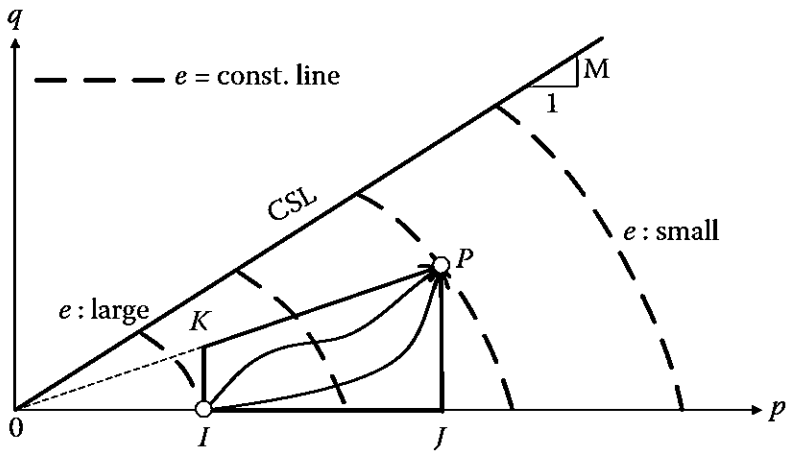

Figure 2.20 Explanation of equivoid ratio lines by Henkel (1960).

In order to construct a proper yield function for soils, the following two experimental findings are taken into consideration. One is the existence of the lines of equal void ratio in the q versus p space for normally consolidated clays as found by Henkel (1960) and shown by broken lines in Figure 2.20. Therefore, the change in void ratio ($-\Delta e$) of a normally consolidated clay is determined only by the initial and current stress states alone

and does not depend on the stress paths between the initial and current states (e.g., from point I to point P in Figure 2.20).

From another experiment, it is shown that for NC soils, the relation between stress ratio and deviatoric strain is independent of the mean principal stress as shown in Figure 2.4.

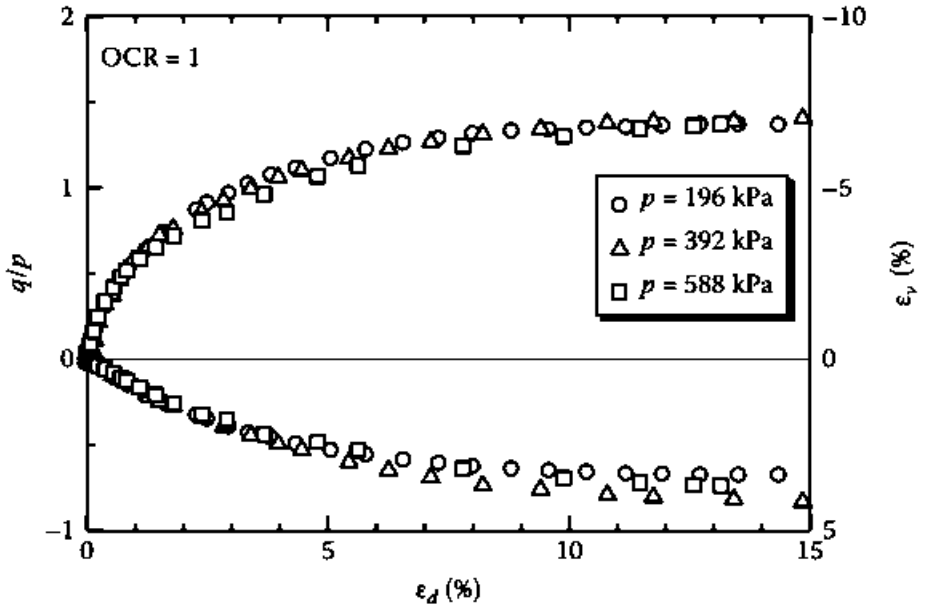

(a) Stress-strain relation

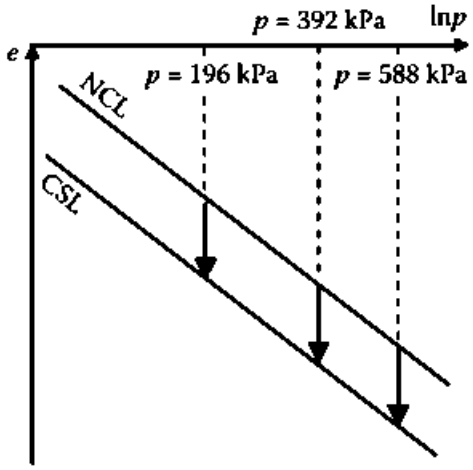

(b) Schematic diagram of e-lnp relation

Figure 2.21 (a) Triaxial compression test of a NC soil under different constant mean principal stresses (b) e-lnp relation of a normally consolidated soil (Nakai, 2013).

It is observed from Figure 2.20 and Figure 2.21 that the positive volumetric strain occurs with the increase of stress ratio and it reaches to the constant at the critical state of stress.

$$\varepsilon_v = \xi(\eta) \tag{2.39}$$

Where, $\xi(0) = 0$

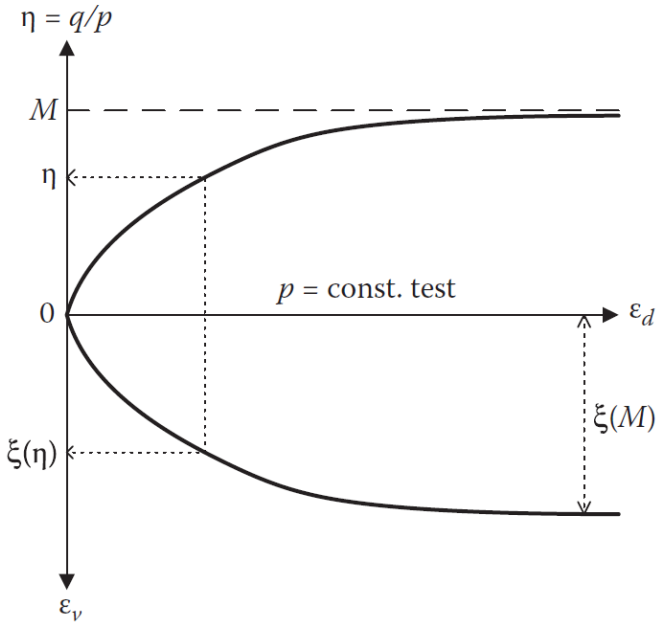

Figure 2.22 Stress ratio (η) versus deviatoric strain (ε_d) versus volumetric strain (ε_v) curves under constant mean principal stresses.

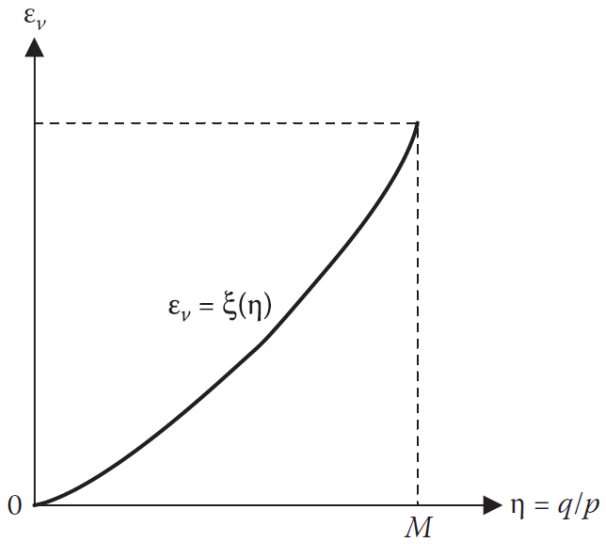

Figure 2.23 Relation between volumetric strain, ε_v and stress ratio, η for normally consolidated soils under constant mean principal stresses.

As shown in Figure 2.23, the volumetric strain under constant mean stress can be expressed as increasing function of ξ(η) in spite of the magnitude of the mean stress or in a linear form in terms of stress ratio,

$$\varepsilon_v = \xi(\eta) = D\eta, \tag{2.40}$$

Where, the coefficient D is called Shibata's dilatancy coefficient (Shibata, 1963).

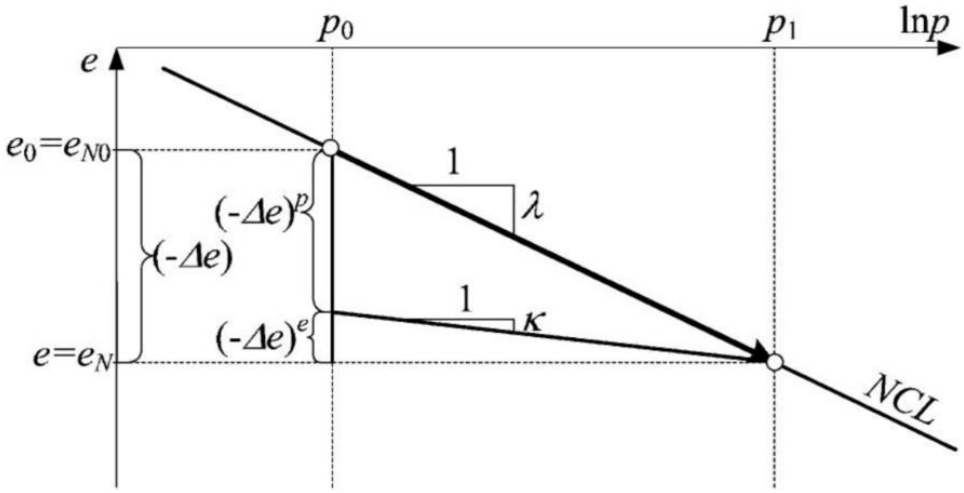

Figure 2.24 Relationship between void ratio and effective pressure in a normally consolidated (NC) soil.

In Figure 2.20, the path I to J represents the isotropic consolidation and the path J to P represents the pure shear. Then the total change in void ratio (-Δ*e*) occurred due to the state of stress that evolves from point I to point P is the summation of the change in void ratio along the path I to J and J to P. The total change of void ratio (-Δ*e*) can be derived as follows:

$$(-\Delta e) = e_0 - e = \lambda \ln \frac{p}{p_0} + (1 + e_0)\, \xi(\eta) \tag{2.41}$$

or

$$(-\Delta e) = e_0 - e = \lambda \ln \frac{p}{p_0} + (1 + e_0) D\eta \tag{2.42}$$

Here, the first part of the equation (2.42) comes from the isotropic compression shown in Figure 2.24, where λ is the compression index. The second part is due to the shear stress.

As explained in Figure 2.24, the elastic change in void ratio is expressed as follows:

$$(-\Delta e)^e = \kappa \ln \frac{p}{p_0} \tag{2.43}$$

Hence, the plastic change in the void ratio becomes,

$$(-\Delta e)^p = (-\Delta e) - (-\Delta e)^e = (\lambda - \kappa) \ln \frac{p}{p_0} + (1 + e_0)\xi(\eta) \tag{2.44}$$

The yield function is then expressed as,

$$f = F(p, \eta = q/p) - H((-\Delta e)^p) = 0 \tag{2.45}$$

Where,

$$F = (\lambda - \kappa) \ln \frac{p}{p_0} + \zeta(\eta) \tag{2.46}$$

$$H = (-\Delta e)^p = (1 + e_0)\varepsilon_v^p \tag{2.47}$$

Here, $\zeta(\eta) = \{(1 + e_0)/(\lambda - \kappa)\}\xi(\eta)$ is a function of η that satisfies $\zeta(\eta) = 0$.

If a NC soil is consolidated isotropically from $p=p_o$ to $p=p_1$, the void ratio changes from e_{N0} to e_N as shown in Figure 2.24. Plastic change of the void ratio is then expressed as,

$$(-\Delta e)^p = (-\Delta e) - (-\Delta e)^e = (\lambda - \kappa) \ln \frac{p_1}{p_0} \tag{2.48}$$

Rewriting the equation 2.42,

$$(\lambda - \kappa) \ln \frac{p}{p_0} + \zeta(\eta) - (\lambda - \kappa) \ln \frac{p_1}{p_0} = 0$$

Or

$$(\lambda - \kappa) \ln p + \zeta(\eta) - (\lambda - \kappa) \ln p_1 = 0 \tag{2.49}$$

The stress ratio function $\zeta(\eta)$ in Cam-clay model (Schofield and Wroth, 1968) and the modified Cam-clay model (Roscoe and Burland, 1968) are given as below.

Original:

$$\zeta(\eta) = \frac{1}{\mathrm{M}} \eta \tag{2.50}$$

Modified:

$$\zeta(\eta) = \frac{M^2+\eta^2}{M^2}\,\eta \tag{2.51}$$

Here, M is the stress ratio, η at critical state as shown in Figure 2.21. Figure 2.25 shows the initial and current yield surface with the direction of plastic flow in the Cam-clay model. The shape of the yield surface of Cam-clay and modified Cam-clay model is shown in the in Figure 2.26 (a) and 2.26 (b), respectively.

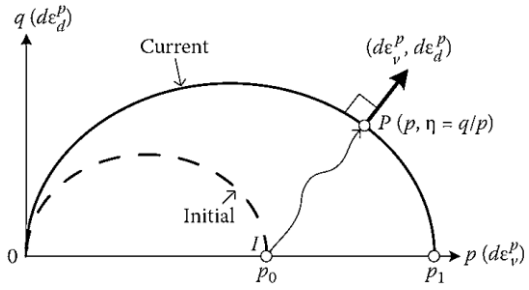

Figure 2.25 Initial and current yield surface in the p-q plane and direction of plastic flow in the Cam-clay model (Nakai, 2013).

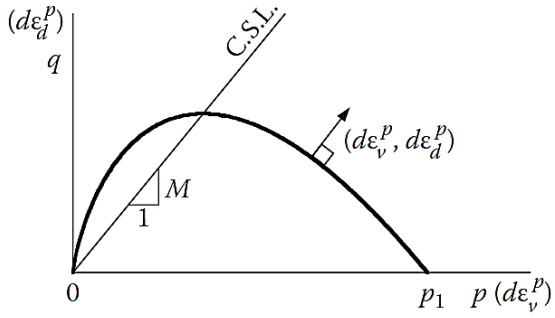

(a) Original

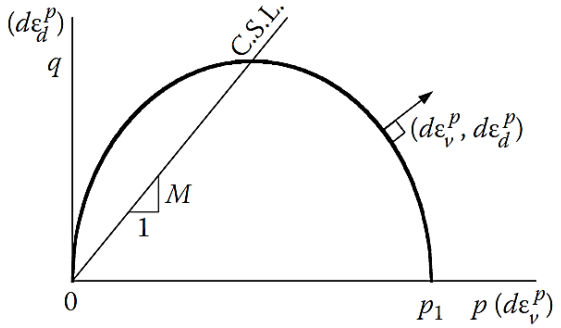

(b) Modified

Figure 2.26 Shape of Yield surface of Cam-clay model on *p-q* plane (Nakai, 2013).

The plastic strain increment assuming associated flow rule then can be expressed as follows (Nakai et al., 2011):

$$\frac{d\varepsilon_v^p}{d\varepsilon_d^p} = \frac{\frac{\partial F}{\partial p}+\frac{\partial F}{\partial \eta}\frac{\partial \eta}{\partial p}}{\frac{\partial F}{\partial \eta}\frac{\partial \eta}{\partial qq}} = \frac{1-\zeta'(\eta).\eta}{\zeta\prime(\eta)} \tag{2.52}$$

Where, $\zeta'(\eta)$ means $d\zeta(\eta)/d\eta$.

The stress-dilatancy relation can be derived as follows:

Original Cam-clay Model:

$$\frac{d\varepsilon_v^p}{d\varepsilon_d^p} = \mathrm{M} - \eta \tag{2.53}$$

Figure 2.27 shows the linear stress-dilatancy relationship derived from equation (2.53).

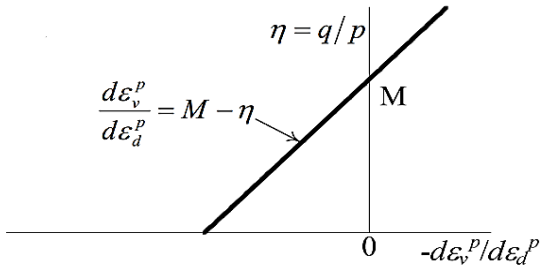

Figure 2.27 Stress-dilatancy relation of Original Cam-clay model (Nakai, 2013).

Modified Cam-clay Model:

$$\frac{d\varepsilon_v^p}{d\varepsilon_d^p} = \frac{\mathrm{M}^2-\eta^2}{2\eta} \tag{2.54}$$

Figure 2.28 shows the linear stress-dilatancy relationship of modified Cam-clay model.

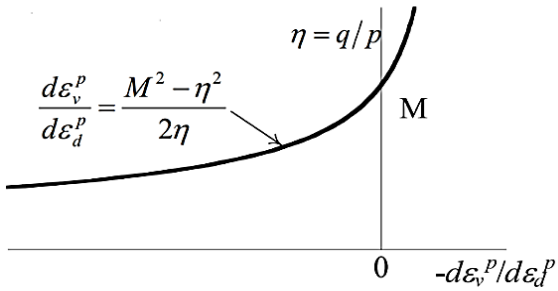

Figure 2.28 Stress-dilatancy relation of modified Cam-clay model (Nakai, 2013).

Table 2.1 Comparison between the original and modified Cam-clay model (Hicher and Shaao 2002)

Cam-Clay model	Original version	Modified form
Stress-dilatancy rule	$\frac{d\varepsilon_v^p}{d\varepsilon_d^p} = M - \frac{q}{p}$	$\frac{d\varepsilon_v^p}{d\varepsilon_d^p} = \frac{M^2 - \left(\frac{q}{p}\right)^2}{2\frac{q}{p}}$
Yield surface	$\frac{q}{Mp} - \ln\left(\frac{p_c}{p}\right) = 0$	$\frac{q^2}{M^2p^2} + 1 - \frac{p_c}{p} = 0$
Non-linear elastic law	$d\varepsilon_v^e = \frac{\kappa}{1+e_o}\frac{dp}{p}$ $d\varepsilon_q^e = 0$	$d\varepsilon_v^e = \frac{\kappa}{1+e_o}\frac{dp}{p}$ $d\varepsilon_q^e = \frac{1}{3G}dq$

2.8 Applicability of Cam-clay Model

The Cam-clay predicts an unrealistically long elastic range when subjected to highly over-consolidated soils, which leads to a wrong peak strength and also initial stiffness. Therefore, the Cam-clay model is not very suitable for the over-consolidated soils (Brinkgreve, 2005).

From Figure 2.29, it is observed that there is no unique stress-stain relation that can be obtained for Fujinomori clay when subjected to extension and compression loading during a triaxial test.

Figure 2.30 and Figure 2.31 show the stress-dilatancy plots for Fujinomori (Nakai et al., 2013) clay and Dhaka clay (Rahman, Shahin and Nakai, 2018). It is observed that there is no unique stress-dilatancy relation at compression and extension.

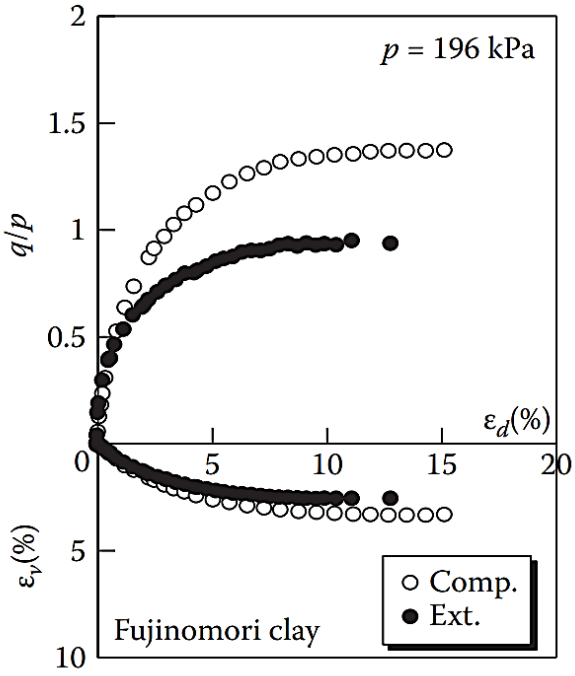

Figure 2.29 Observed stress-starin relation of a NC Fujinomori clay under extension and compression (Nakai 2013).

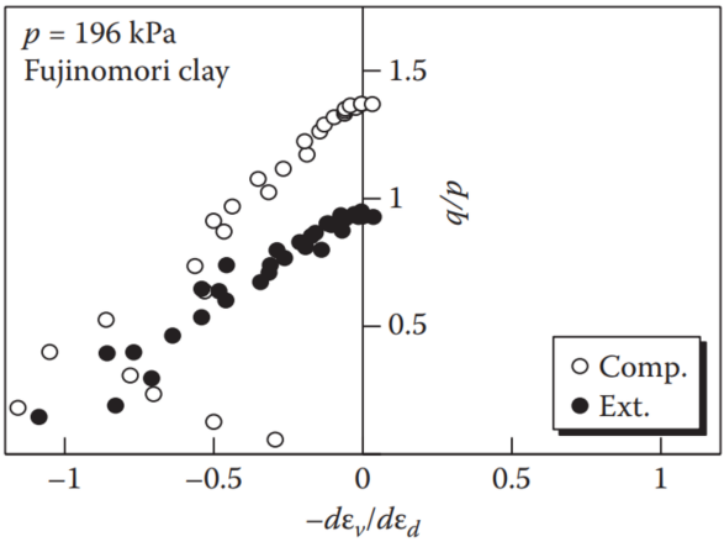

Figure 2.30 Observed stress-dilatancy relation of a NC Fujinomori clay under extension and compression (Nakai et al 2013).

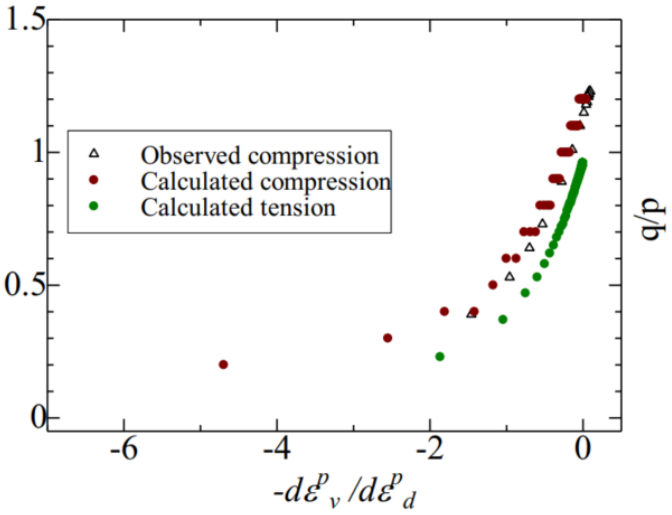

Figure 2.31 Stress-dilatancy relation of a NC Dhaka clay under extension and compression (Rahman et al. 2018).

2.9 Modeling of Soil Behavior Based on the t_{ij} Concept

2.9.1 Definition of stress and strain invariants

To take into account the influence of intermediate principal stress, Nakai and Mihara (1984) developed a model by introducing the modified stress tensor t_{ij}. The sides AB, AC and BC in Figure 2.32 is the plane where shear-normal stress ratio is maximum between two corresponding principal stresses as shown in Figure 2.33. Moreover, the plane AB at which the shear normal stress ratio is maximized is called the 'plane of maximum mobilization' and all the three sides AB, AC, BC together is called 'compound mobilized plane' (Matsuka, 1974).

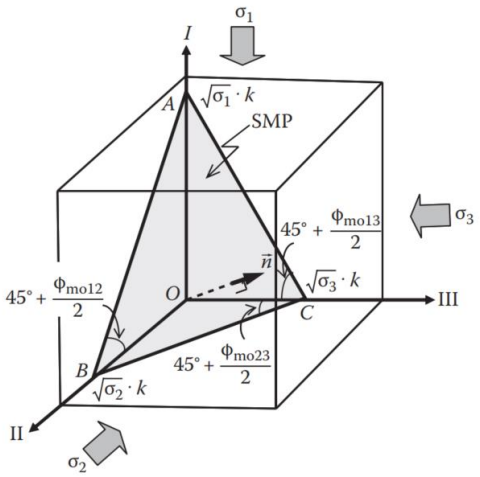

Figure 2.32 Spatially mobilized plane the three-dimensional space (Nakai, 2013).

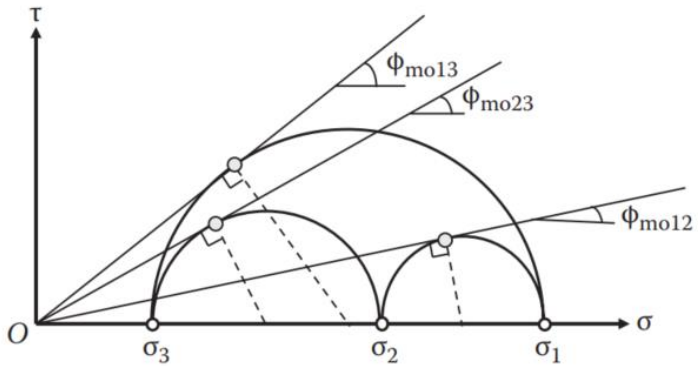

Figure 2.33 Plane of maximum mobilization at different principal stresses (Nakai, 2013).

From the Figure 2.33, corresponding principal stress ratio can be expressed as follows,

$$\tan 45^\circ + \frac{\Phi_{moij}}{2} = \sqrt{\frac{1+sin\Phi_{moij}}{1-sin\Phi_{moij}}} = \sqrt{\frac{\sigma_i}{\sigma_j}} \qquad (i, j = 1,2,3;\ i < j) \qquad (2.55)$$

The direction cosines are expressed as follows (Nakai, 1989):

$$a_1 = \sqrt{\frac{I_3}{I_2\sigma_1}}, a_2 = \sqrt{\frac{I_3}{I_2\sigma_2}},\ a_3 = \sqrt{\frac{I_3}{I_2\sigma_3}}, \qquad (i, j = 1,2,3;\ i < j) \qquad (2.56)$$

$$a_{ij} = \sqrt{\frac{I_3}{I_2}}.r_{ij}^{-1} = \sqrt{\frac{I_3}{I_2}}.\left(\sigma_{ij} + I_{r2}\delta_{ik}\right)\left(I_{r1}\sigma_{kj} + I_{r3}\delta_{kj}\right)^{-1} \qquad (2.57)$$

Where,

δ_{ij} is the unit tensor

I_1, I_2, I_3 are the first, second and third invariants of σ_{ij}

I_{r1}, I_{r2}, I_{r2} are the first, second and third invariants of r_{ij} , which is the square root of the stress tensor or $r_{ik}r_{kj} = \sigma_{ij}$

The expression of the stress invariants are expressed as follows,

$$I_1 = \sigma_1 + \sigma_2 + \sigma_3 = \sigma_{ii}$$

$$I_2 = \sigma_1\sigma_2 + \sigma_2\sigma_3 + \sigma_3\sigma_1 = \frac{1}{2}\{(\sigma_{ii})^2 - \sigma_{ij}\sigma_{ji}\}$$

$$I_3 = \sigma_1\sigma_2\sigma_3 = \frac{1}{6}e_{ijk}e_{lmn}\sigma_{il}\sigma_{jm}\sigma_{kn} \qquad (2.58)$$

$$I_{r1} = \sqrt{\sigma_1} + \sqrt{\sigma_2} + \sqrt{\sigma_3} = r_{ii}$$

$$I_{r2} = \sqrt{\sigma_1\sigma_2} + \sqrt{\sigma_2\sigma_3} + \sqrt{\sigma_3\sigma_1} = \frac{1}{2}\{(r_{ii})^2 - r_{ii}r_{ii}\}$$

$$I_{r3} = \sqrt{\sigma_1\sigma_2\sigma_3} = \sqrt{\frac{1}{6}e_{ijk}e_{lmn}r_{il}r_{jm}r_{kn}} \tag{2.59}$$

The modified stress tensor t_{ij} is then defined by the product of a_{ik} and σ_{kj} and can be expressed as:

$$t_{ij} = a_{ik}\sigma_{kj} \tag{2.60}$$

Principal values as shown in Figure 2.34 are expressed as follows:

$$t_1 = a_1\sigma_1, t_2 = a_2\sigma_2, t_3 = a_3\sigma_3 = 3\frac{I_3}{I_2} = \sigma_{SMP} \tag{2.61}$$

The stress invariants, t_N, t_S, and strain increment invariants $d\varepsilon_N^*, d\varepsilon_S^*$ as shown in Figure 2.35 are expressed as follows:

$$t_N = t_1a_1 + t_2a_2 + t_3a_3 = t_{ij}a_{ij} \tag{2.62}$$

$$t_S = \sqrt{(t_1a_2 - t_2a_1)^2 + (t_2a_3 - t_3a_2)^2 + (t_3a_1 - t_1a_3)^2} = \sqrt{t_{ij}t_{ij} - \left(t_{ij}a_{ij}\right)^2}$$

$$=3\frac{\sqrt{I_1I_2I_3 - 9I_3^2}}{I_2} = \tau_{SMP} \tag{2.63}$$

$$d\varepsilon_N^* = d\varepsilon_1a_1 + d\varepsilon_2a_2 + d\varepsilon_3a_3 = d\varepsilon_{ij}a_{ij} \tag{2.64}$$

$$d\varepsilon_S^* = \sqrt{(d\varepsilon_1a_2 - d\varepsilon_2a_1)^2 + (d\varepsilon_2a_3 - d\varepsilon_3a_2)^2 + (d\varepsilon_3a_1 - d\varepsilon_1a_3)^2}$$

$$= \sqrt{d\varepsilon_{ij}d\varepsilon_{ij} - \left(d\varepsilon_{ij}a_{ij}\right)^2} \tag{2.65}$$

Stress ratio, X is expressed as follows

$$X = \frac{t_S}{t_N} = \frac{2}{3}\sqrt{\frac{(\sigma_1-\sigma_2)^2}{4\sigma_1\sigma_2} + \frac{(\sigma_2-\sigma_3)^2}{4\sigma_2\sigma_3} + \frac{(\sigma_3-\sigma_1)^2}{4\sigma_3\sigma_1}} = \sqrt{\frac{I_1I_2}{9I_3} - 1} \tag{2.66}$$

When X is constant, following criterion is established:

$$\frac{I_1 I_2}{9I_3} = constant \tag{2.67}$$

This is called Matsuoka-Nakai criterion or the SMP criterion (Matsuoka and Nakai 1974). Figure 2.36 shows the shape of Matsuoka-Nakai SMP criterion compared with the shape of von Mises criterion and Mohr-Coulomb criterion on the octahedral plane in three principal stresses space. The comparison between the ordinary concept and t_{ij} concept is listed in Table 2.2.

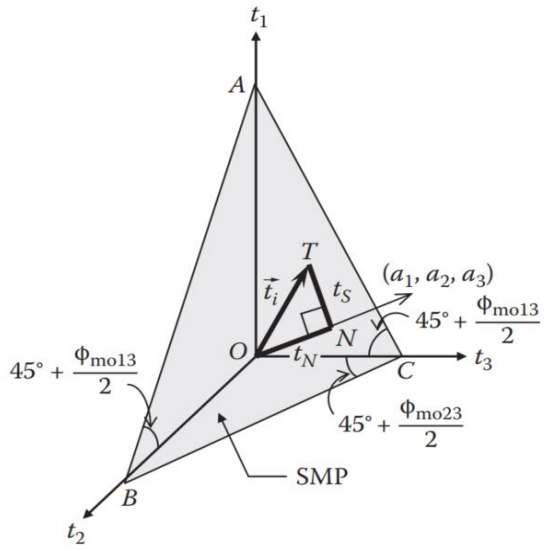

Figure 2.34 Definitions of t_N and t_S (Nakai, 2013).

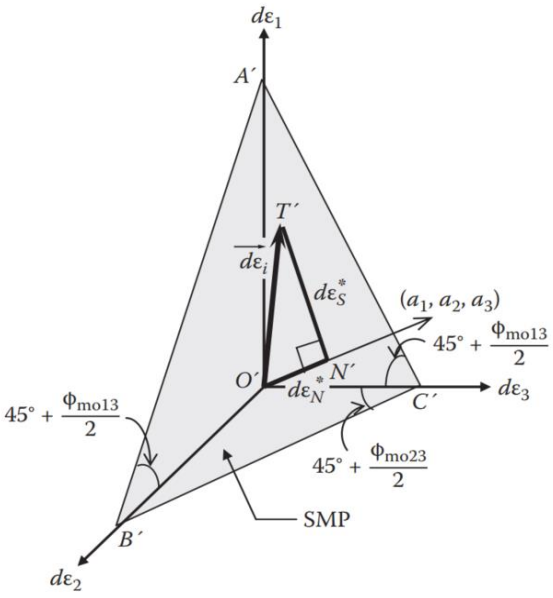

Figure 2.35 Definitions of $d\varepsilon_N^*$ *and* $d\varepsilon_S^*$ (Nakai, 2013).

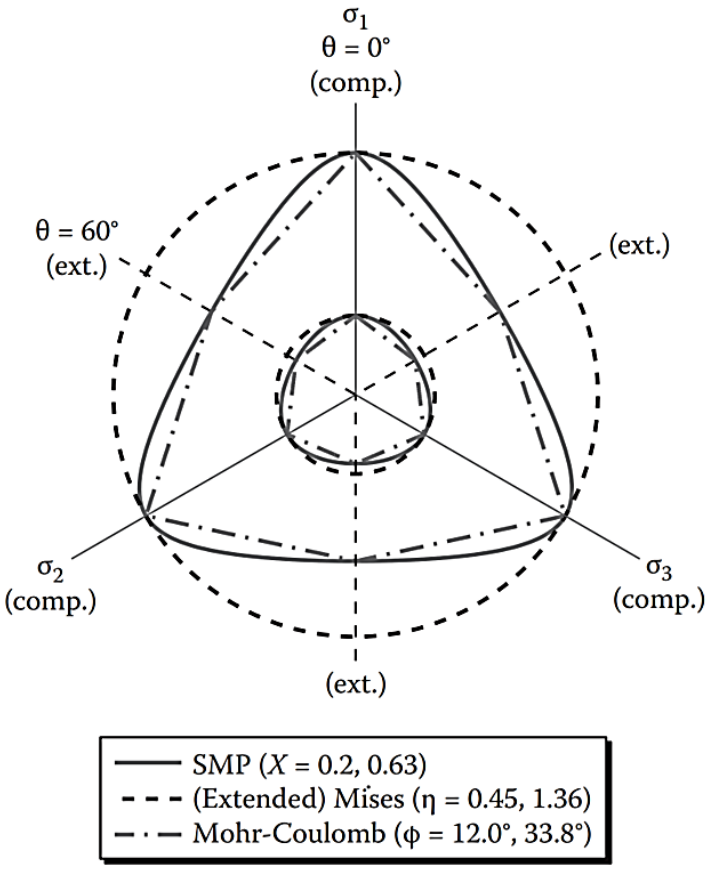

Figure 2.36 Definitions of $d\varepsilon_N^*, d\varepsilon_S^*$ (Nakai, 2013). Shape of Matsuoka–Nakai SMP criterion, (extended) von Mises criterion, and Mohr–Coulomb criterion on the octahedral plane in three principal stresses space. (a) Stress quantities used in the ordinary concept; (b) stress quantities used in the t_{ij} concept.

Table 2.2 Comparison between tensors and scalars related to stress and strain in the ordinary concept and the t_{ij} concept.

Tensor	Ordinary concept	t_{ij} concept
Tensor normal to reference plane	δ_{ij} (unit tensor)	a_{ij} (tensor normal to SMP)
Stress tensor	σ_{ij}	t_{ij}
Mean stress	$p = \sigma_{ij}\,\delta_{ij}/3$	$t_N = t_{ij}a_{ij}$
Deviatoric stress tensor	$s_{ij} = \sigma_{ij} - p\delta_{ij}$	$t'_{ij} = t_{ij} - t_N a_{ij}$
Deviatoric stress	$\sqrt{(3/2)s_{ij}s_{ij}}$	$\sqrt{t_{ij}t_{ij}}$
Stress ratio tensor	$\eta_{ij} = s_{ij}/p$	$x_{ij} = t'_{ij}/t_N$
Stress ratio	$\eta = q/p$	$X = t_s/t_N$
Strain increment normal to reference plane	$d\varepsilon_v = d\varepsilon_{ij}\delta_{ij}$	$d\varepsilon^*_N = d\varepsilon_{ij}a_{ij}$

Deviatoric strain increment tensor Strain increment parallel to reference plane	$de_{ij} = d\varepsilon_{ij} - d\varepsilon_v \delta_{ij}/3$ $de_{ij} = \sqrt{(2/3) de_{ij} de_{ij}}$	$d\varepsilon'_{ij} = d\varepsilon_{ij} - d\varepsilon^*_N a_{ij}$ $d\varepsilon^*_{ij} = \sqrt{d\varepsilon_{ij}\varepsilon_{ij}}$

2.9.2 Modelling of Normally Consolidated Soil

In the subloading t_{ij} model (Nakai and Hinoko, 2004) yield function can be achieved simply by replacing p and q in the Eqs. (2.42), (2.43) and (2.44). Expression is as follows:

$$f = F - H = 0 \tag{2.68}$$

$$F = (\lambda - \kappa) ln \frac{t_{N1}}{t_{N0}} = (\lambda - \kappa) \left\{ ln \frac{t_N}{t_{N0}} + \zeta(X) \right\} \tag{2.69}$$

$$H = (-\Delta e)^p = (1 + e_0)\varepsilon_v^p$$

The stress ratio function $\zeta(X)$ is then given by the equation below (Chowdhury and Nakai, 1998; Nakai and Hinokio, 2004):

$$\zeta(\mathrm{X}) = \frac{1}{\beta} \left(\frac{X}{\mathrm{M}^*}\right)^{\beta} \tag{2.70}$$

Where β (≥1) is the parameter which controls the shape function. Figure 2.37 shows the shape of yield surface in the t_N–t_S plane and direction of plastic flow for the model based on the t_{ij} concept.

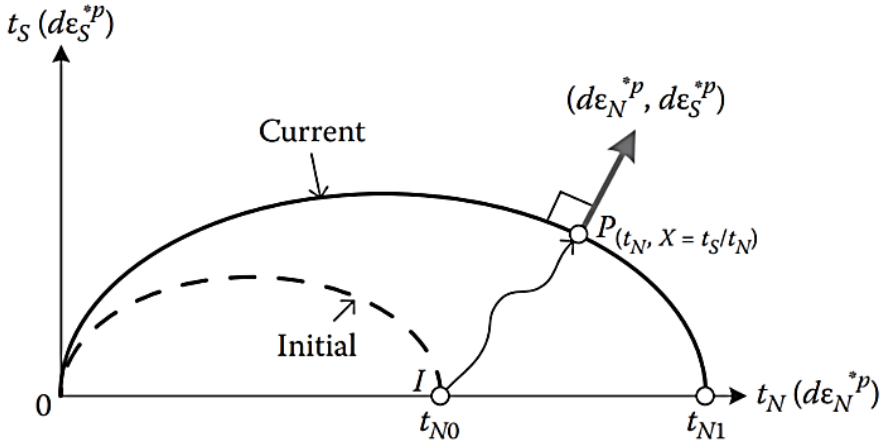

Figure 2.37 Initial and current yield surfaces in the t_N–t_S plane and direction of plastic flow for the model based on the t_{ij} concept (Nakai et al., 2011).

The plastic strain increment assuming associated flow rule is expressed as following:

$$d\varepsilon_{ij}^{p} = \frac{dF}{(1+e_0)\frac{\partial F}{\partial t_{kk}}} \left(\frac{\partial F}{\partial t_N}\frac{\partial t_N}{\partial t_{ij}} + \frac{\partial F}{\partial X}\frac{\partial X}{\partial t_{ij}}\right) \tag{2.71}$$

The elastic strain increment can be expressed as follows:

$$d\varepsilon_{ij}^{e} = \frac{1+v_e}{E_e}\ d\left(\frac{\sigma_{ij}}{1+X^2}\right) - \frac{v_e}{E_e} d\left(\frac{\sigma_{kk}}{1+X^2}\right)\delta_{ij} \tag{2.72}$$

Here,

$$t_N = \frac{p}{1+X^2} \tag{2.73}$$

$$E_e = \frac{3(1-2v_e)(1+e_0)t_N}{\kappa} \tag{2.74}$$

The stress-dilatancy relation as shown in Figure 2.38 can be expressed as,

$$\frac{d\varepsilon_N^{*p}}{d\varepsilon_S^{*p}} = \frac{1-\zeta'(X).X}{\zeta\prime(X)} = \frac{(\mathrm{M}^*)^{\beta}-X^{\beta}}{X^{\beta-1}} \tag{2.75}$$

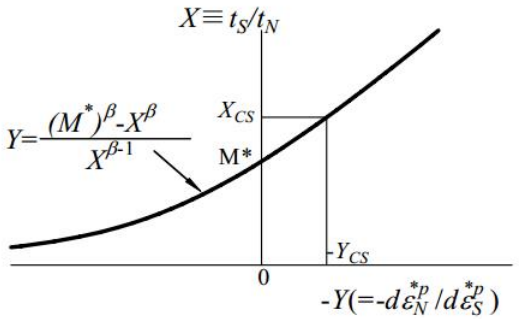

Figure 2.38 Stress-dilatancy relation of subloading t_{ij} model (Nakai et al., 2013).

Here, M^* expressed using X_{CS} and Y_{CS}, which are the stress ratio X and Y at critical state ($d\varepsilon_v^p = 0$).

$$\mathrm{M}^* = (X_{CS}{}^{\beta} + X_{CS}{}^{\beta-1}Y_{CS})^{1/\beta} \tag{2.76}$$

Xcs and Ycs are expressed as follows (e.g., Nakai and Mihara, 1984):

$$X_{CS} = \frac{\sqrt{2}}{3}\left(\sqrt{R_{CS}} - \frac{1}{\sqrt{R_{CS}}}\right) \tag{2.77}$$

$$Y_{CS} = \left(\frac{1-\sqrt{R_{CS}}}{\sqrt{2}(\sqrt{R_{CS}}+0.5)}\right) \quad (2.78)$$

Where, R_{CS} is the critical stress ratio and expressed as follows:

$$R_{CS} = \left(\frac{\sigma_1}{\sigma_3}\right)_{CS(comp)} \quad (2.79)$$

Figure 2.39 and Figure 2.40 show observed stress-dilatancy relation of normally consolidated Fujinomori clay and Dhaka clay based on subloading t_{ij} model. It is observed that there is a unique stress-dilatancy relation is established under drained compression and extension condition.

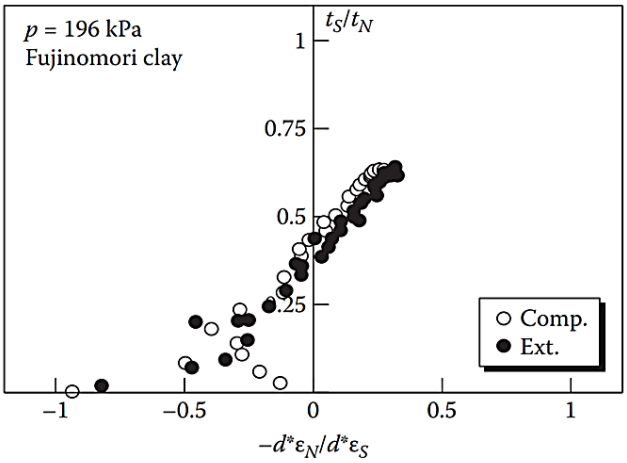

Figure 2.39 Observed stress-dilatancy relation of drained triaxial compression and extension test on Fujinomori clay (Nakai et al., 2011).

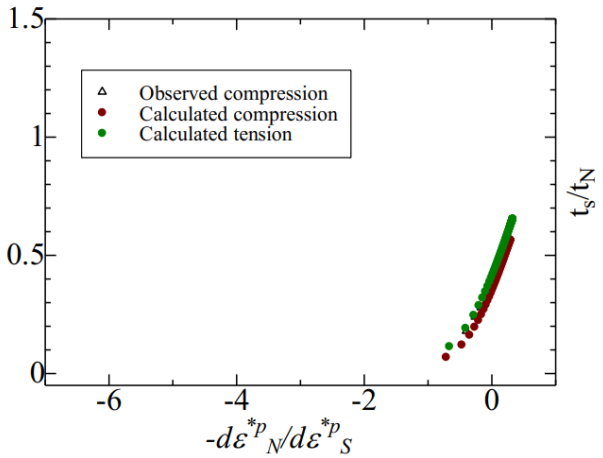

Figure 2.40 Stress-starin relation of a NC Dhaka clay under extension and compression (Rahman et al., 2018).

2.9.3 Modelling of Over-consolidated Soil

As discussed in section 2.6.2, various expressions based on Subloading t_{ij} model are as follows:

Plastic change of void ratio:

$$(-\Delta e)^p = (\lambda - \kappa) \ln \frac{t_{N1}}{t_{N0}} - (\rho_0 - \rho) \tag{2.80}$$

Yield Function:

$$f = F - \{H + (\rho_0 - \rho)\} = 0 \tag{2.81}$$

From consistency condition (*df=0*) and the flow rule,

$$df = dF - \{dH - d\rho\} = dF - \{d(-e)^p - d\rho\}$$

$$= dF - \left\{(1 + e_0)\Lambda \frac{\partial F}{\partial t_{ij}} - d\rho\right\} = 0 \tag{2.82}$$

Evolution rule of the density variable, ρ is expressed as follows:

$$d\rho = -(1 + e_0) \frac{G(\rho)}{t_N} \Lambda \tag{2.83}$$

Where,

$$G(\rho) = sign(\rho).a\rho^2 \tag{2.84}$$

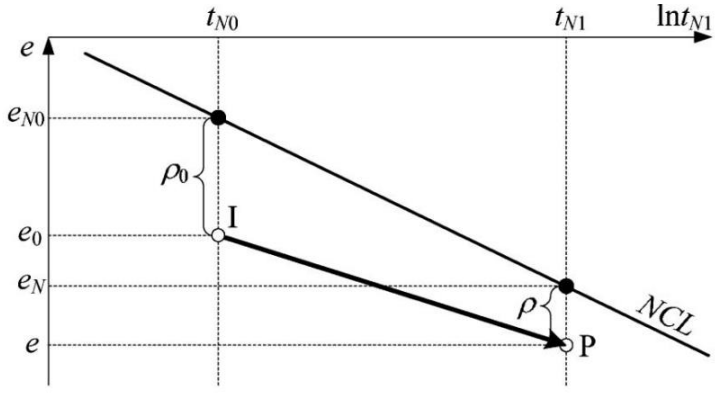

Figure 2.41 $e - lnt_N$ relation of an OC soil (Nakai, 2013).

2.9.4 Modelling of Structured Soil

As discussed in Section 2.6.3, the behavior of structured soil depends on density as well as effect of bonding. The evolution rule of ρ is expressed as follows:

$$d\rho = -(1+e_0)\left\{\frac{G(\rho)}{t_N} + \frac{Q(\omega)}{t_N}\right\}\Lambda \tag{2.85}$$

$$d\omega = -(1+e_0)\frac{Q(\omega)}{t_N}\Lambda \tag{2.86}$$

Where,

$$Q(\omega) = b\omega \tag{2.87}$$

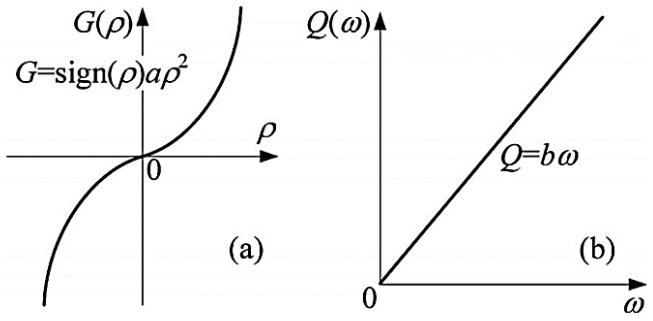

Figure 2.42 Function $G(\rho)$ and $Q(\omega)$ for evolution rule of ρ (Nakai, 2013).

2.10 Other Constitutive Models and Their Features

In the following Sub-section various features of well-known constitutive models are discussed briefly. Some of the constitutive models with their attributes and capabilities are listed in Table 2.3.

2.10.1 The Mohr-Coulomb model (MC)

As shown in Figure 2.43, the Mohr-Coulomb is an elastic-perfectly plastic model formulated combining the Hook's law of elasticity and Coulomb's failure criterion (Brinkgreve, 2005). Figure 2.44 shows that the real soil behavior cannot be captured by this model providing inaccurate stiffness. However, this model adopt the non-associated flow rule and can be applicable to the granular soil like sand with reasonable accuracy. To overcome the limitations, Elastic-hardening plastic Mohr-Coulomb model, Mohr-Coulomb model with stress dependent on state variable, Kinematic hardening Mohr – Coulomb have been developed (Wood & Gajo, 2005). The Mohr-Coulomb model is being used by several FEM program because of its simplicity in determining the model parameters.

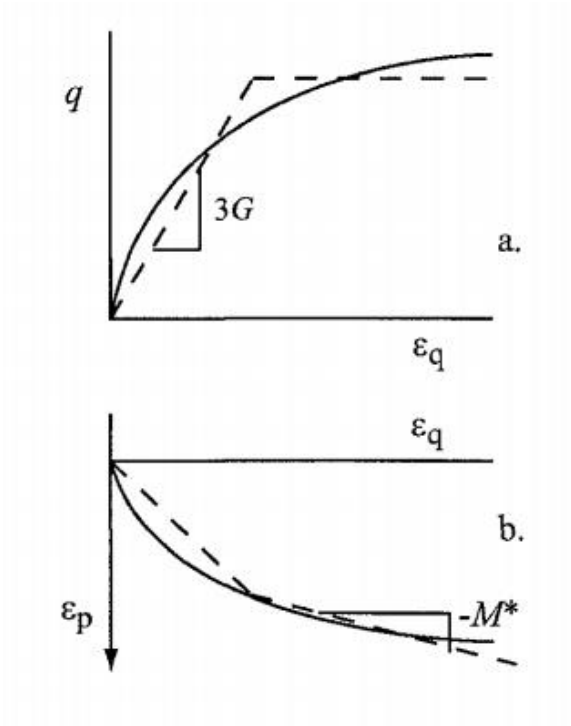

Figure 2.43 Elastic-perfectly plastic Mohr-Coulomb model compared with typical soil under drained triaxial compression test (Wood & Gajo, 2005).

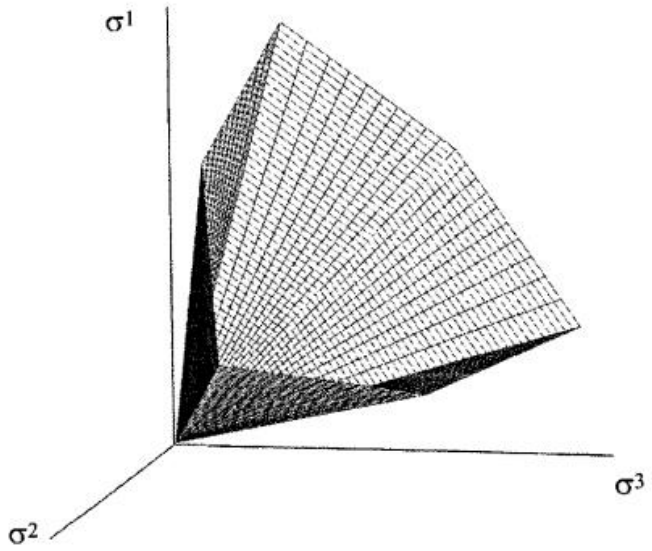

Figure 2.44 Mohr-Coulomb criterion on the octahedral plane in three principal stresses (Brinkgreve, 2005).

2.10.2 Drucker-Prager (MC)

In the drucker - Prager model (Drucker & Prager, 1952), hexagonal shape of the failure contour is simplified to a conical shape as shown in Figure 2.45. It facilitates during analysis by numerical methods. It has the similar limitations as described for the Mohr-Coulomb model.

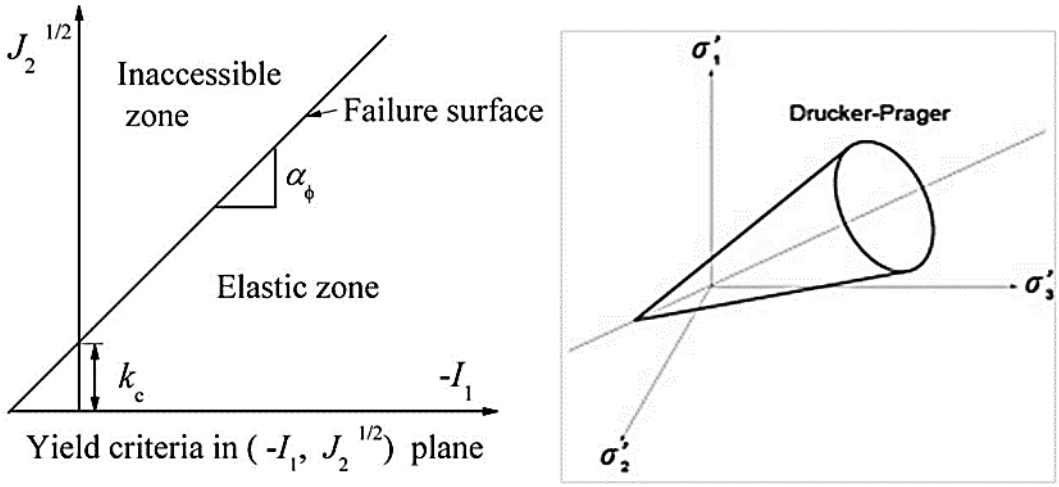

Figure 2.45 Drucker-Prager yield criteria (Islam, 2014)

2.10.3 Hyperbolic Model

Duncan and Chang (1970) developed a non-linear soil model based on the concept of hyperbola that can predict the stress-strain behavior (Kondner,1963) and a power law that can formulate the stiffness of the soil as a stress-dependent parameter (Ohde, 1939). One of the disadvantage of the model is that, it cannot describe the dilatancy behavior of the soil, since this would require a Poisson's ratio larger than 0.5, which is invalid (Wood & Gazo, 2005).

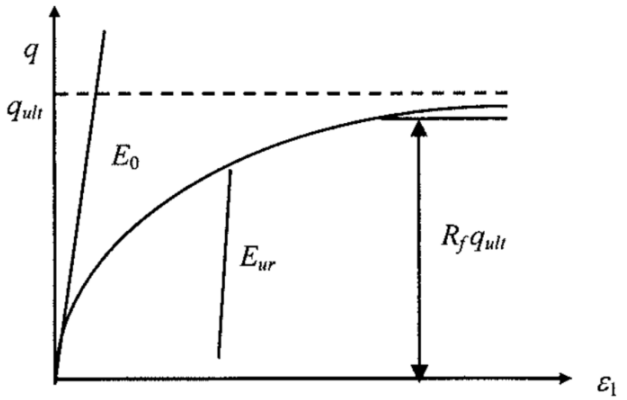

Figure 2.46 Hyperbolic model perdition of a drained triaxial test (Wood & Gazo, 2005).

Table 2.3 Some Constitutive Models, Their Attributes and Their Capabilities (Lade, 2005)

Model	Types of Soil			Failure Surface	Plastic Potential	Experiments Required	No of Parameters
	Sand	Clay	Cemented Soil				
Plaxis Hardening (Brinkgreve and Vermeer, (1977)	Yes	Yes	Yes	Mohr-Coulomb	Nonassociated and Associated	3 Triax Comp & 1 Iso-Comp	11
MIT-E3 (Whittle, 1993)	No	Yes	No	Rotated, Extended von Mises	Nonassociated	2 CK_oU Triax. Compt. 1 CK_oU Triax. Ext. 1 CD Triax. Comp. K_o-Comp. Resonant Column/ Bender Element	15
MIST-S1 (Pestana and Whittle, 1990)	Yes	Yes	No	Smooth, Triangular, Conical	Nonassociated	CU Triax Comp (Iso/K_o) CD Triax Comp (Iso/K_o) Iso/K_o-Comp Resonant Column/ Bender Element	13
Nor-Sand (Jefferies, 1993)	Yes	Yes	No	Smooth, Triangular, Conical	Associated	2 CD Triax Comp 2 CU Triax Comp 1 Iso Comp	7
Single Hardening (Kim and Lade, 1993)	Yes	Yes	Yes	Smooth, Triangular, Conical	Nonassociated	3 Triax Comp 1 Iso Comp	12
Structured Cam Clay (Liu and Carter, 2002)	No	Yes	No	Smooth, Triangular, Conical	Associated	3 Triax Comp & 1 Iso-Comp	10

2.11 Geological Aspects of Dhaka Clay

Dhaka the capital city of Bangladesh is geologically placed on the southern part of the Madhupur tract which is formed by older Pleistocene terrace sediments. The tropical clay soils of Dhaka are mainly composed of illite, kaolinite, chlorite and some non-clay minerals (Hossain and Toll, 2006). The Dhaka clay varies from light-yellowish-gray to brick red in color. Monsur (1995) stated that the red color is the result of iron compounds. In general, the soil is in slightly to heavily overconsolidated state (Uddin, 1990) and of intermediate to high plasticity (Islam, Siddique & Muqtadir, 2004). The soil is developed in place without transportation (Vaughan et al. 1988). The void ratio of residual soils is very variable and does not vary systematically with soil type, parent rock etc (Hossain and Toll, 2006). The top layer of the Dhaka clay extends up to 8~30 meter which contains silts and sands. The present study mainly covered with this layer of soil.

2.12 Studies on Modelling of Dhaka Clay

Some studies were carried on constitutive modelling of Dhaka sub-soil. Islam, Suravi & Shahin (2013) applied Subloading t_{ij} model to bearing capacity estimation for Dhaka sub-soil. They determined the model parameters from undrained triaxial test for Dhaka clay as shown in Table 2.4. Later, Azam, Sharif & Shahin (2016) applied Subloading t_{ij} model in tunnel simulation.

Table 2.4 Parameters of Subloading t_{ij} model for Dhaka clay (Islam et al., 2013)

Parameters	Notation	Value
Compression index	λ	0.080
Swelling index	κ	0.0078
Void ratio on normally consolidation line at p= 98 kPa	N	0.80
Critical state stress ratio,	R_{cs}	3.82
Poisson's ratio	v_e	0.20
Shape of yield surface (same as original Cam clay at β= *1)*	β	1.50
Influence of density and confining pressure	a	600
Influence of structure of soil	b	2.5

2.13 Conclusions

It is important to calibrate the parameters of any constitutive model before applying it to a particular soil. A very limited number of study has been carried on the application of constitutive model to Dhaka clay as discussed in section 2.12. The study carried out by Islam et al. (2013) and Azam et al. (2016) is restricted to undrained simulation at constant minor principal test. To evaluate the model performance, it is important to compare with other models at various stress conditions.

The present study emphasizes on determination of various parameters of simple elastoplastic constitutive models at drained and undrained conditions under different stress conditions. Also, their performance in describing stress-strain characteristics of Dhaka clay is evaluated at various stress paths.

Chapter Three
RESEARCH METHODOLOGY

3.1 General

The present study is mainly covered with the validation of constitutive models that could be able to estimate the stress strain behavior of Dhaka soil. In this chapter, details of the experimental program are presented. It includes the details of site selection, data collection from field, disturbed and undisturbed sample collection and laboratory testing. Also, steps to calculate the various soil features like stress, strain, dilatancy is discussed based on the Cam-clay (both original and modified) model and Subloading t_{ij} model.

3.2 Study Area

Dhaka city is placed on the Madhupur tract which stretches from administrative district Jamalpur in the north to the district Narayonganj in the south. It covers most of the portions of the Gazipur, Dhaka (Figure 3.1) and Savar area which also the study area. For the study, total six locations were selected inside and near the Dhaka city. Subsoil exploration program is carried out at Mirpur DOHS, Shagufta Housing of Mirpur, Baridhara DOHS, Rokeya Sarani at Shewrapara area and near Dhaka city locations includes Bagher Bazar at Gazipur and Savar. Locations for the subsoil investigation program inside the Dhaka city is marked on the Figure 3.2. Table 3.1 presents the details information about the study locations.

Table 3.1 Soil investigation locations

Ser	Location	Latitude & Longitude	Sample ID	Depth	Remarks
1	Rokeya Sarani, Shewrapara, Dhaka	24.165481, 90.432233	Rk-UD-01	3.0 m	Drained Analysis
2	Baridhara DOHS, Dhaka	23.810905, 90.413767	Br-UD-01	2.6 m	Undrained Analysis
3	Mirpur DOHS, Dhaka	23.836236, 90.373283	Dh-UD-02	5.0 m	Drained Analysis
4	Shagufta Housing, Mirpur	23.834224, 90.375354	Sh-UD-02	5.0 m	Undrained Analysis

5	Bagher Bazar, Gazipur	24.165073, 90.432361	Gz-UD-01	2.5 m	Drained Analysis
6	Karnapara, Savar	23.825909, 90.257421	Sv-UD-02	5.0 m	Drained Analysis

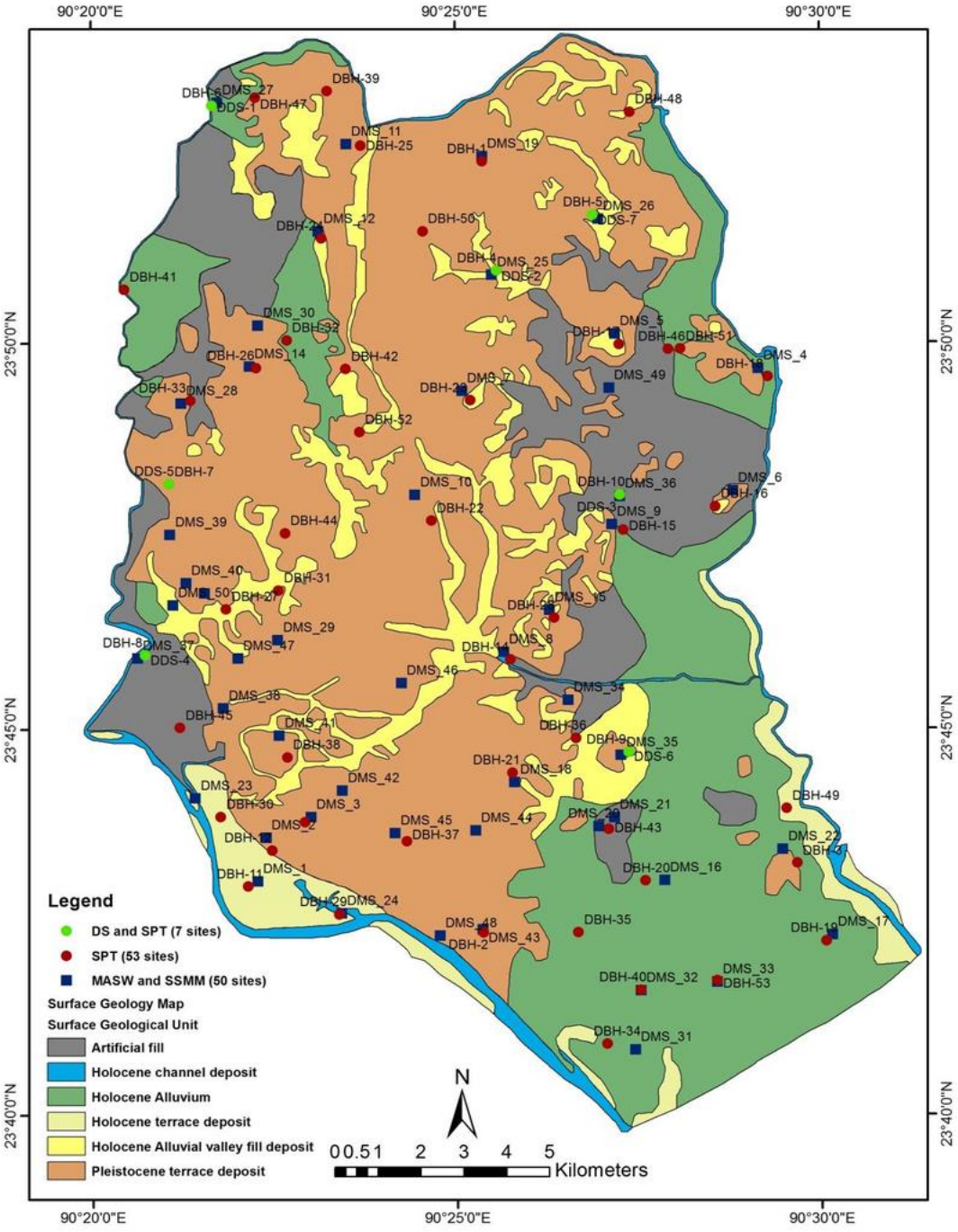

Figure 3.1 Map showing the area covered by the Madhupur track inside the Dhaka city.

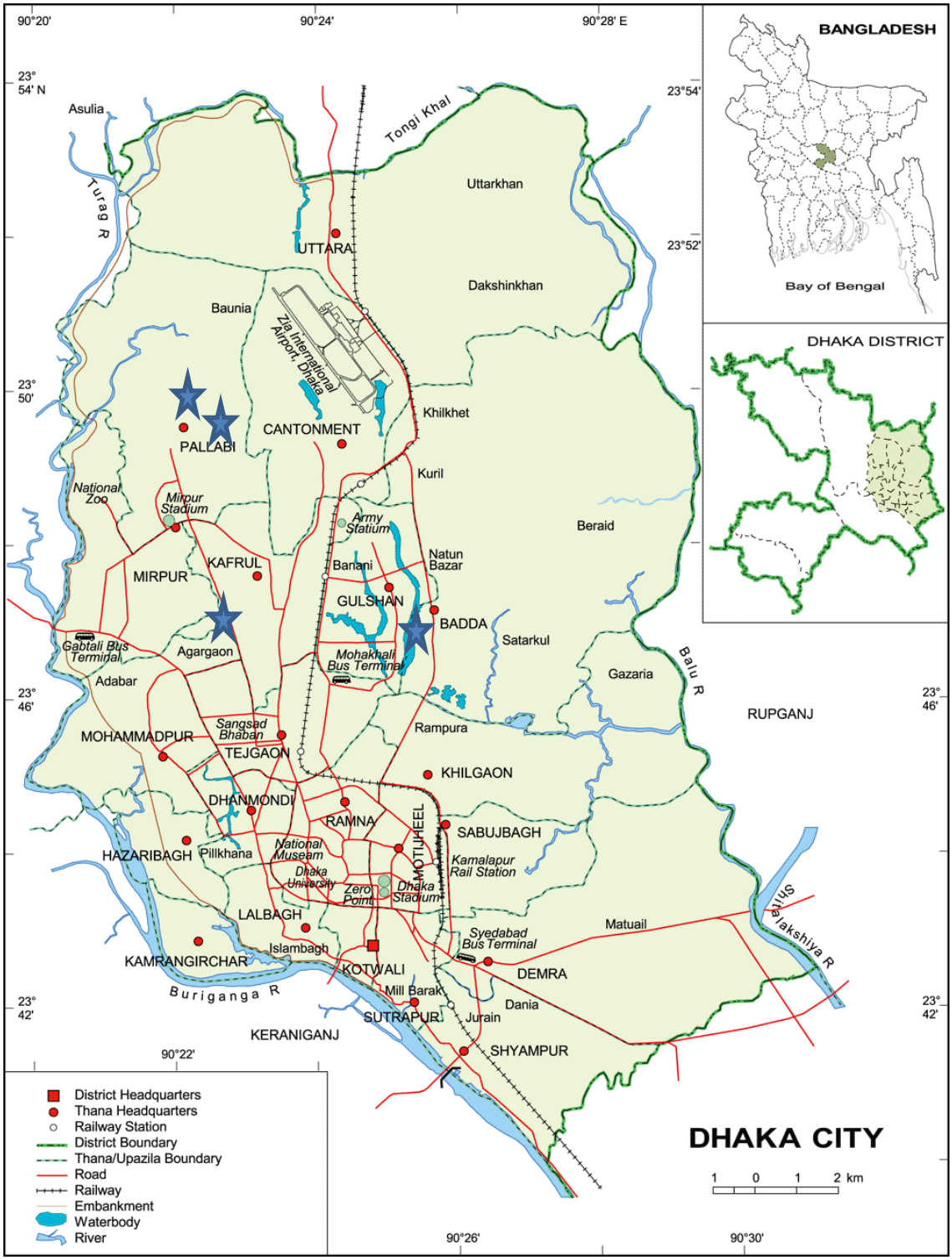

Figure 3.2 Map showing the locations of soil sample collection inside the Dhaka city.

3.3 Research Scheme

This study is consisted of sample collection from several locations, laboratory testing and numerical simulations. The sequence of the study is represented by a flowchart as shown below:

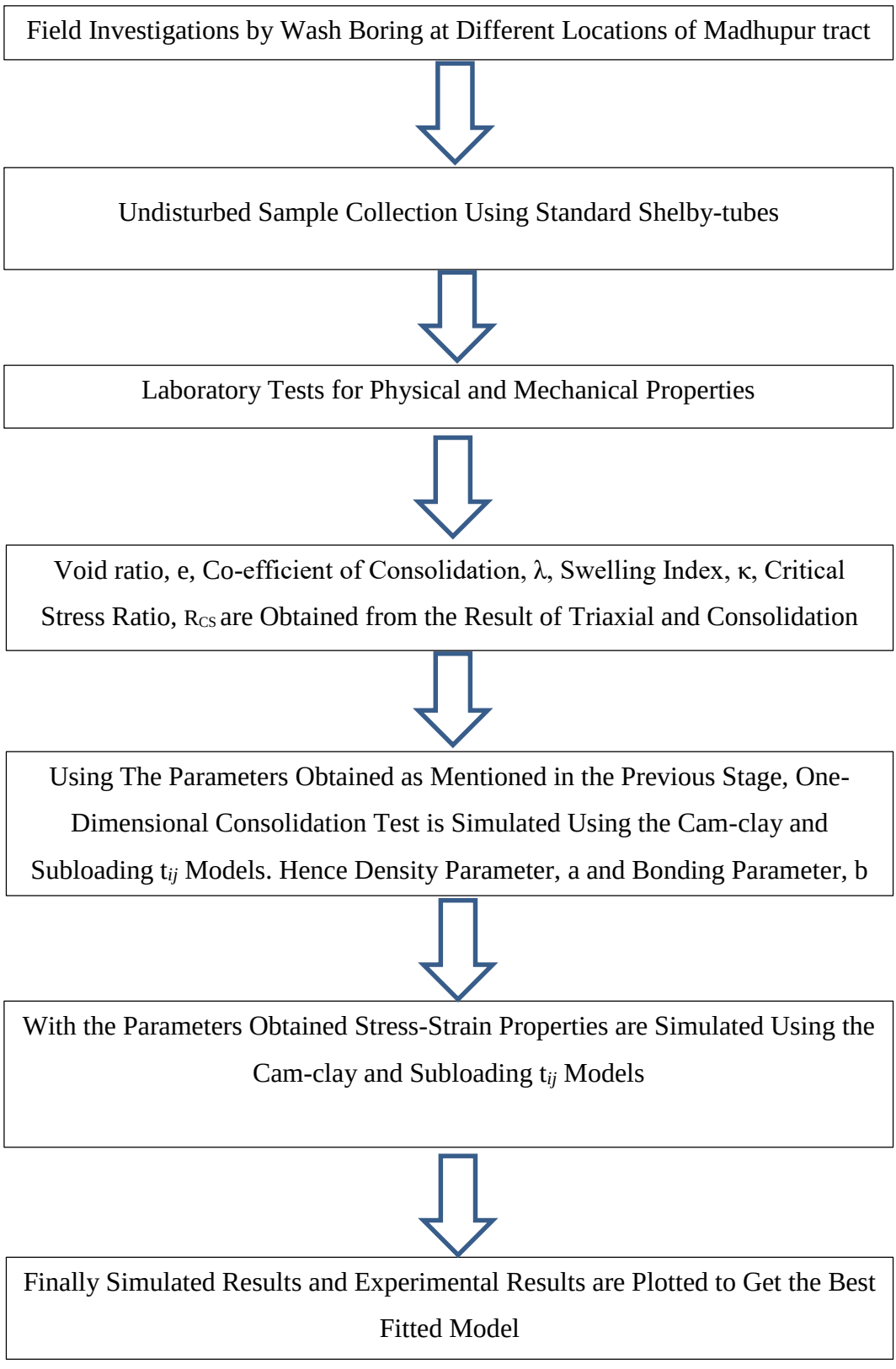

3.4 Sample Collection

This study focuses on the natural undisturbed soils to understand its behavior more sophisticatedly. Hence, mainly undisturbed samples are collected from the selected sites. Undisturbed samples are collected using Thin-walled Shelby tubes following the ASTM D1587. The Shelby tubes are of 75 mm diameter and wall thickness is of 3 mm. This specification provides a disturbance of 8.5 % (<10%) which indicates a good quality undisturbed samples. The sample tubes are transported with shipping box following the ASTM D 4220.

3.5 Preservation and Preparation of Sample

After collection from the field, samples are brought in the MIST geotechnical engineering laboratory. To ensure the undisturbed condition sample tubes are stored in humid chamber at a constant temperature of 25^{o}C and constant humidity >95 %.

3.6 Laboratory Test

Laboratory test is divided into two types, i.e. physical test and mechanical test. Physical tests mialy includes Atterberg limit tests, specific gravity test, and grain size analysis. Mechanical test covers the one-dimensional consolidation test, consolidated drained triaxial test (CD), consolidated undrained triaxial test (CU). All the tests are conducted in MIST geotechnical engineering laboratory.

3.7 Physical Properties Test

To determine the physical properties, atterberg limit tests, specific gravity test and grain size analysis tests are conducted. All tests are conducted according to the corresponding ASTM standards. Table 3.2 shows the details of the tests for physical properties.

Table 3.2 Physical property tests

Test Name	Properties	ASTM Standard	Test Method
Atterberg limit	Liquid limit, Plastic limit, Plasticity index	ASTM 4318	Casagrande type liquid limit device
Specific gravity	Particle density	ASTM D854	Small pycnometer
Grain size analysis	Particle size distribution	ASTM D6913 ASTM D7928	Wash sieving and Hydrometer

3.8 Mechanical Properties Test

This study focuses on the stress-strain behavior of soil. Therefore, stress-strain behavior of the soil in drained and undrained condition is tested. The tests are conducted according to the corresponding ASTM standards. All the tests are conducted in MIST geotechnical engineering laboratory. Details of the tests are appended below.

3.8.1 Preparation of Sample

3.8.1.1 Sample Extrusion

Samples are extruded first using the horizontal motorized extruder to ensure uniform pressure and best quality undisturbed samples.

3.8.1.2 Specimen Preparation

For consolidated drained and undrained triaxial test, after extrusion of the sample, it is brought to the soil lathe and cut off by a wire saw to the required shape. In the present study, usually two specimen size was adopted, one was 38 mm diameter and 76 mm height and another was 50 mm diameter and 100 mm height.

For consolidation test, enough height of extruded sample is placed on a glass plate. The consolidation ring is then pushed and additional amount is trimmed off.

3.8.2 Triaxial Compression Test

Prepared specimen are placed in triaxial cell with necessary caution to maintain the undisturbed condition. The test procedure is summarized in the following steps:

(i) After placing the specimen, triaxial cell is fitted and pressurized as shown in Figure 3.3.

(ii) At first, degree of saturation is checked by calculating pore pressure coefficient B. If B is equal to or greater than 0.95, the specimen can be considered to be saturated and the consolidation stage can be started. Alternate cell pressure and back pressure increment was used to achieve the target B value to ensure saturated condition. The objective of the saturation stage is to ensure that all the voids in the specimen are filled with water. This enables reliable readings of pore pressure changes during subsequent consolidation and shearing stages.

(iii) After saturation, consolidation is done to bring the specimen to the state of effective stress required for carrying out the compression test.

(iv) All the tests are conducted at constant confining pressure. From the consolidation stage, based on the time required for consolidation, rate of shear displacement is calculated. Enough slow rate was applied so that no pore pressure is developed during drained test. During drained test drainage path is kept open and for undrained test drainage path is closed and no water is allowed to pass. Test is stopped when the specimen is failed at ultimate deviator stress.

Figure 3.3 triaxial test in progress.

3.8.3 One-dimensional Consolidation Test

Consolidation properties are mandatory for simulation of both Cam-clay and Subloading t_{ij} model. Specimen prepared in section 3.4.1.2 is placed in the consolidation cell with necessary caution (Figure 3.4). Subsequent loading is applied until the final effective stress is achieved. Load increment ratio of 2.0 is applied. Subsequent unloading is done and returned to the starting loading point to determine the swelling potential. Load increment ratio of 4 is adopted for unloading stage. In the present study following loading and unloading sequences are adopted in general:

Loading:

25, 50, 100, 200, 400, 800, 1600 kPa.

Unloading:

400, 100, 25 kPa.

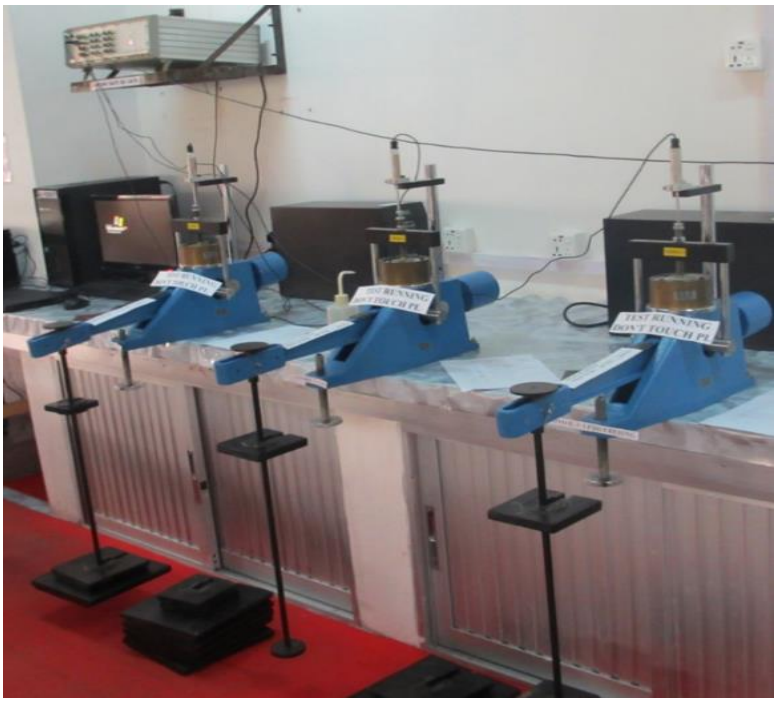

Figure 3.4 Consolidation test in progress.

3.8.4 Data Collection and Calculation

Sophisticated data loggers were integrated both with the consolidation and triaxial machine to record data. For calculation and analysis DS7.2 software was used which is integrated with consolidation and triaxial machine. This software also provides live monitoring of different test stages.

3.9 Simulation Steps

To predict the various soil features, Subloading t_{ij} Element Simulation Software version 3.2 was used. The software was developed in Nagoya Institute of Technology (NIT) and has been used in various research projects. This software can calculate various soil features based on the input parameters both for Cam-clay and Subloading t_{ij} model. The simulation steps are appended below:

(i) Input the test type (i.e. drained or undrained), loading condition (i.e. isotropic or one dimensional), target effective stress, target deviator stress in path.txt file of the program.

(ii) Input the parameters obtained from triaxial and consolidation tests in the para.txt file of the program. The input parameters required are listed in the table 3.3.

Table 3.3 Input parameters for numerical simulation

Ser.	Parameter	Notations
1	Compression index	λ
2	Swelling index	κ
3	Void ratio at atmospheric pressure (98 kPa)	N
4	Critical state stress ratio	R_{CS}
5	Poisson's ratio	v_e

(iii) Using the parameters as shown above, one dimensional consolidation test is simulated both using Cam-clay and Suloading t_{ij} model. This simulation will provide density parameter, *a*, bonding parameter, *b*, yield surface shape parameter, β.

(iv) Cam-clay model requires the parameters obtained as shown in table 3.3 and density parameter, *a* obtained from consolidation simulation to calculate stress-strain values at target effective stresses. Subloading t_{ij} model requires the bonding parameter, *b* and yield surface shape parameter, β in addition to parameters for Cam-clay model.

(v) Finally predicted results of stress-strain are plotted against the observed results obtained from the test results.

Chapter Four
RESULTS AND DISCUSSIONS

4.1 General

In this chapter results obtained from physical index properties are presented which will provide basic concept on the sample type. For all the six locations, Observed stress-strain results of triaxial drained and undrained tests are plotted and compared against the predicted stress-strain behavior using Cam-clay and Subloading t_{ij} model. Observed test results of one-dimensional consolidation test is also plotted against the predicted results using both the models. Description of the specimen, test conditions and test stages are presented in tabular form.

4.2 Index Properties

To evaluate the physical and index properties of Dhaka clay, grain size analysis, specific gravity test, liquid limit and plastic limit tests were conducted according to relevant ASTM standards as mentioned in Section 3.7 of Chapter 3. Grain size analysis results show that in general the sample has 30 - 34 % clay, 60 - 66 % silt and 4-8 % sand. The specific gravity of the various locations ranges from 2.67 to 2.70. The liquid limit result found ranges from 27 % to 32 % and plastic limit ranges from 24 % to 26 %. In general the collected samples are of higher unit weight ranges from 19.6 kN/m^3 to 21.6 kN/m^3 and less initial void ratio ranges from 0.50 to 0.63. This indicates that the samples are heavily compacted and perform as over consolidated soil at normal stress conditions.

4.3 Model Parameters Obtained at Drained Condition

In this study, samples from various locations of Madhupur tract was collected and tested at drained and undrained condtions. Samples collected from Bagher Bazar at Gazipur, Mirpur DOHS and Rokeya Sarani at Dhaka and Savar area tested at drained condition. Details of the sample collection procedure and test procedures were already discussed in the Chapter 3.

Both the Cam-clay and Subloading t_{ij} model requires few parameters which can be obtained from simple tests. To obtain the compression and swelling properties one dimensional consolidation test was conducted. To obtain critical stress ratio, consolidated drained triaxial tests are conducted according to the relevant ASTM standards.

4.3.1 One-dimensional Consolidation Properties

Table 4.1 presents the specimen details for consolidation test at natural condition. The samples were collected from a depth in the range of 2.5 m to 5.0 m below the existing ground level. Figure 4.1 shows the observed $e - lnp$ relationship of the samples collected for drained analysis. From Figure 4.1, compression index, C_c was found in the range of 0.13 to 0.16 (λ = 0.057 to 0.07) and swelling index, C_r was found in the range of 0.02 to 0.03 (κ = 0.015). The pre-consolidation pressure from graphical method was obtained in the range of 250 to 300 kPa.

Table 4.1 Consolidation Specimen Description

Sample Locations	Gazipur	Mirpur DOHS	Rokeya Sarani	Savar
Initial Unit Weight	19.8 kN/m^3	20.0 kN/m^3	19.7 kN/m^3	20.0 kN/m^3
Initial Moisture Content	19 %	24 %	19 %	25 %
Initial Void Ratio	0.556	0.606	0.506	0.62
Initial Degree of Saturation	90 %	88 %	85 %	86 %
Final Degree of Saturation	100 %	100 %	100 %	100 %
Depth below EGL	2.5 m	5.0 m	3.0 m	5.0 m
Preconsolidation Pressure	300 kPa	250 kPa	250 kPa	260 kPa

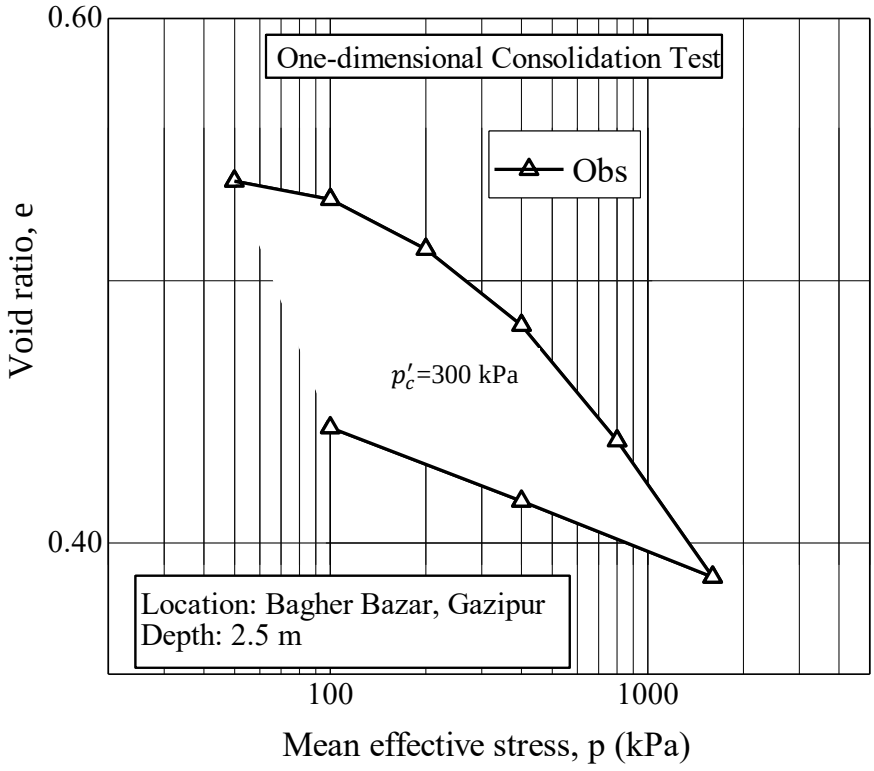

(a) Bagher Bazar, Gazipur

Figure 4.1 Observed $e - lnp$ relationship of the Sample of (a) Gazipur

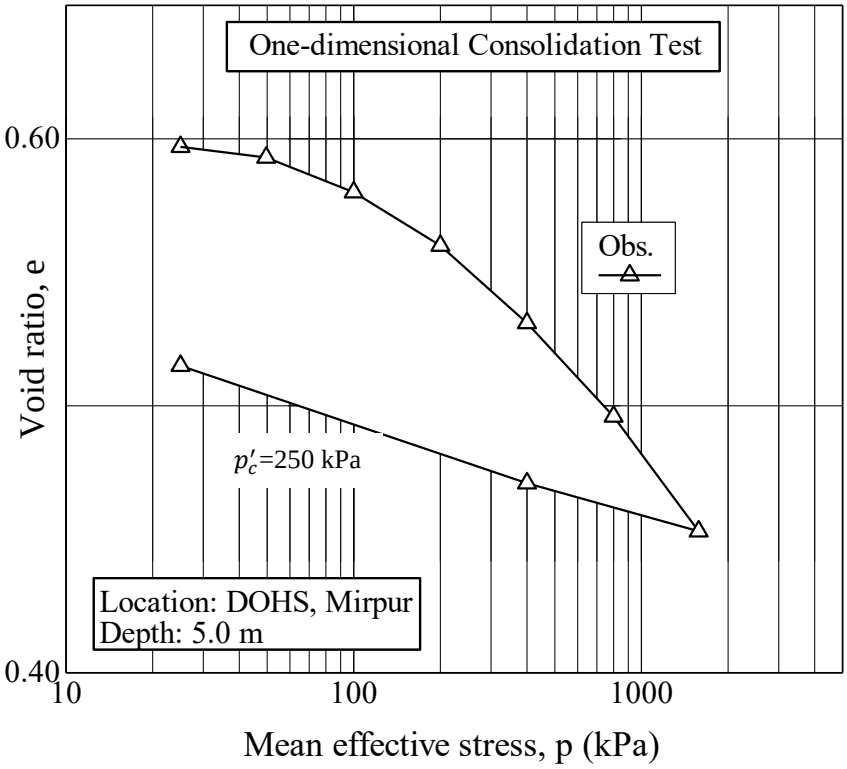

(b) Mirpur DOHS, Dhaka

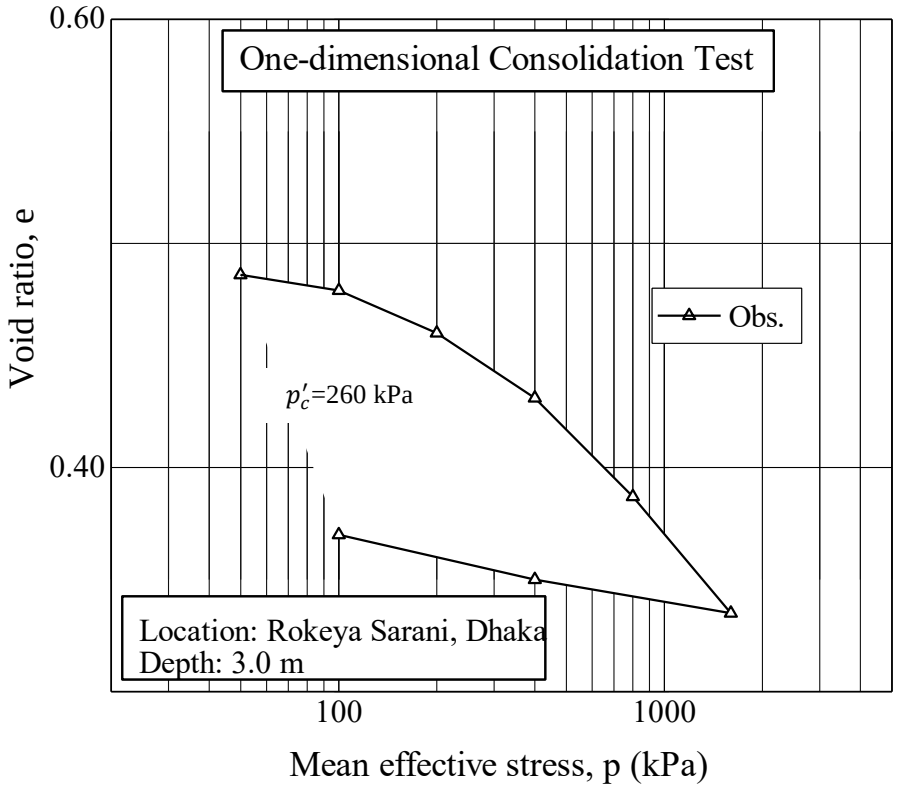

(c) Rokeya Sarani, Dhaka

Figure 4.1 (Cont.) Observed $e - lnp$ relationship of the Samples of (b) Mirpur DOHS, (c) Rokeya Sarani.

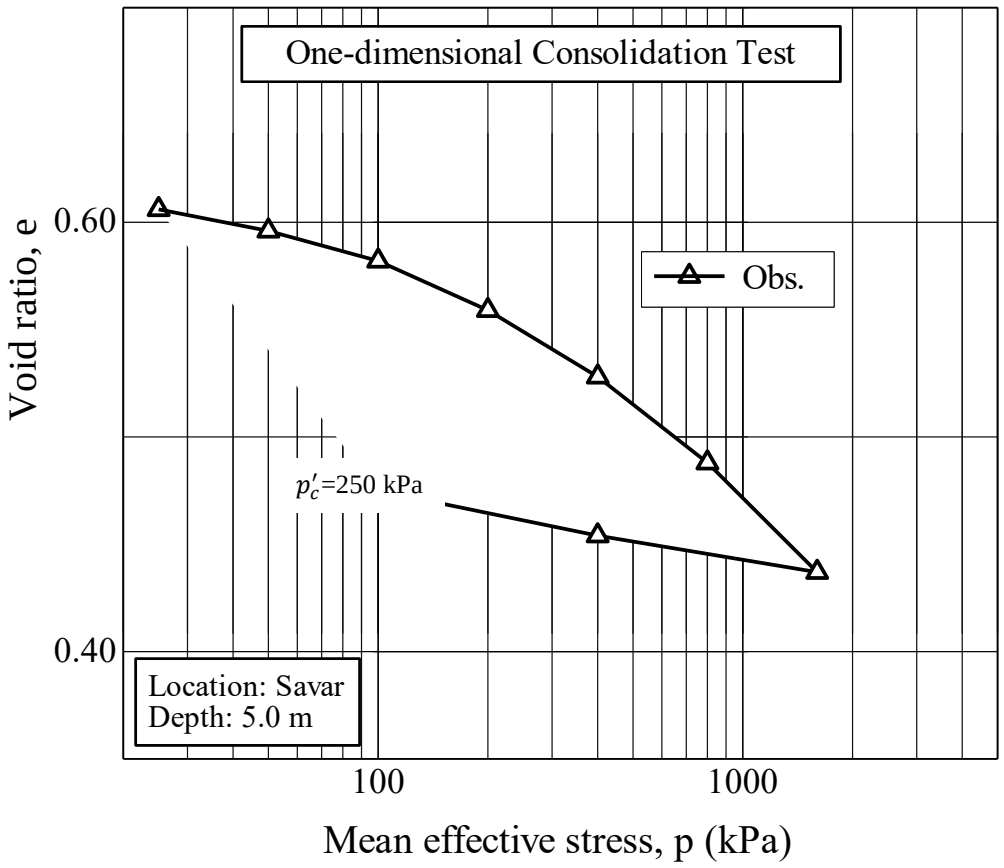

(d) Savar

Figure 4.1 (Cont.) Observed $e - lnp$ relationship of the Sample of (d) Savar.

4.3.2 Consolidated Drained Triaxial Properties

Table 4.2 presents the specimen details for specimen of various locations for consolidated drained triaxial tests. In general, specimen A, B and C were tested at effective stress of 100 kPa, 200 kPa and 400 kPa respectively. From consolidation test results in Sec 4.3.1, the initial OCR of specimen was obtained in the range of 1.0 to 3.0. From the observed stress-strain relationship of the specimen as shown in Figure 4.2 to Figure 4.5, the critical stress ratio, η was found in the range of 2.8 to 3.0

Table 4.2 Triaxial Specimen Description

Specimen	A	B	C
Location: Gazipur			
Initial Unit Weight	20.2 kN/m^3	20.1 kN/m^3	-
Moisture Content	22 %	21 %	-
Void Ratio	0.56	0.56	-
B Value	0.95	0.94	-
Effective Confining Stress	95 kPa	201 kPa	-
Initial OCR	3.1	1.5	-
Critical Stress Ratio	2.8		
Location: Mirpur DOHS			
Initial Unit Weight	20.0 kN/m^3	20.0 kN/m^3	20.0 kN/m^3
Moisture Content	24 %	24 %	25 %
Void Ratio	0.61	0.61	0.61
B Value	0.97	0.95	0.97
Effective Confining Stress	102 kPa	202 kPa	400 kPa
Initial OCR	2.5	1.25	1.0
Critical Stress Ratio	2.8		
Location: Rokeya Sarani			
Initial Unit Weight	20.6 kN/m^3	20.7 kN/m^3	-
Moisture Content	19 %	20 %	-
Void Ratio	0.50	0.50	-
B Value	0.96	0.95	-
Effective Confining Stress	97 kPa	201 kPa	-
Initial OCR	2.7	3.0	-
Critical Stress Ratio	3.0		
Location: Savar			
Initial Unit Weight	-	19.9 kN/m^3	19.8 kN/m^3
Moisture Content	-	25 %	24 %
Void Ratio	-	0.62	0.62
B Value	-	0.97	0.96
Effective Confining Stress	-	196 kPa	394 kPa
Initial OCR	-	1.25	1.0
Critical Stress Ratio	3.0		

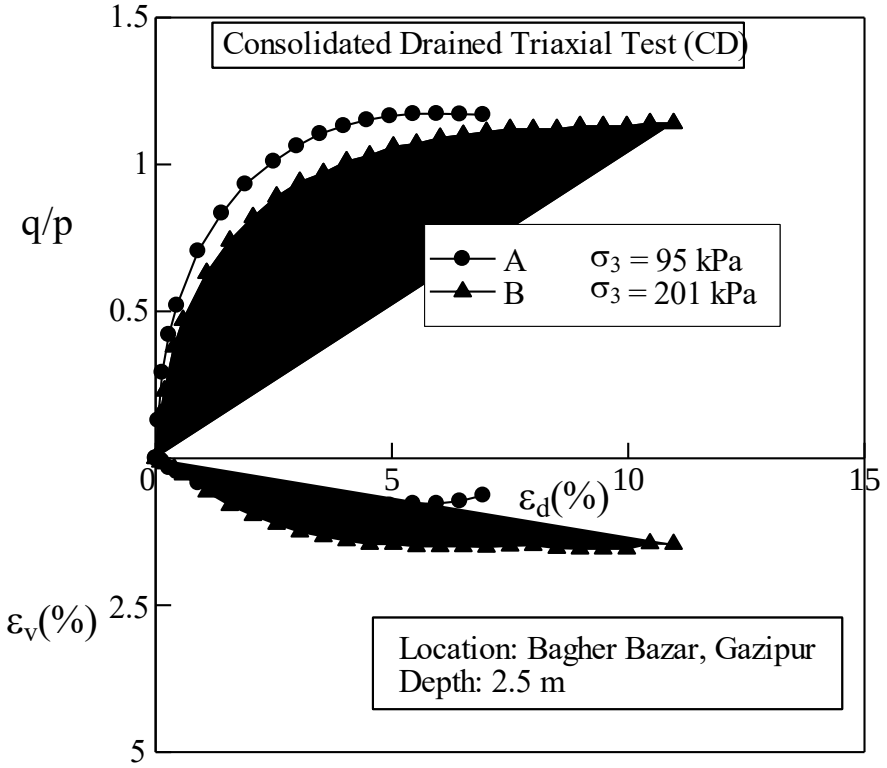

(a)

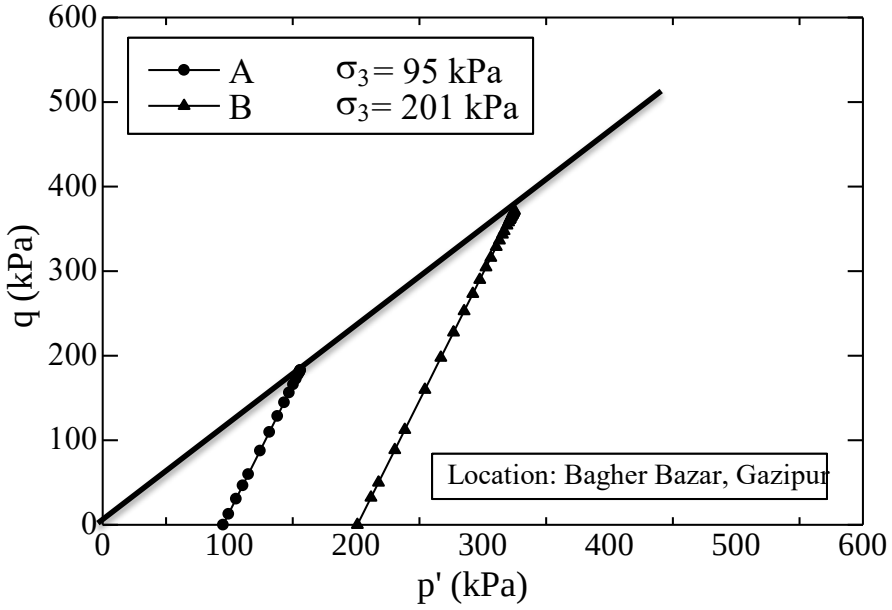

(b)

Figure 4.2 Observed (a) stress-deviator strain-volumetric strain relationship, (b) effective stress path of Gazipur Sample in CD triaxial compression test

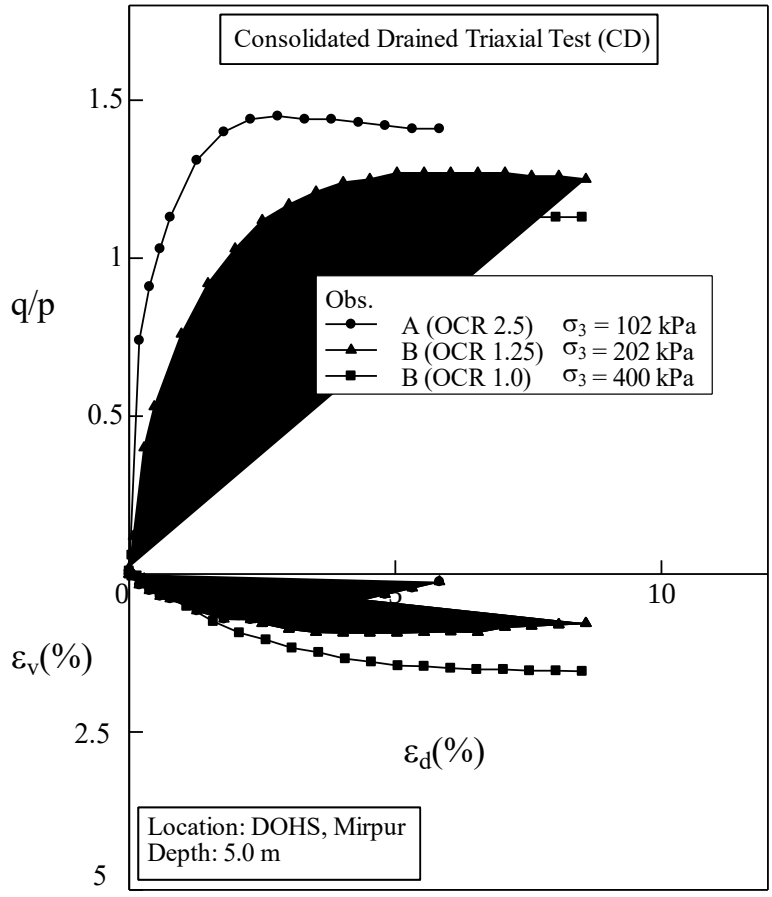

(a)

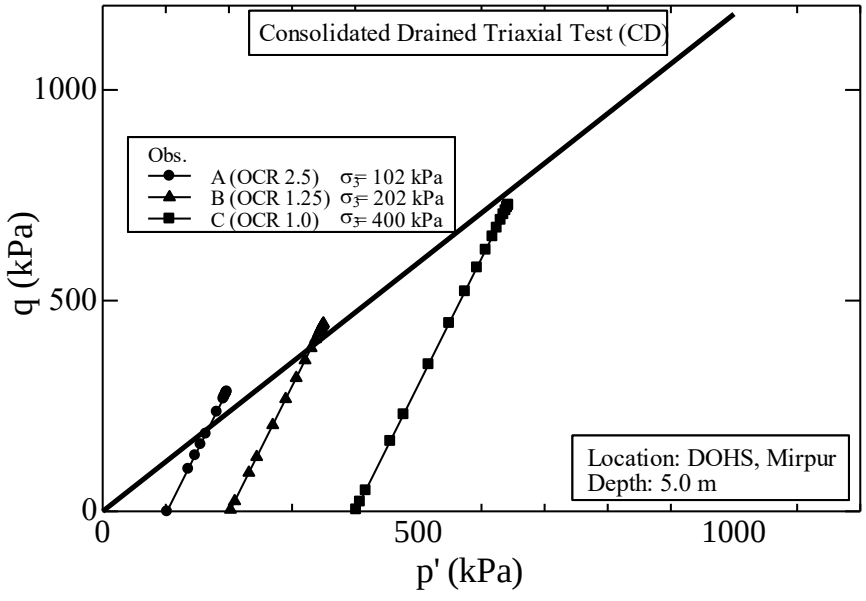

(b)

Figure 4.3 Observed (a) stress-deviator strain-volumetric strain relationship, (b) effective stress path of Mirpur DOHS Sample in CD triaxial compression test

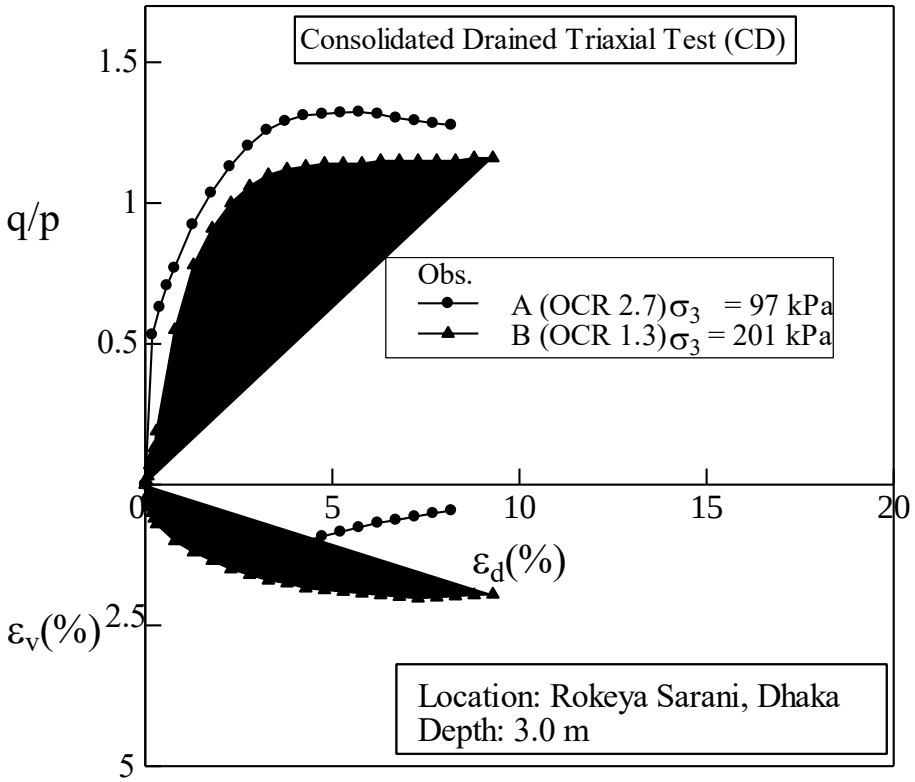

(a)

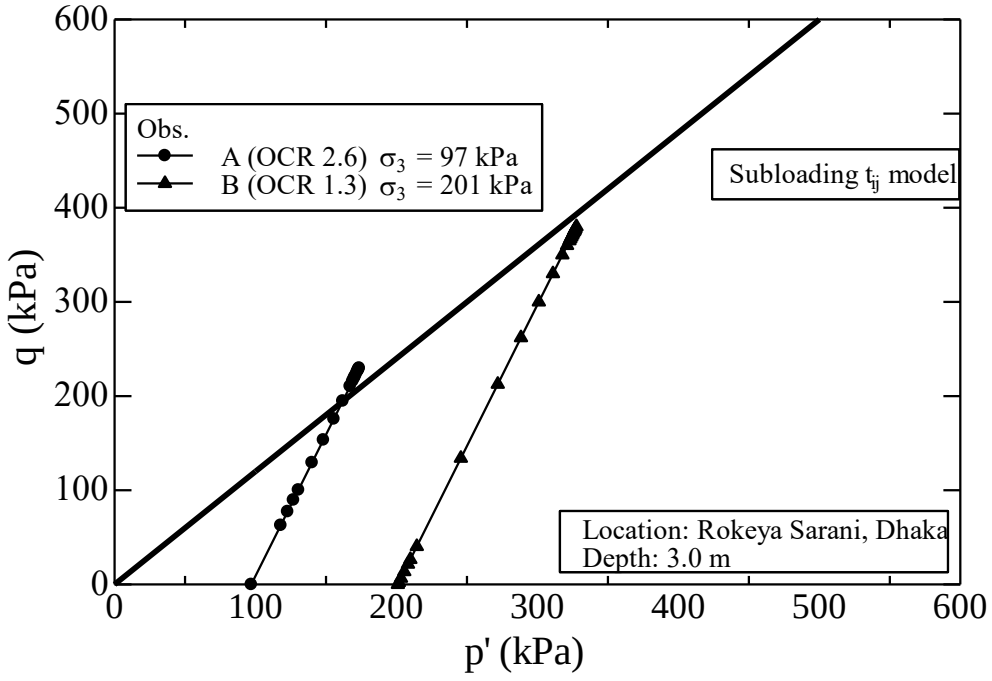

(b)

Figure 4.4 Observed (a) stress-deviator strain-volumetric strain relationship, (b) effective stress path of Rokeya Sarani Sample in CD triaxial compression test

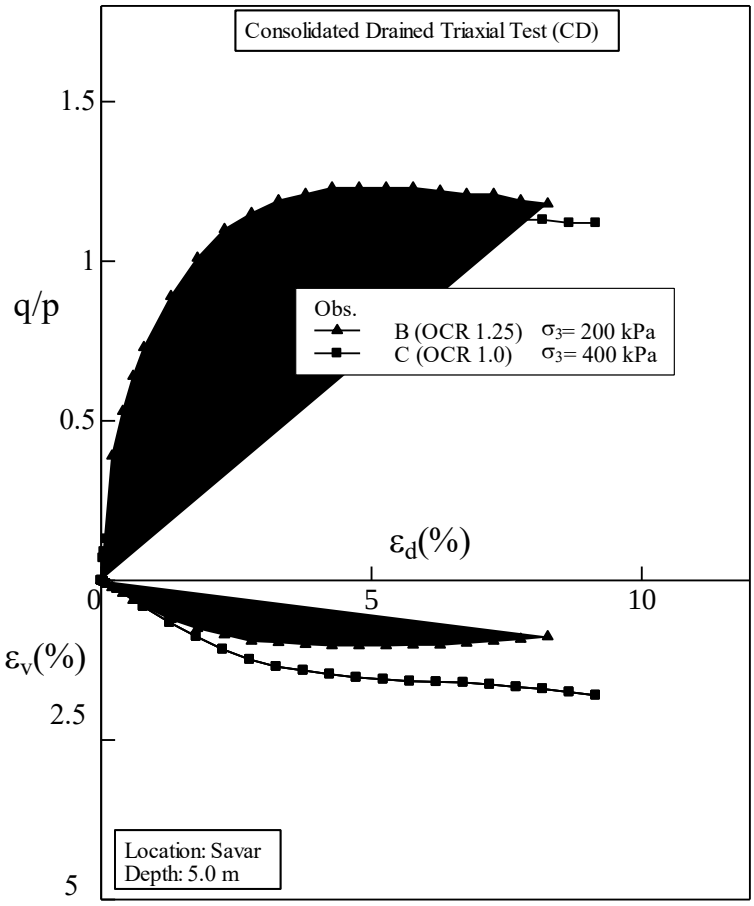

(a)

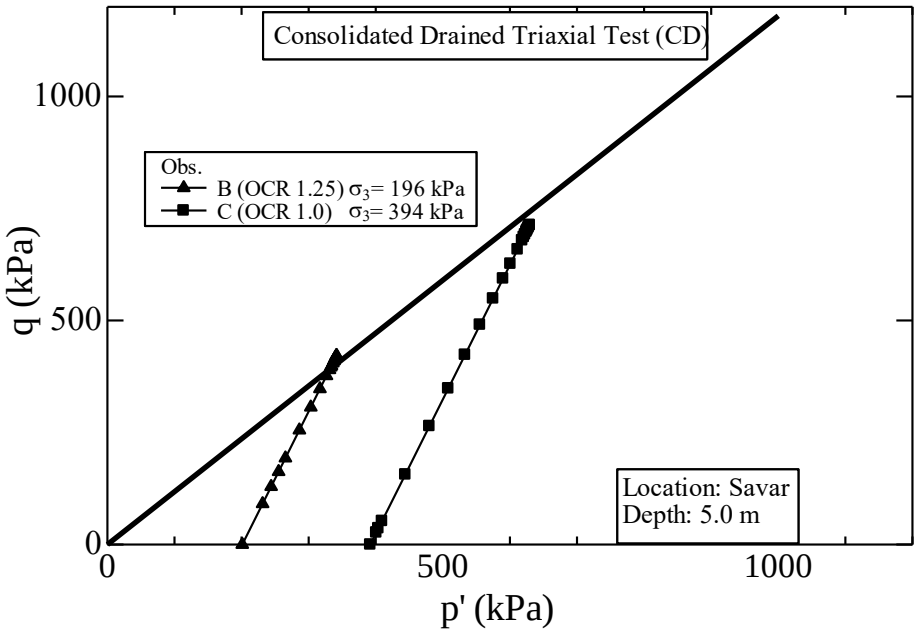

(b)

Figure 4.5 Observed (a) stress-deviator strain-volumetric strain relationship, (b) effective stress path of Savar Sample in CD triaxial compression test

4.3.3 Simulations of the Test Results

In this study for simulation, Subloading t_{ij} model, Cam-clay and Modified Cam-clay models were used. Results predicted by the models are compared against the observed results of one-dimensional and triaxial compression test. The parameters obtained from the one-dimensional consolidation test and consolidated triaxial test are listed in Table 4.3. Here, parameters obtained from the one-dimensional consolidation and triaxial compression tests are required by both the models. In addition, to take into account the effect of density and bonding, Subloading t_{ij} model requires the density parameter, a and bonding parameter, b.

Table 4.3 Material parameters at drained condition

Parameter	Notations	Gazipur	Mirpur DOHS	Rokeya Sarani	Savar
Compression index	λ	0.07	0.057	0.065	0.06
Swelling index	κ	0.015	0.013	0.010	0.012
Void ratio at atmospheric pressure (98 kPa)	N	0.60	0.63	0.52	0.63
Critical state stress ratio	R_{CS}	2.8	2.80	3.00	3.0
Poisson's ratio	v_e	0.2	0.2	0.2	0.2
Shape of yield surface	β	1.5	1.5	1.5	1.5
Influence of density	a	480	400	380	480
Influence of bonding	b	10	10	15	10

4.3.3.1 Subloading t_{ij} model

In the Subloading t_{ij} model influence of density and bonding was taken into account by introducing two parameters, a and b. These two parameters can be obtained by fitting the predicted results of $e - lnp$ relation with the observed results. Several trial may be required to obtain the best fitted predicted $e - lnp$ curve.

Table 4.3 shows the model parameters including density and bonding obtained from the best fitted predicted $e - lnp$ curve with the observed result. Figure 4.6 shows that the simulated $e - lnp$ relation fits well with observed results of Gazipur sample using the parameters listed in Table 4.3.

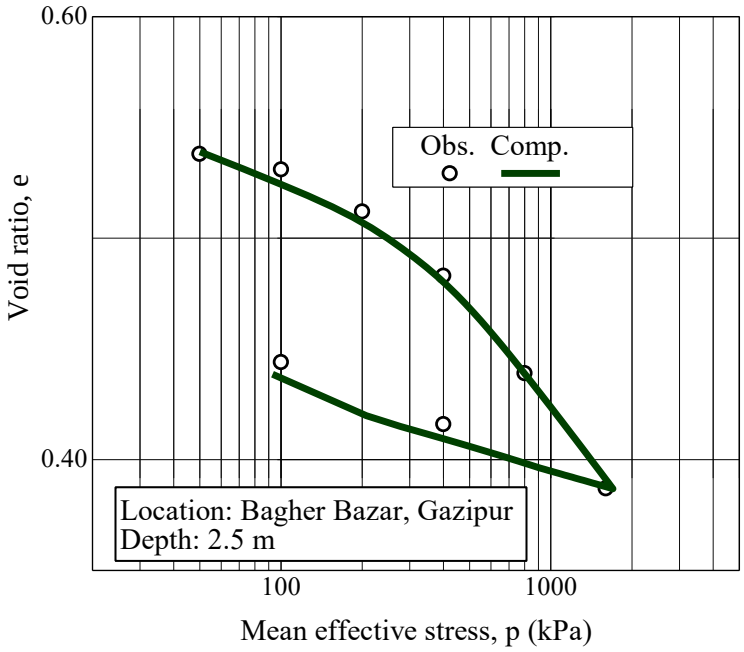

Figure 4.6 Observed and Predicted $e - lnp$ relationship of Gazipur sample.

In Figure 4.7, predicted results using Subloading t_{ij} model is plotted with the observed stress-strain results from CD triaxial test. It was observed that the predicted stress ratio, deviator strain, volumetric strain fitted well with observed results from test.

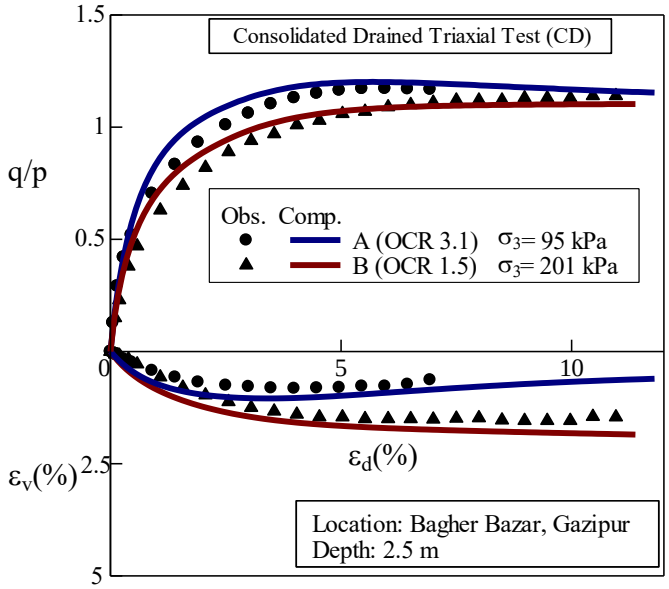

Figure 4.7 Observed and predicted stress-strain relation of Gazipur soil at drained condition.

Figure 4.8 shows the observed and predicted effective stress path of the specimen A and B in drained compression test. It is observed that the predicted results fits well with the observed test results.

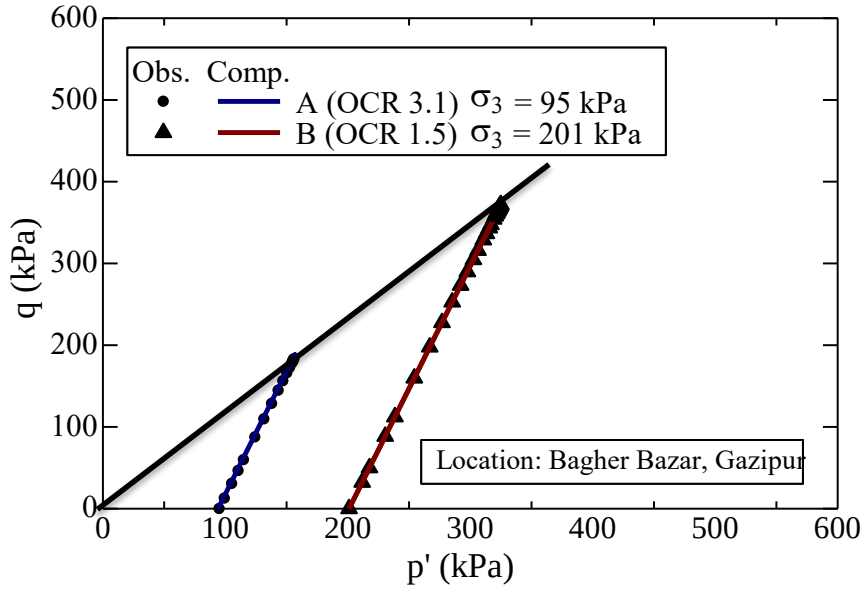

Figure 4.8 Observed and predicted effective stress path in CD triaxial compression test

4.3.3.2 Cam clay model

Performance of both Cam-clay and Modified Cam-clay models is evaluated by plotting the predicted results against the observed test results. Figure 4.9 shows the predicted stress-strain relation using the Cam-clay model. Material parameters obtained from the consolidation and triaxial test as listed in Table 4.3 are used for the simulation. It is observed that for both the specimen A and B, predicted results of stress ratio, deviator stress and volumetric strain are found unsatisfactory when plotted with the test results. Here, specimen A and B have very high initial stiffnesses than the observed results. Volumetric strain curve of specimen A has failed to describe its dilation behavior whereas for specimen B, volumetric change predicted is quit higher than the observed results.

Figure 4.10 shows the predicted stress-strain relation using the Modified Cam-clay model. It is observed that for both the specimen A and B, predicted results of stress ratio, deviator stress and volumetric strain are inaccurate when plotted with the test results providing a larger stiffness than the observed results. However, the stress ratio at failure fits well with the observed results. For specimen A, volumetric strain curve does not fit

well with observed result providing excess positive dilation. On the other hand, for specimen B, c predicted volumetric strain is found satisfactory. This is mainly caused by not taking the bonding and density behavior of Dhaka clay under considerations.

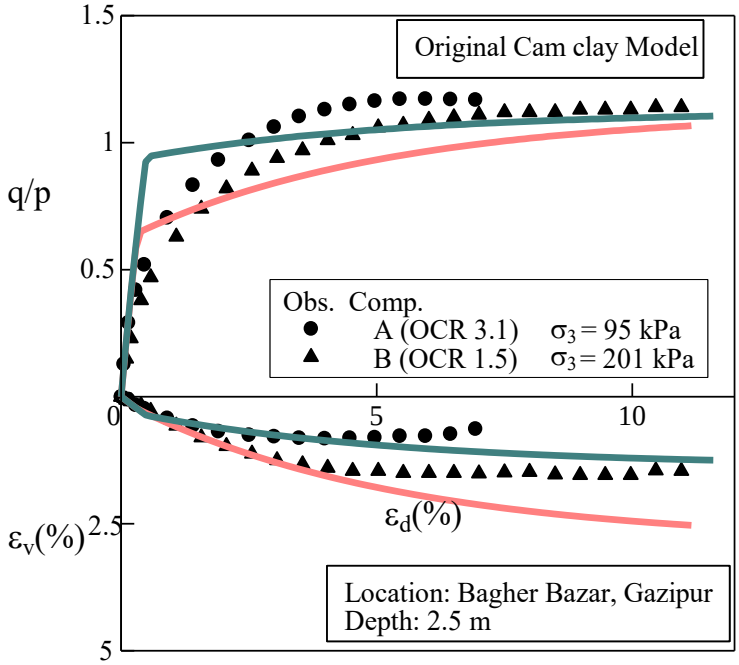

Figure 4.9 Observed and predicted stress-strain relation of Gazipur soil under CD triaxial test.

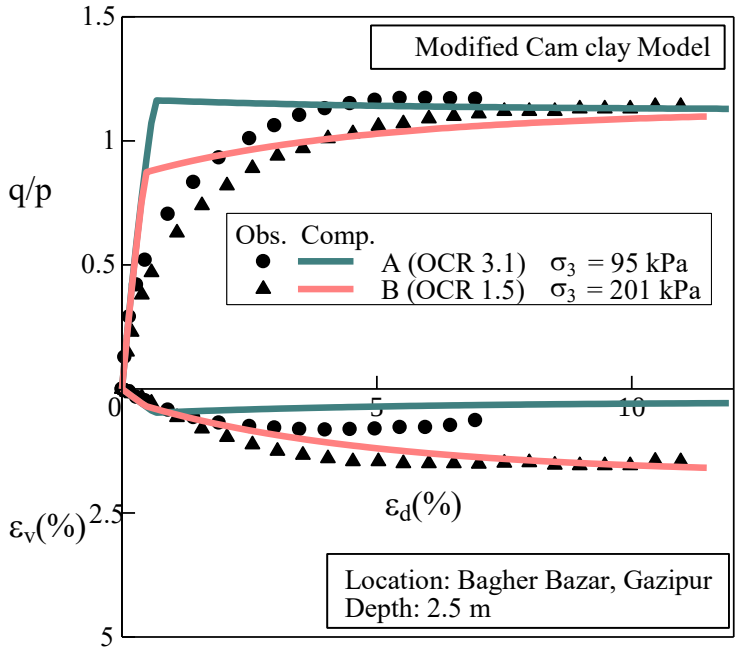

Figure 4.10 Observed and predicted stress-strain relation of Gazipur soil under CD triaxial test.

Figure 4.11 (a) and (b) shows the simulated results using Cam-clay model and Modified Cam-clay model respectively. It is observed that both the simulated results do not fit well with the tested results as the Subloading t_{ij} model as shown in Figure 4.4.

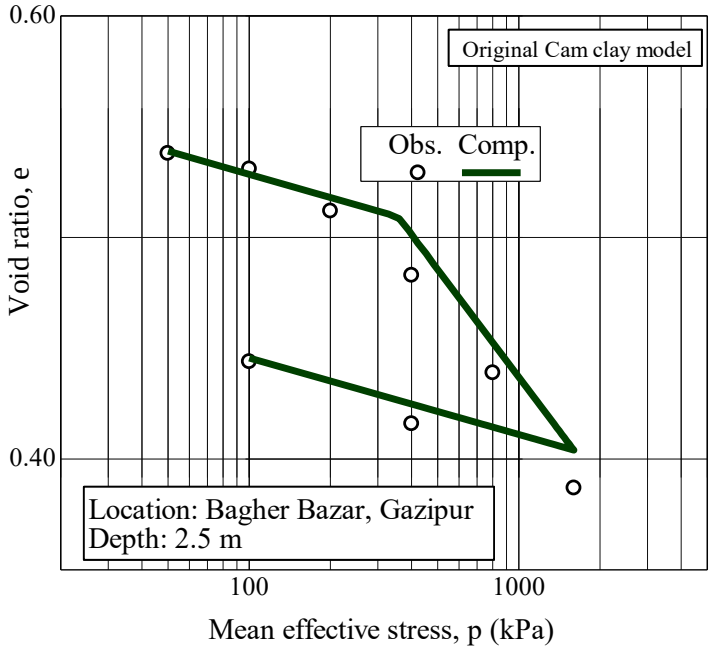

(a)

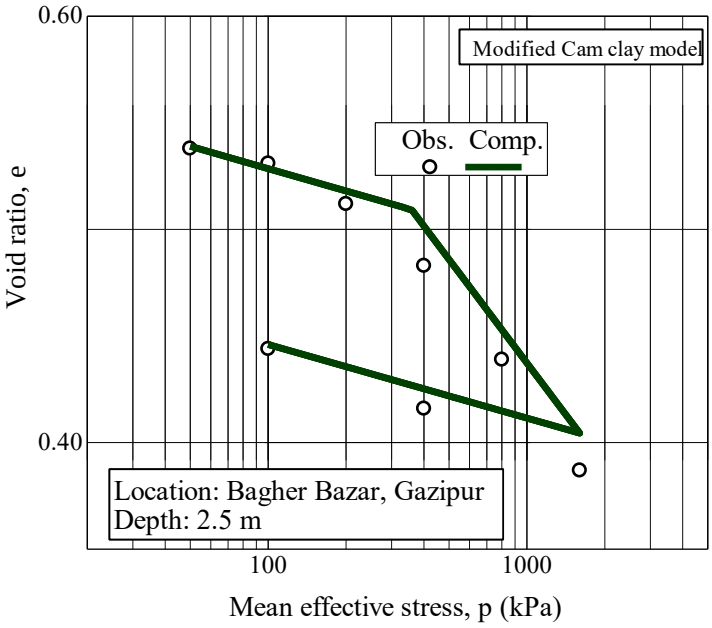

(b)

Figure 4.11 Observed and Predicted $e - lnp$ relationship of Gazipur sample (a) Cam-clay model (b) Modified Cam-clay model.

4.3.3.3 Simulations at different Initial OCR

Figure 4.12 shows the predicted results of stress strain at initial OCR 6.0 and 1.5. It is observed that, at the both OCR value soil meets the other observed and predicted results almost at the same critical stress ratio. Thus providing a realistic predicted results. At Initial OCR 1.5, it is observed that realistic dilation is predicted while using Subloading t_{ij} model.

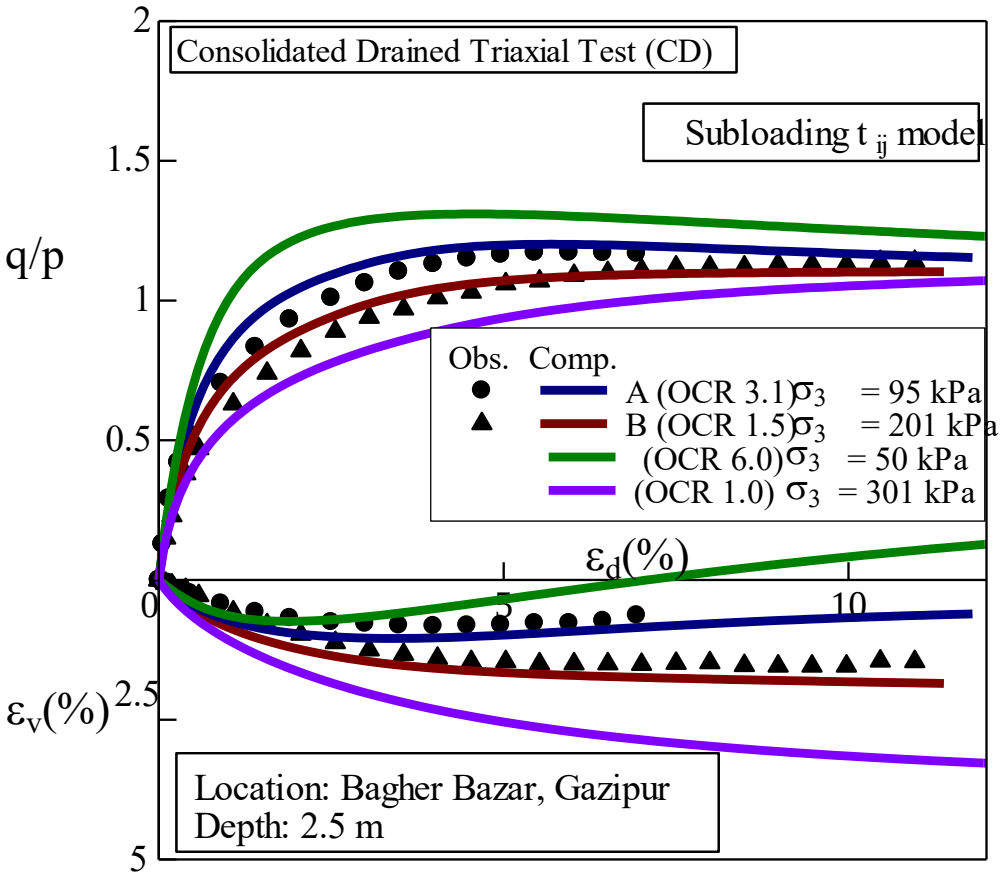

Figure 4.12 Predicted results at initial OCR 6.0 and OCR 1.0 in CD Triaxial test.

Figure 4.13 shows the predicted results at different initial OCR using Cam-clay model. It is observed that for both original and modified Cam-clay model, it is not possible describe the real soil behavior at higher OCR. However, at the normally consolidated condition, the stress-strain results can be considered to be satisfactory where the influence of density and bonding are less. On the contrary, volumetric changes are seemed to be overestimated than the real one.

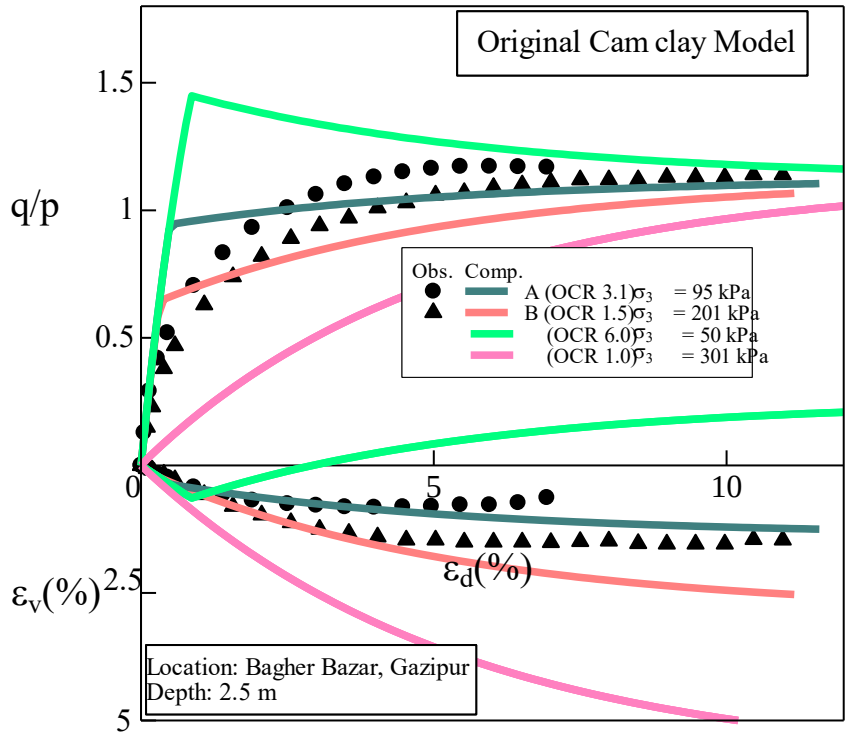

(a)

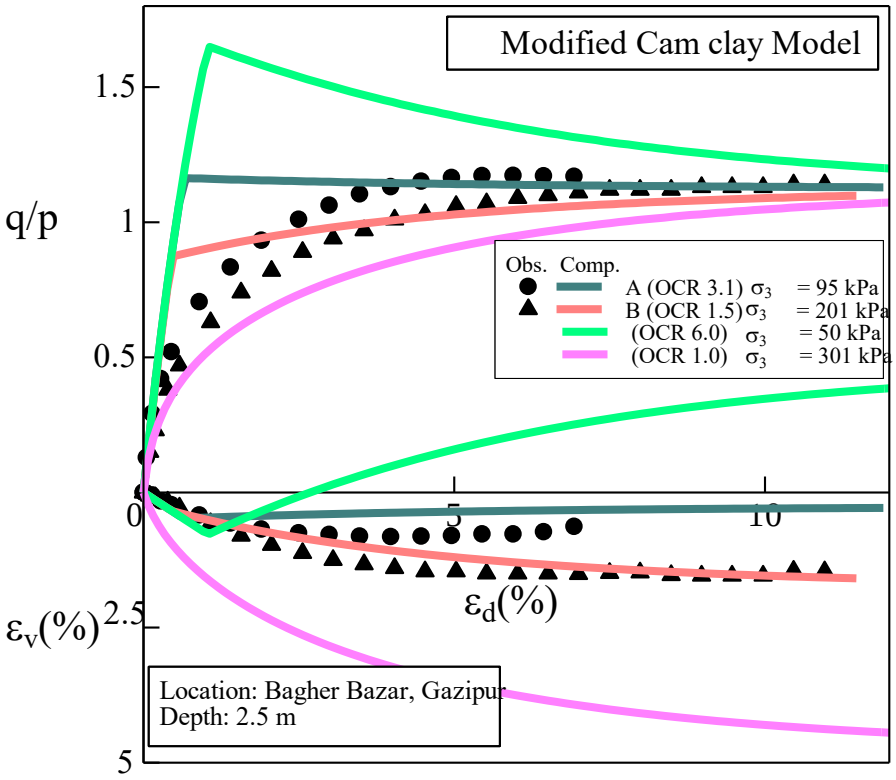

(b)

Figure 4.13 Predicted results at Initial OCR 6.0 and OCR 1.0 in CD Triaxial test using (a) Cam-clay model (b) Modified Cam-clay model.

4.3.3.4 Simulation of stress path test

In this study, all tests were conducted at constant minor effective confining pressure, σ_3. Besides this stress path, other stress path tests such as constant mean principal stress, p and major effective confining pressure, σ_1, are simulated as shown in Figure 4.14 and Figure 4.15 using the parameters obtained for Gazipur sample. In Figure 4.14 simulated results at p constant condition is presented at compression and extension condition. In Figure 4.15 simulated results are presented both at compression and extension condition under constant major principal stress. It is observed, for the same soil the stress and deformation characteristics cannot be defined uniquely using the stress invariants of ordinary models such as Cam-clay model.

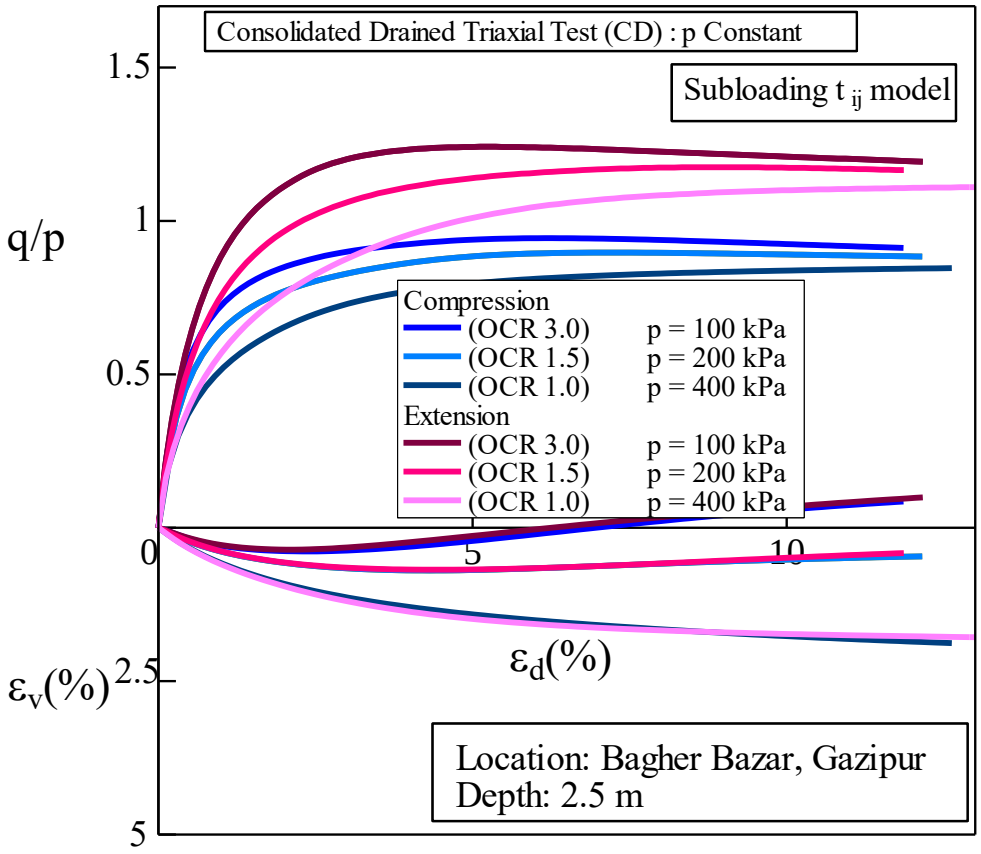

Figure 4.14 Simulated results at constant mean effective stresses, p for different OCR.

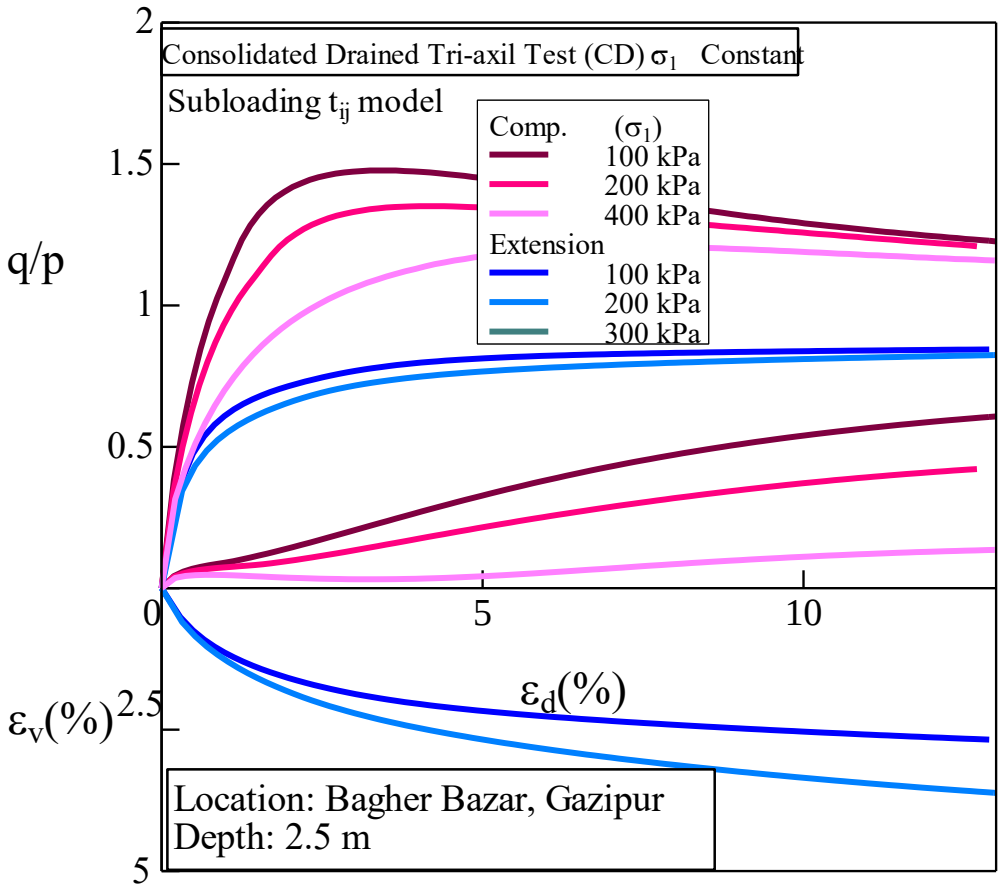

Figure 4.15 Simulated results at constant mean effective stresses, σ_3 for different OCR.

4.3.3.5 Stress-dilatancy relation

In Figure 4.16 shows the experimental and simulated results of stress-dilatncy relation using Cam-clay and Subloading t_{ij} model. In Figure 4.16 (a), for Subloading t_{ij} model it is shown that there is a unique stress-dilatancy relationship obtained at different stress path and OCR of the same soil specimen. This is because of the independency of the t_{ij} concept from the influence of intermediate principal stress. On the contrary, Cam-clay model as shown in Figure 4.16 (b) and (c) cannot describe the stress dilatancy relation uniquely under different stress conditions. It is caused by the strong influence of the intermediate principal stress on the direction of plastic strain increment.

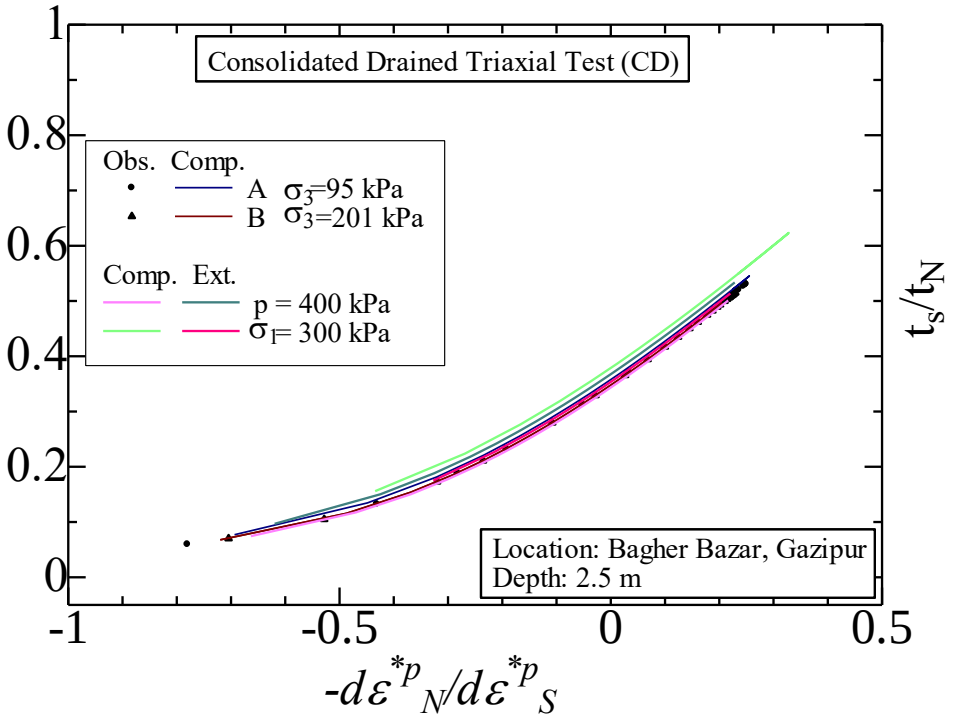

(a)

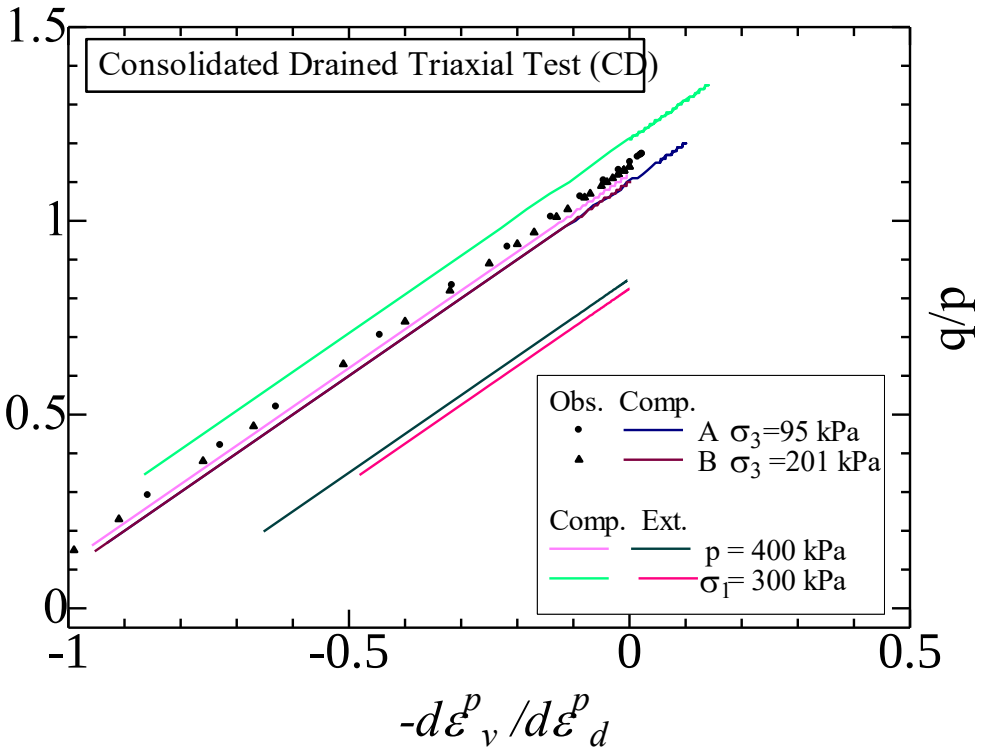

(b)

Figure 4.16 Observed and Predicted Stress-dilatancy relation of (a) Subloading t_{ij} (b) Cam-clay model

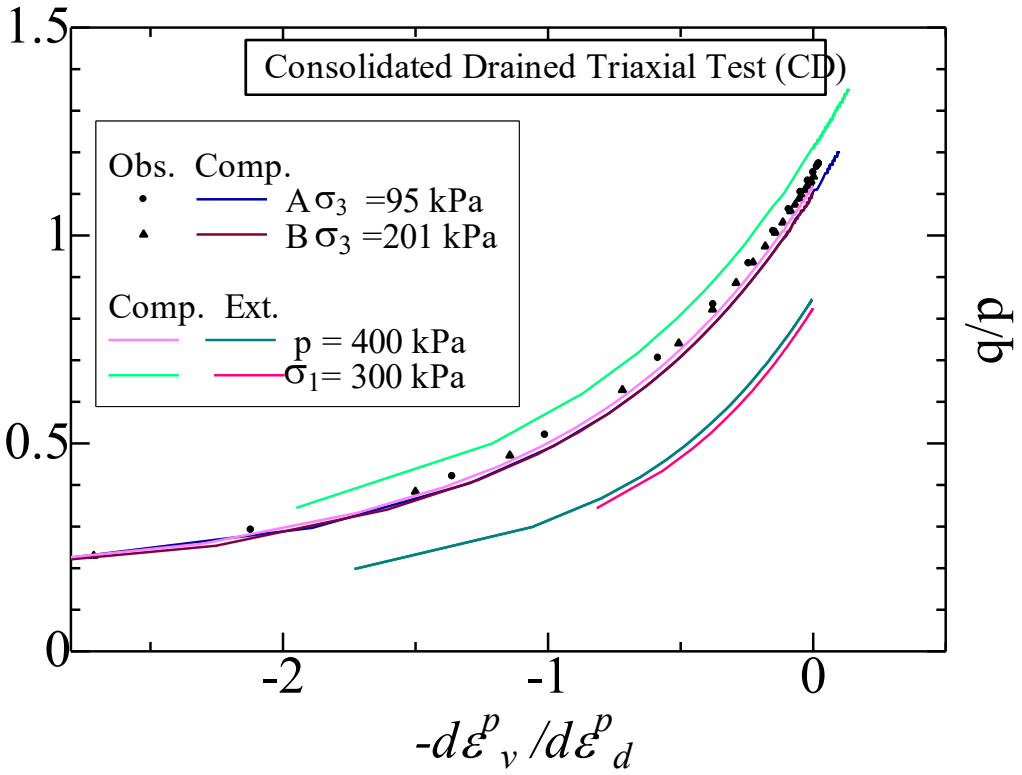

(c)

Figure 4.16 (Cont.) (c) Modified Cam-clay model under compression and extension at different stress paths.

4.3.3.6 Observed and simulated results of other locations

In the previous sections, observed and simulated results of Gazipur sample was presented. In this section from Figure 4.17 to Figure 4.28 shows the observed and simulated results of Mirpur DOHS, Rokeya Sarani and Savar samples. From the simulations it was found that, Subloading t_{ij} can describe well the stress-strain properties of the samples accurately. On the contrary, both Cam-clay and Modified Cam-clay model cannot describe it satisfactorily.

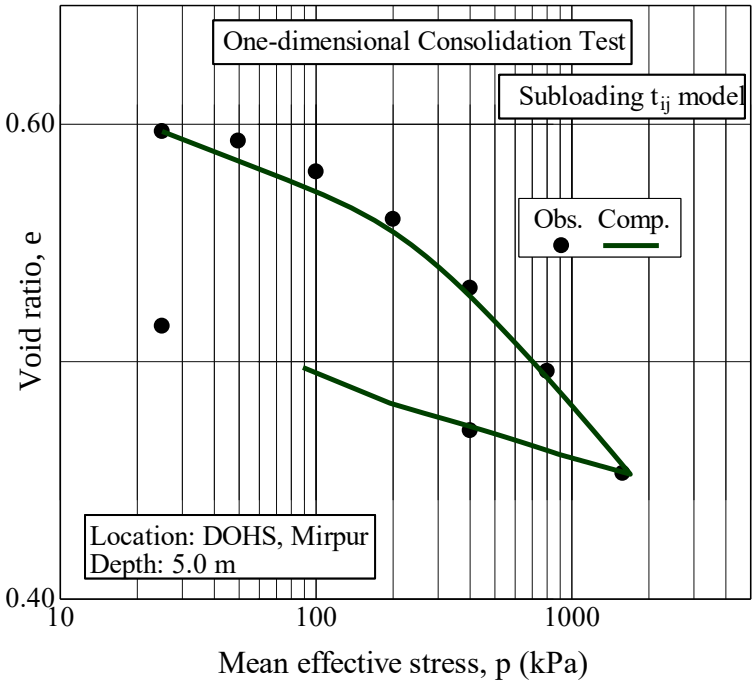

Figure 4.17 Observed and Predicted $e - lnp$ relationship of Mirpur DOHS sample.

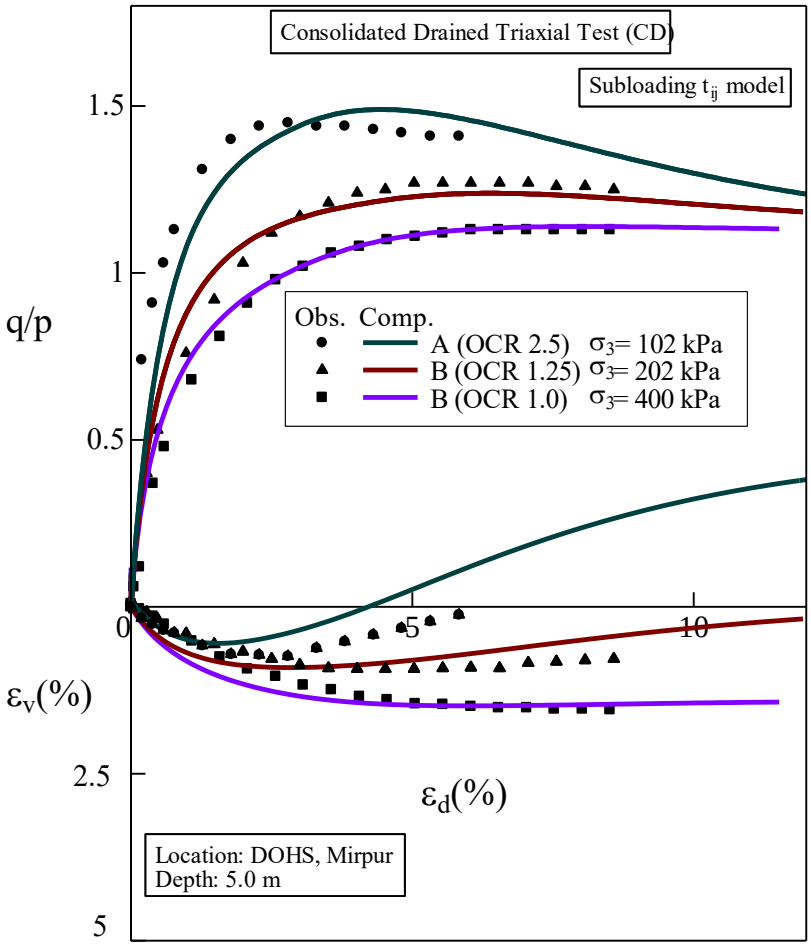

Figure 4.18 Observed and predicted stress-strain relation of Mirpur DOHS soil.

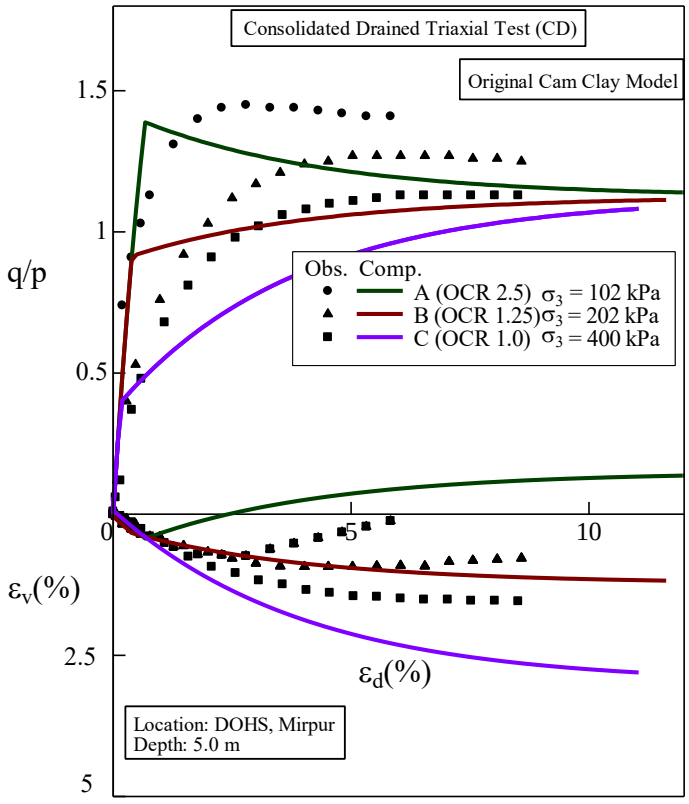

(a)

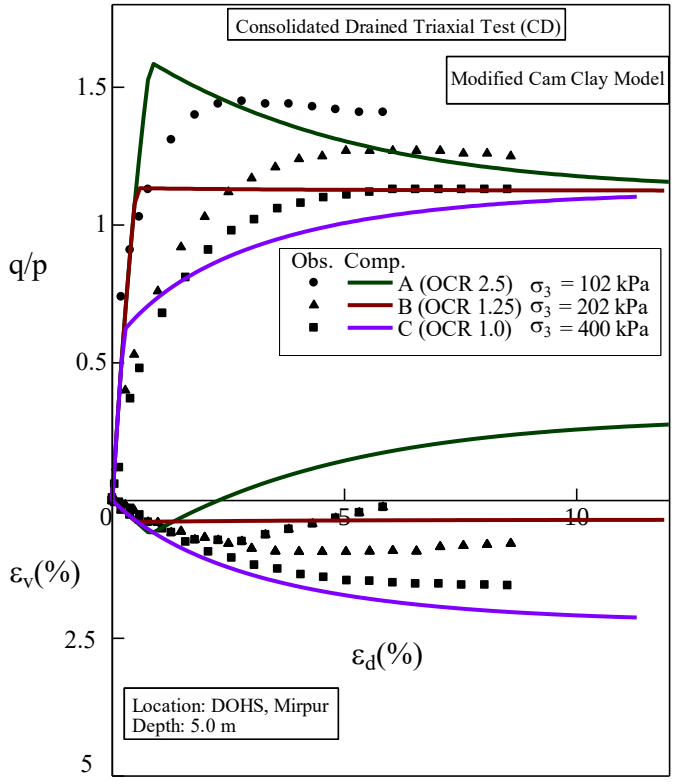

(b)

Figure 4.19 Observed and predicted stress-strain relation of Mirpur DOHS soil (a) Cam-clay (b) Modified Cam-clay model.

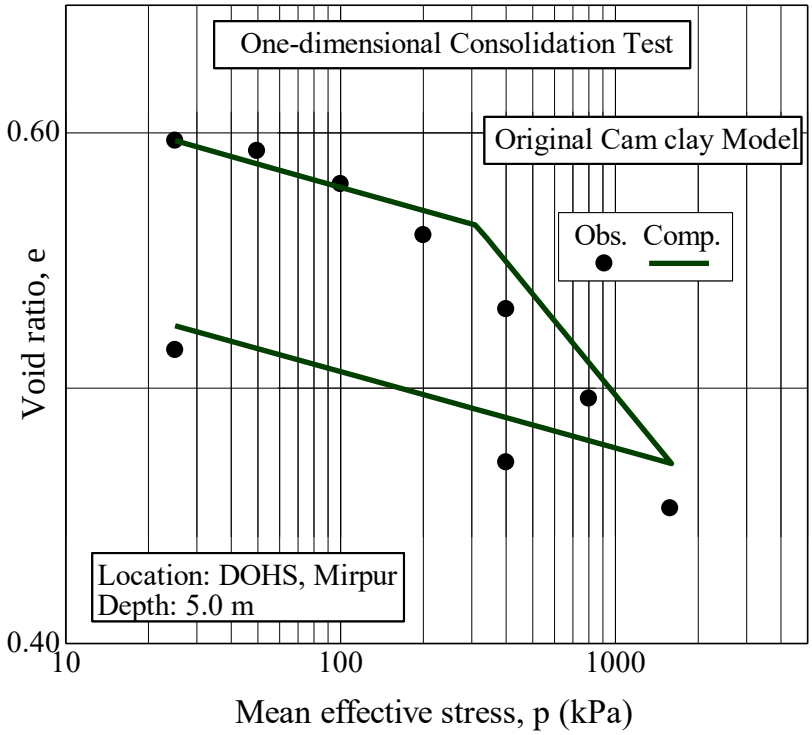

(a)

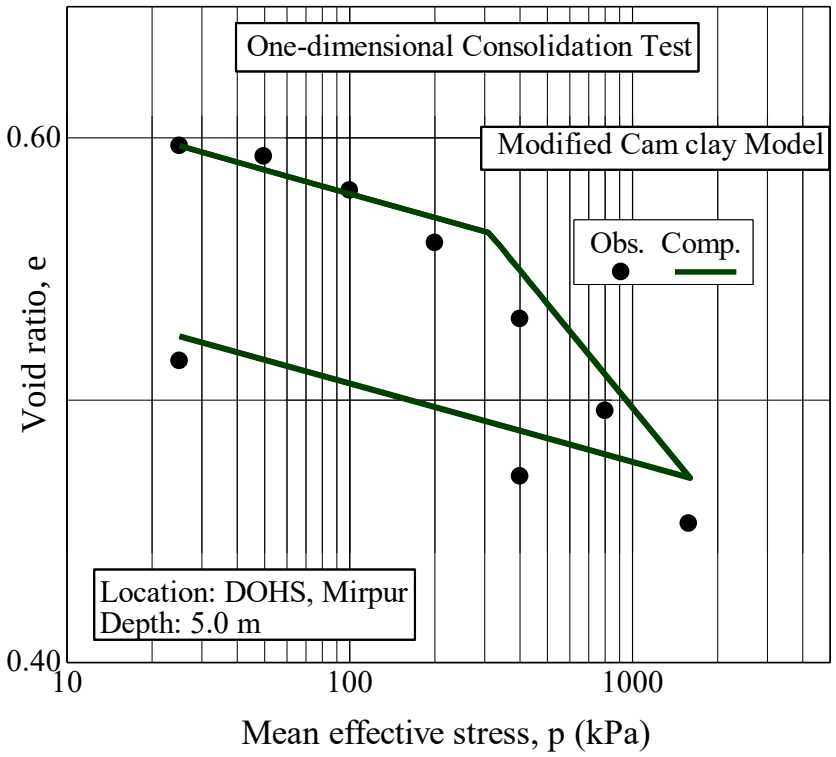

(b)

Figure 4.20 Observed and Predicted $e - lnp$ relationship of Mirpur DOHS sample (a) Cam-clay model (b) Modified Cam-clay model.

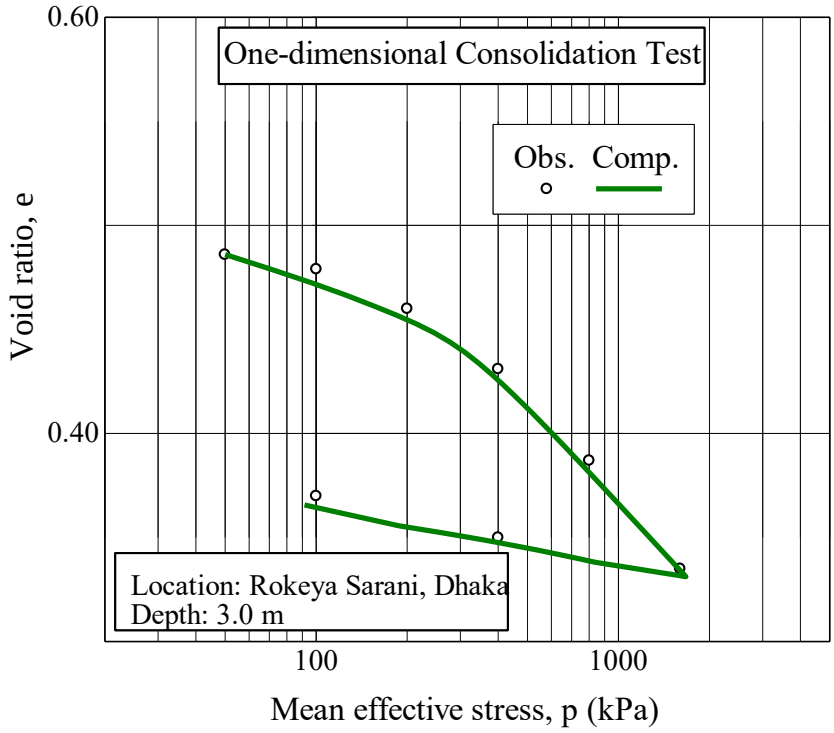

Figure 4.21 Observed and Predicted $e - lnp$ relationship of Rokeya Sarani sample.

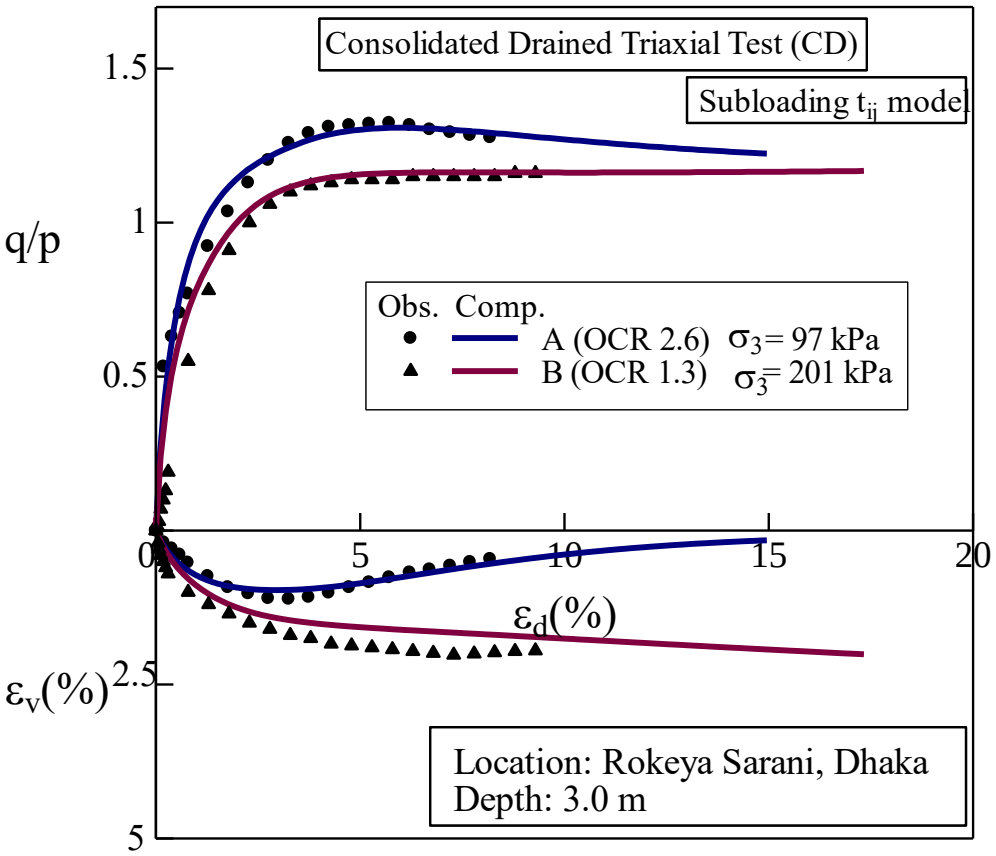

Figure 4.22 Observed and predicted stress-strain relation of Rokeya Sarani soil.

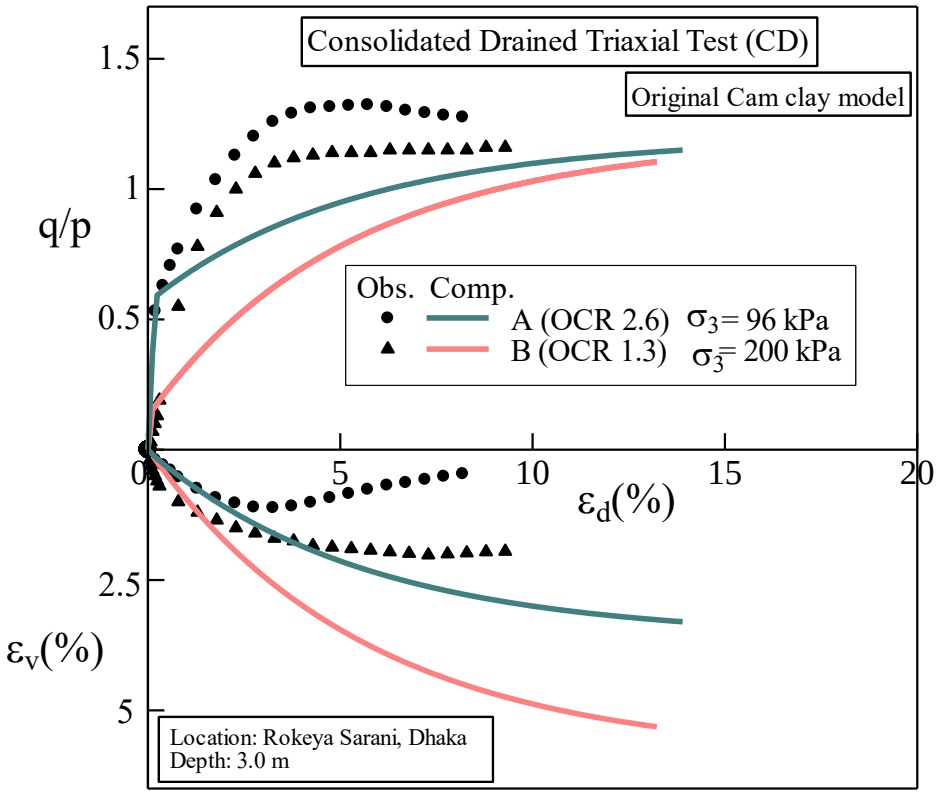

(a)

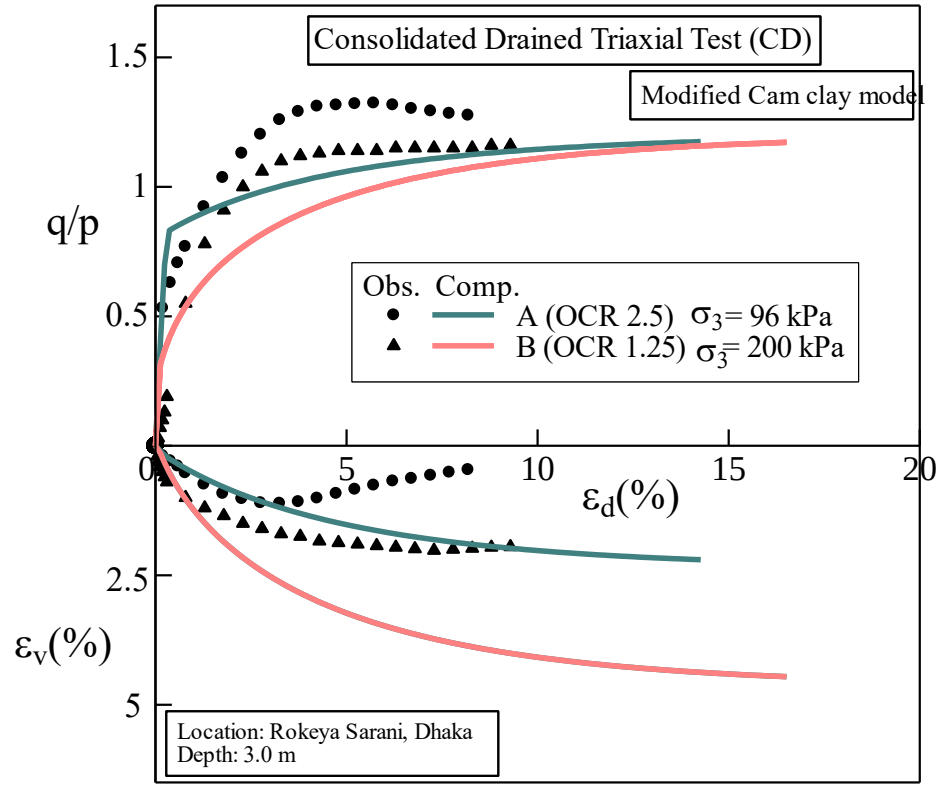

(b)

Figure 4.23 Observed and predicted stress-strain relation of Rokeya Sarani soil (a) Cam-clay (b) Modified Cam-clay model.

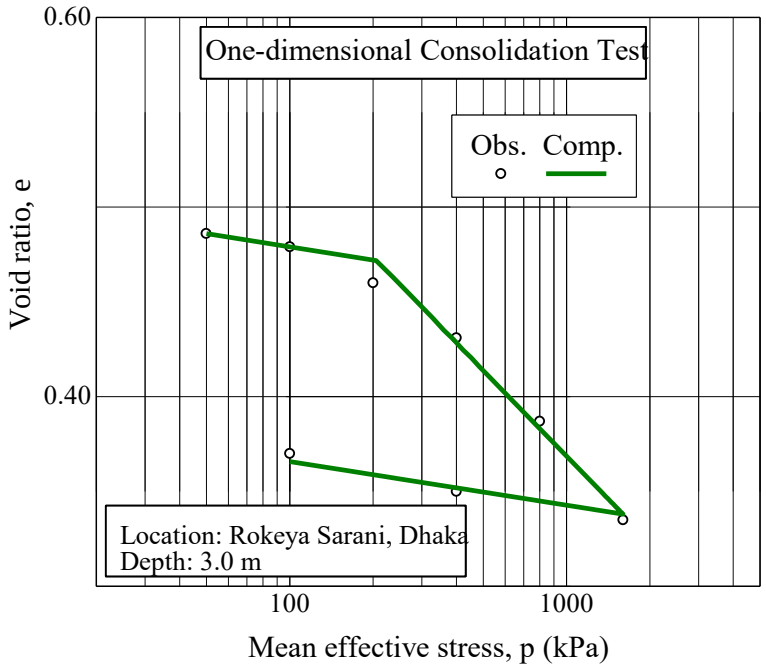

(a)

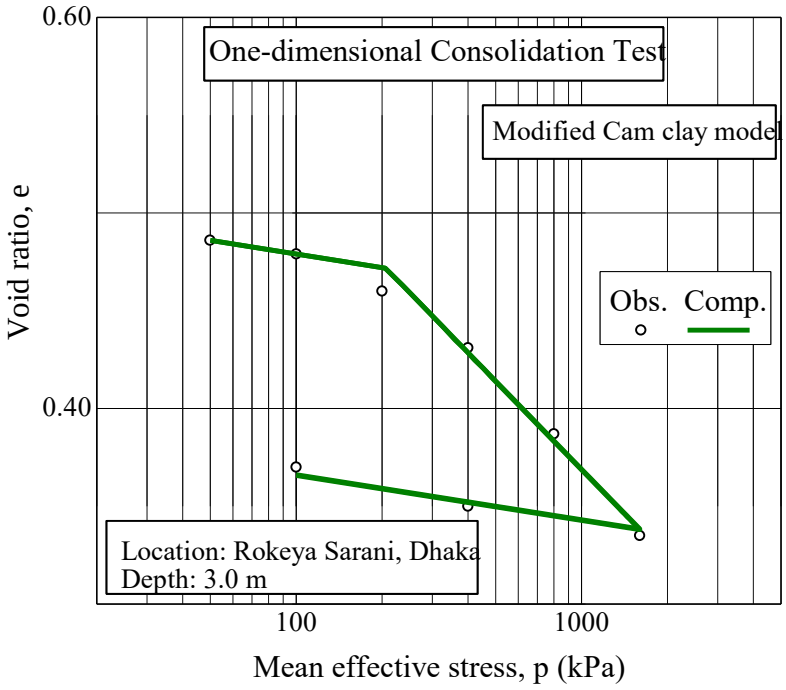

(b)

Figure 4.24 Observed and Predicted $e - lnp$ relationship of Rokeya Sarani sample (a) Original Cam-clay model (b) Modified Cam-clay model.

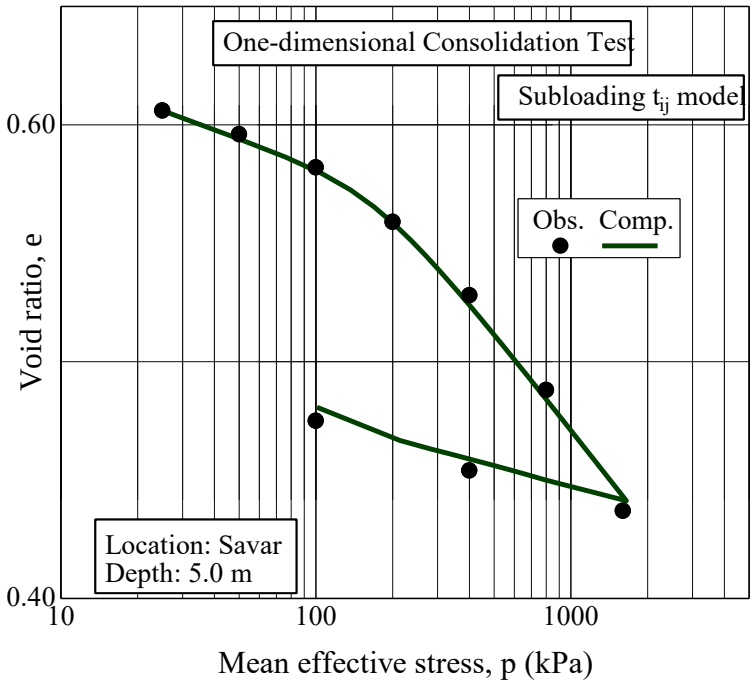

Figure 4.25 Observed and Predicted $e - lnp$ relationship of Savar sample.

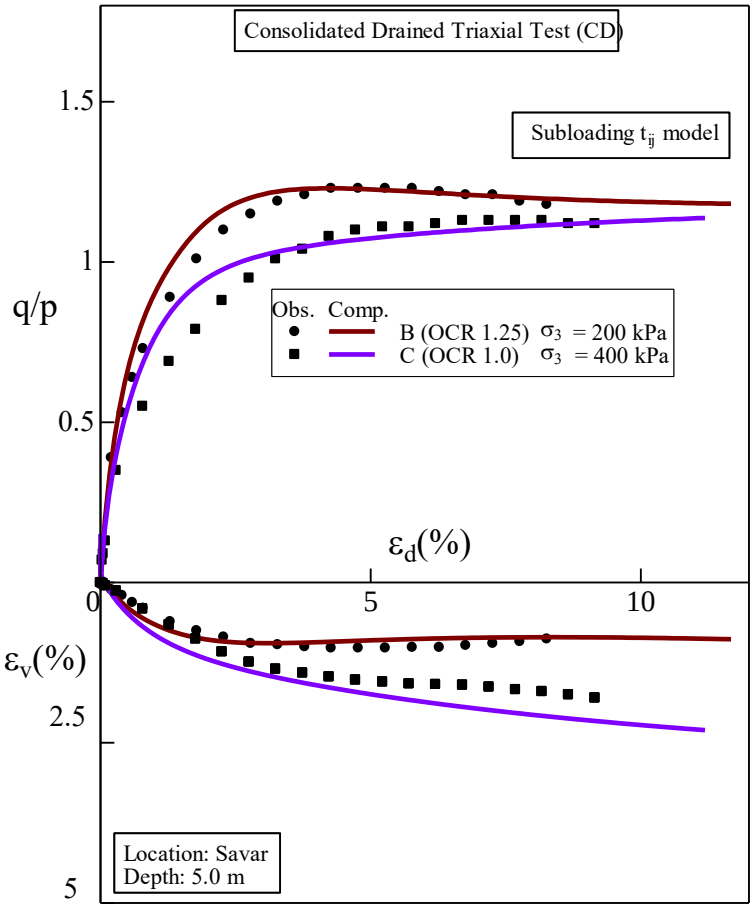

Figure 4.26 Observed and predicted stress-strain relation of Savar soil under CD triaxial compression test.

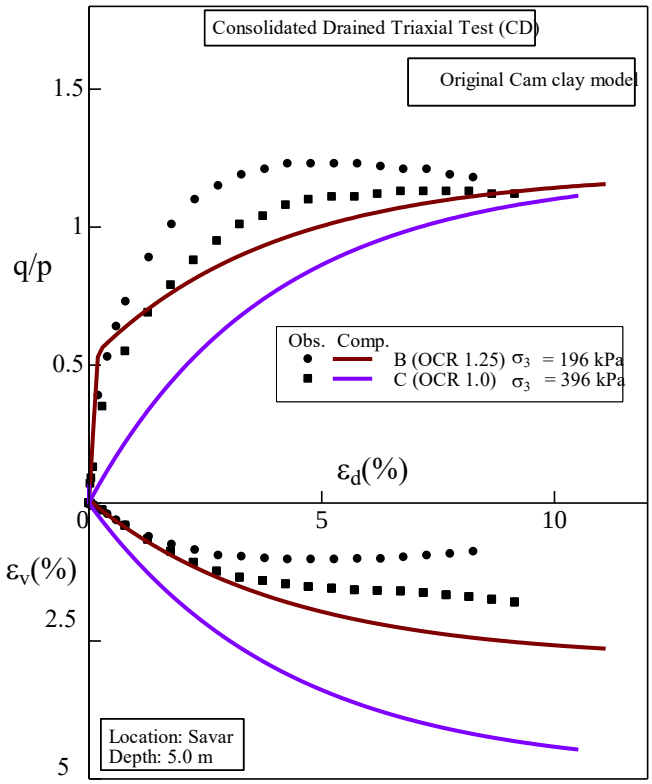

(a)

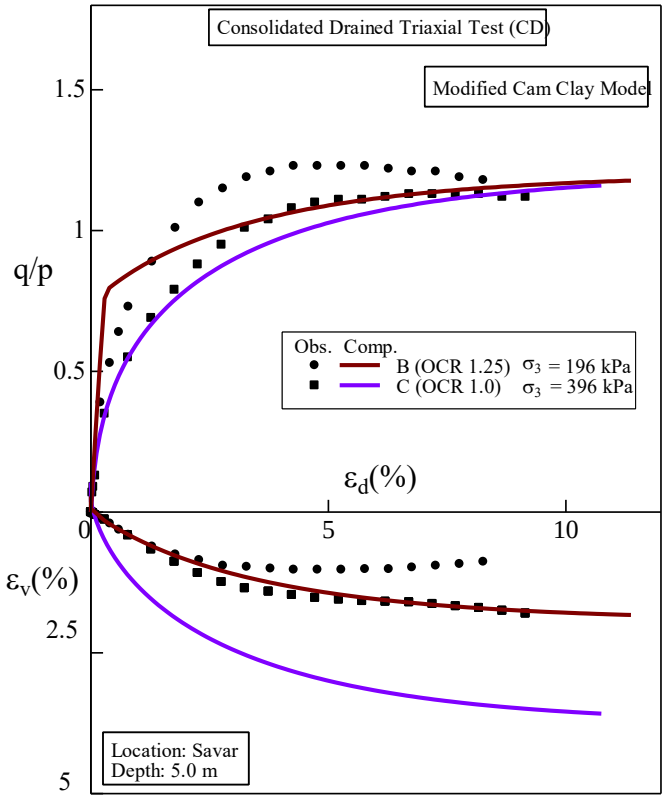

(b)

Figure 4.27 Observed and predicted stress-strain relation of Savar soil.

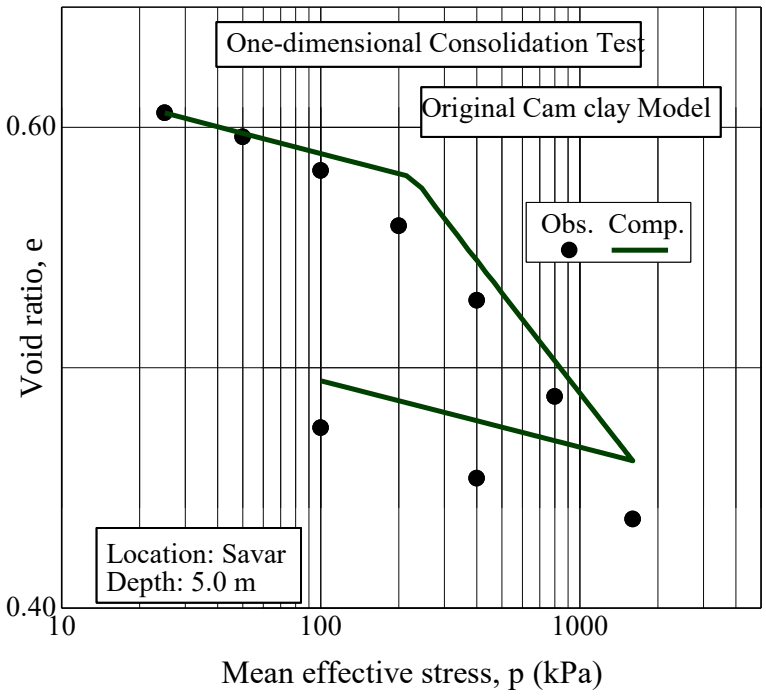

(a)

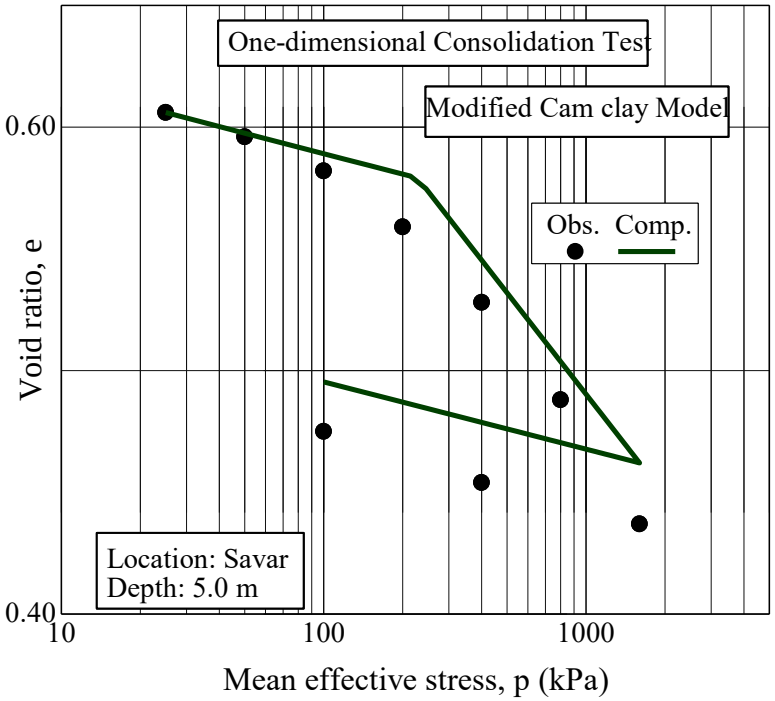

(b)

Figure 4.28 Observed and Predicted $e - lnp$ relationship of Savar sample (a) Original Cam-clay model (b) Modified Cam-clay model.

4.4 Model Parameters Obtained at Undrained Condition

In this study, Samples collected from Shagufta at Mirpur and Baridhara DOHS area are tested at undrained condition. To obtain the compression and swelling properties, one dimensional consolidation test was conducted. To obtain critical stress ratio, consolidated undrained triaxial tests are conducted according to the relevant ASTM standards.

4.4.1 One-dimensional Consolidation Properties

Table 4.4 presents the specimen details for consolidation test at natural condition. The samples were collected from a depth in the range of 5.0 m to 8.0 m below the existing ground level. Figure 4.29 shows the observed $e - lnp$ relationship of the samples collected for undrained analysis. From Figure 4.29, compression index, C_c was found as 0.16 ($\lambda = 0.07$) and swelling index, Cr was found in the range of 0.02 to 0.03 ($\kappa = 0.01$ to 0.015). The pre-consolidation pressure from graphical method was obtained in the range of 170 to 400 kPa.

Table 4.4 Consolidation Specimen Details

Sample Locations	Shagufta	Baridhara DOHS
Initial Unit Weight	20.6 kN/m^3	20.9 kN/m^3
Initial Moisture Content	21 %	30 %
Initial Void Ratio	0.56	0.63
Initial Degree of Saturation	89 %	91 %
Final Degree of Saturation	100 %	100 %
Depth below EGL	8.0 m	5.0 m
Preconsolidation Pressure	400 kPa	170 kPa

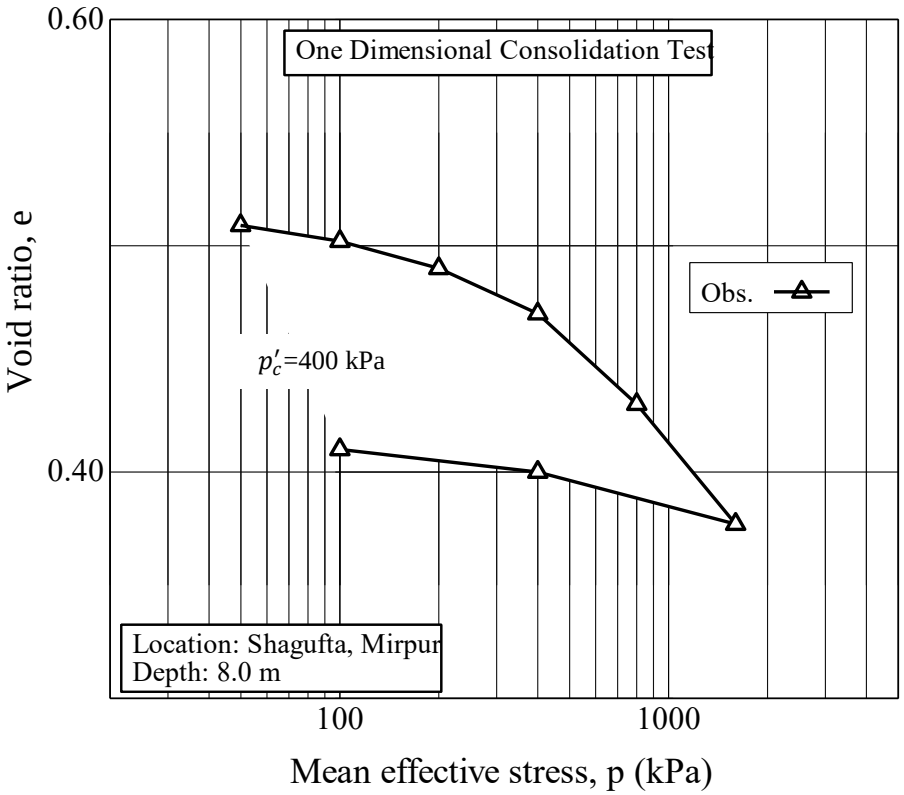

(a) Shagufta, Mirpur

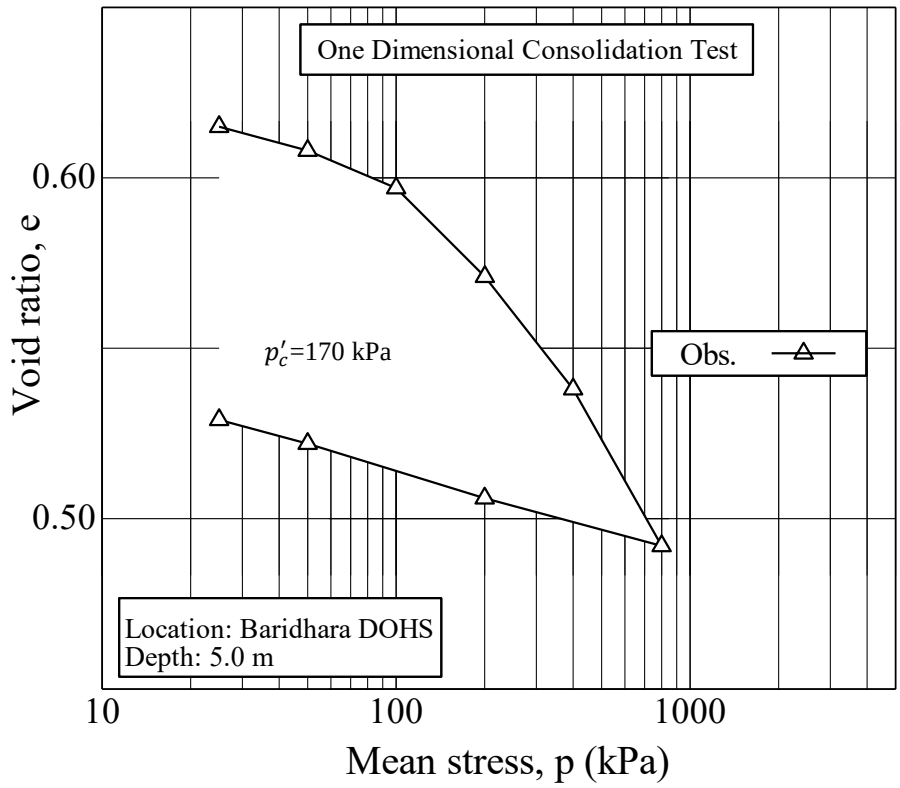

(b) Baridhara DOHS

Figure 4.29 Observed $e - lnp$ relationship of (a) Shagufta (b) Baridhara sample.

4.4.2 Consolidated Undrained Triaxial Properties

Table 4.2 presents the specimen details for specimen of various locations for consolidated drained triaxial tests. In general, specimen A, B and C are tested at effective confining stress of 100 kPa, 200 kPa and 400 kPa respectively. From consolidation test results in Sec 4.4.1, the initial OCR of specimen was obtained in the range of 1.0 to 2.7. From the observed stress-strain relationship of the specimen as shown in Figure 4.30 and Figure 4.32, the critical stress ratio, η was found in the range of 2.5 to 3.3

Table 4.5 Triaxial Specimen Description

Specimen	A	B	C
Location: Gazipur			
Initial Unit Weight	20.6 kN/m^3	20.6 kN/m^3	20.5 kN/m^3
Moisture Content	21 %	21 %	20 %
Void Ratio	0.53	0.53	0.53
B Value	0.95	0.96	0.95
Effective Confining Stress	147 kPa	302 kPa	592 kPa
Initial OCR	2.7	1.3	1.0
Critical Stress Ratio	2.5		
Location: Mirpur DOHS			
Initial Unit Weight	20.9 kN/m^3	20.7 kN/m^3	-
Moisture Content	31 %	30 %	-
Void Ratio	0.63	0.63	-
B Value	0.97	0.96	-
Effective Confining Stress	147 kPa	592 kPa	-
Initial OCR	2.7	1.0	-
Critical Stress Ratio	3.3		

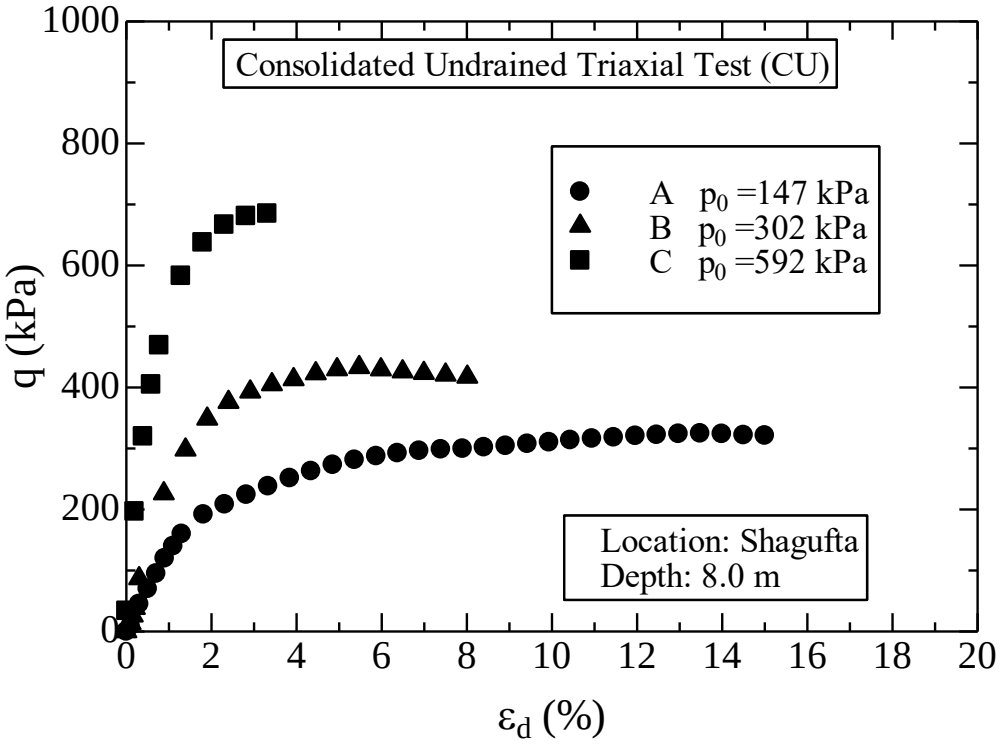

(a)

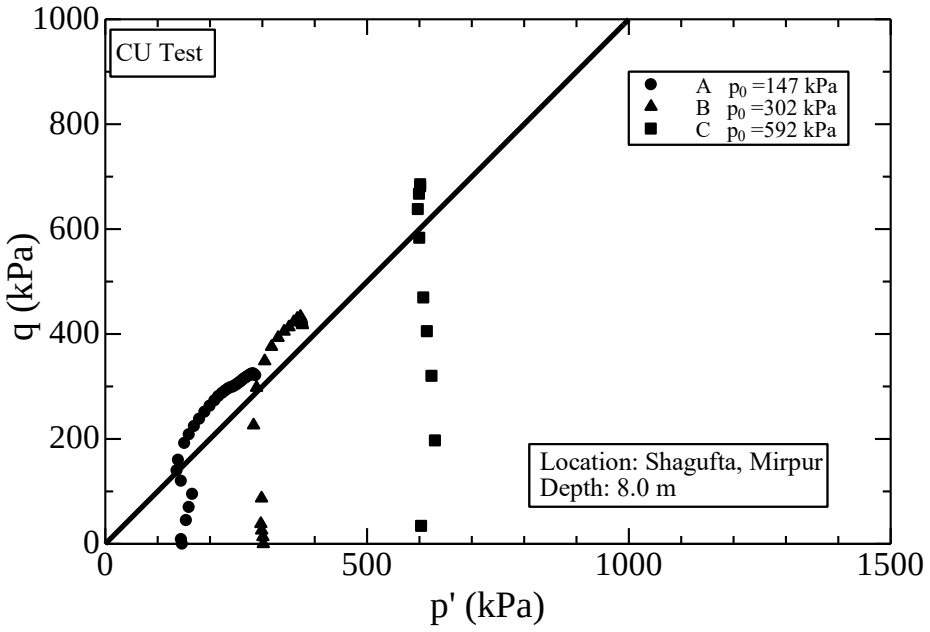

(b)

Figure 4.30 Observed (a) stress-deviator strain-volumetric strain relationship, (b) effective stress path of Shagufta Sample.

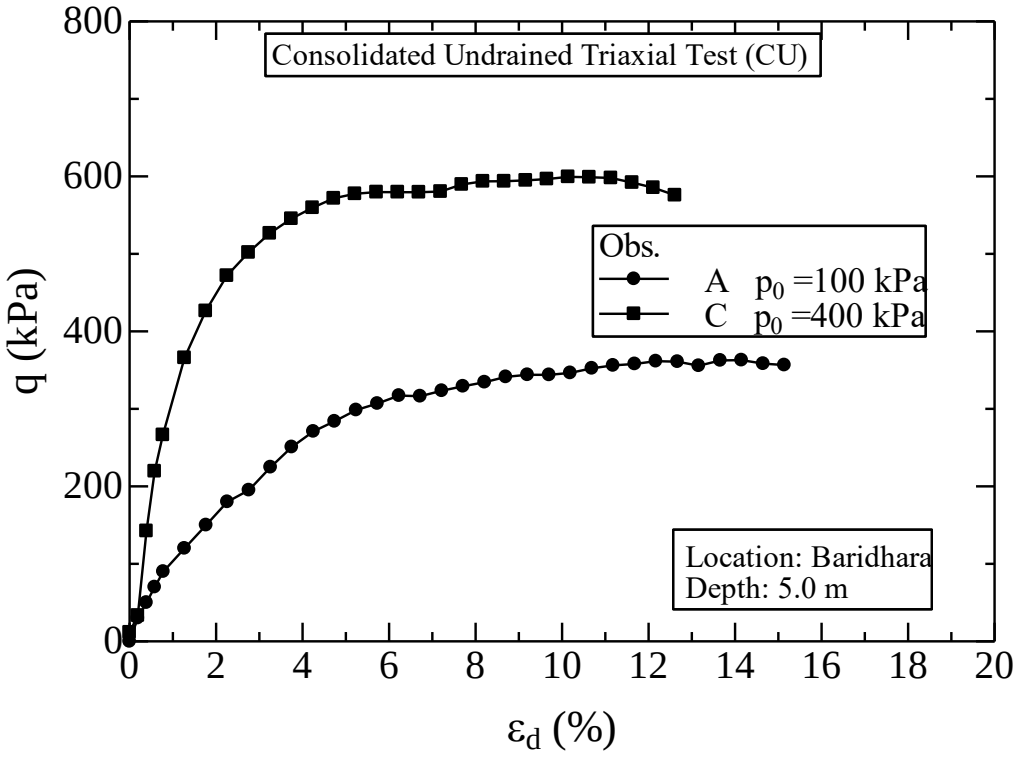

(a)

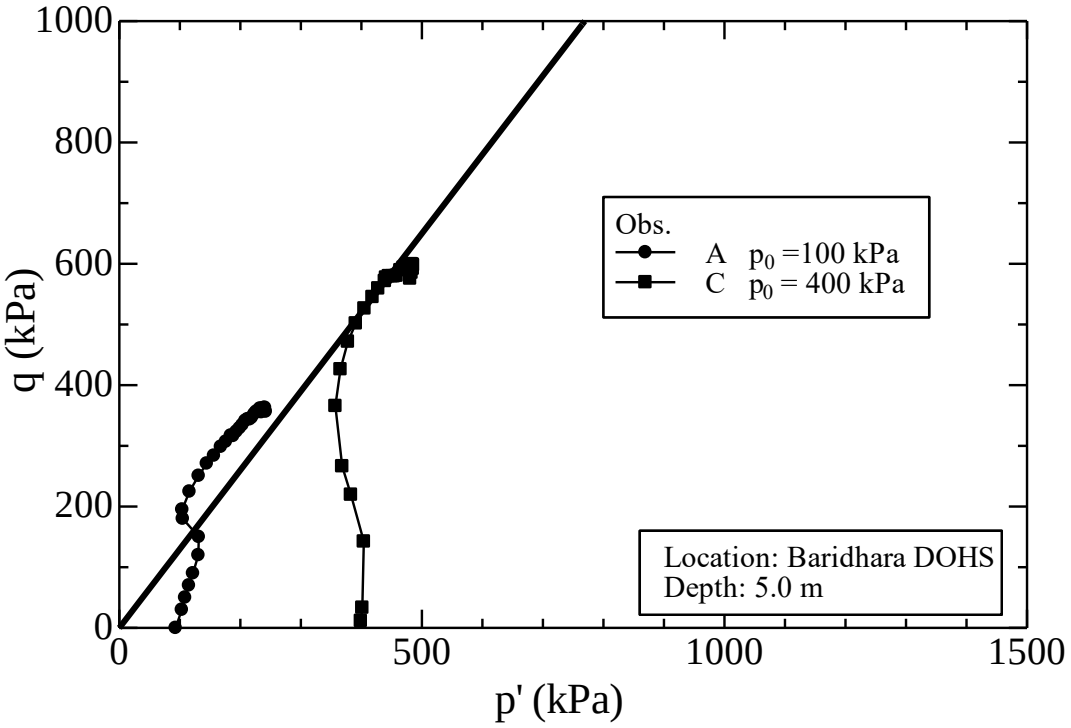

(b)

Figure 4.31 Observed (a) stress-deviator strain-volumetric strain relationship, (b) effective stress path of Baridhara sample.

4.4.3 Simulations of the Test Results

The parameters obtained from the one-dimensional consolidation test and consolidated undrained triaxial test are listed in Table 4.6. As discussed before, parameters obtained from the one-dimensional consolidation and triaxial compression tests are required by both the models. In addition, to take into account the effect of density and bonding, Subloading t_{ij} model requires the density parameter, *a* and bonding parameter, *b*.

Table 4.6 Material parameters at undrained condition

Parameter	Notations	Gazipur	Mirpur DOHS
Compression index	λ	0.07	0.07
Swelling index	κ	0.010	0.015
Void ratio at atmospheric pressure (98 kPa)	N	0.60	0.66
Critical state stress ratio	R_{CS}	2.5	3.3
Poisson's ratio	v_e	0.2	0.2
Shape of yield surface	β	1.5	1.5
Influence of density	a	450	300
Influence of bonding	b	45	30

4.4.3.1 Subloading t_{ij} model

Table 4.6 shows the model parameters including density and bonding obtained from the best fitted predicted $e - lnp$ curve with the observed result. Figure 4.32 shows that the simulated $e - lnp$ relation fits well with observed results of Shagufta sample using the parameters listed in Table 4.6.

From the parameters obtained, it was observed that the influence of bonding is large during undrained condition as compared to drained condition. The value of bonding parameter is 45 whereas during drained condition it was 10. However, both the Gazipur and Shagufta samples are of almost similar density and OCR. Hence the density parameter is found almost same as previous.

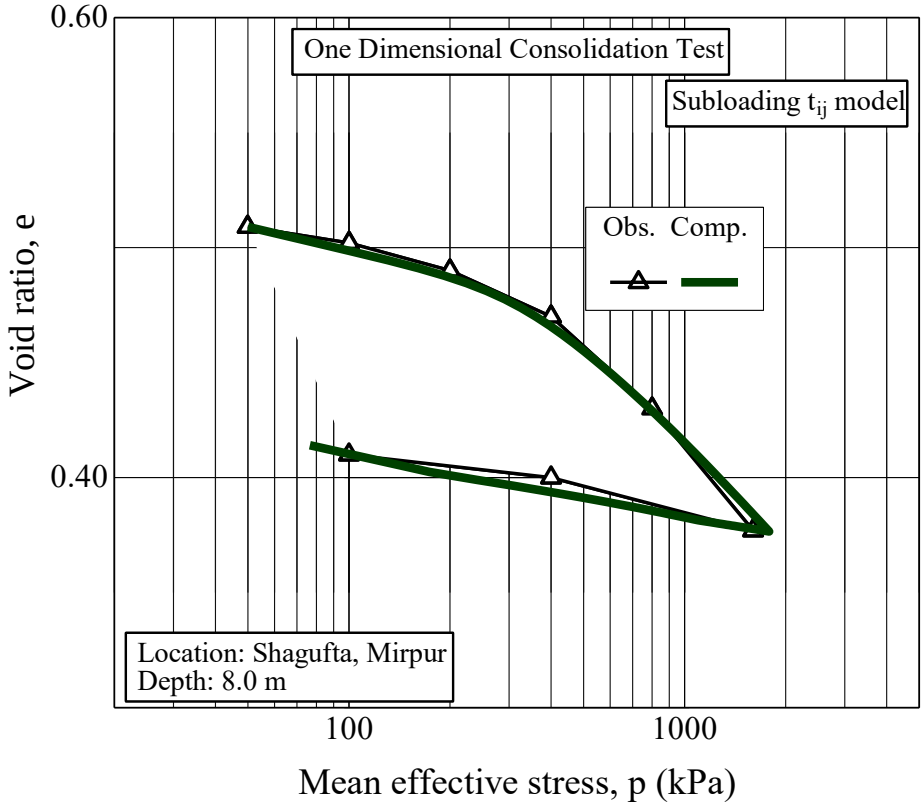

Figure 4.32 Observed and Predicted $e - lnp$ relationship of Shagufta sample.

In Figure 4.33, predicted results using Subloading t_{ij} model is plotted with the observed stress-strain results from CU triaxial test. It was observed that the predicted stress ratio, deviator strain, volumetric strain fitted well with observed results from test.

Figure 4.34 shows the observed and predicted effective stress path of the specimen A and B in drained compression test. It was observed that the predicted results fitted well with the observed test results.

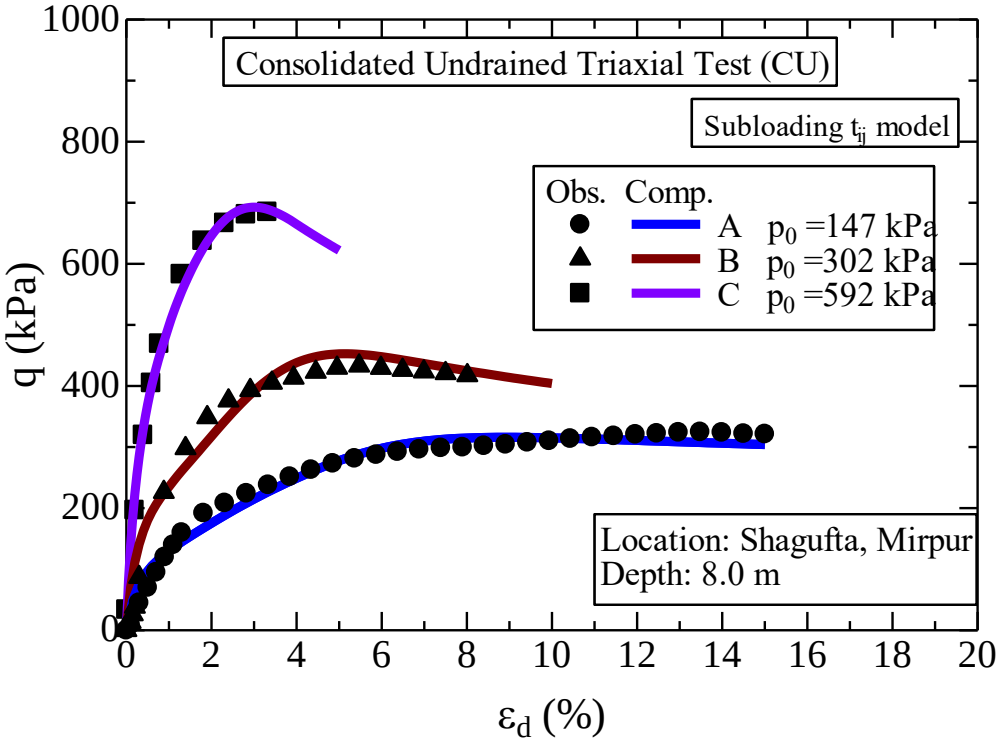

Figure 4.33 Observed and predicted stress-strain relation of Shagufta sample.

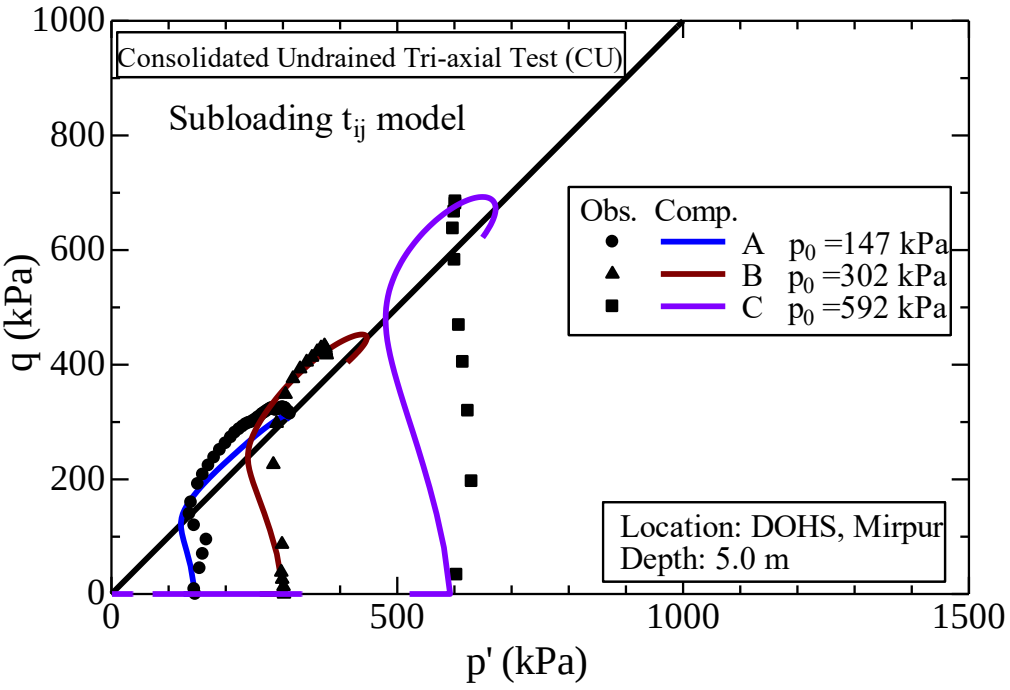

Figure 4.34 Observed and predicted effective stress path of Shagufta sample.

4.4.3.2 Cam-clay model

Performance of both Cam-clay and Modified Cam-clay model was evaluated by plotting the predicted results against the observed test results. Figure 4.35 and Figure 4.36 shows the predicted stress-strain relation and effective stress path plots using the original Cam-clay model. Material parameters obtained from the consolidation and triaxial test as listed in Table 4.6 were used for the simulation. It was observed that the predicted results does not fit with the tested results. All the observed deviator stress results are larger than the predicted results. Also, the stiffness was found unrealistic when compared with the observed results. At undrined condition, it was found that Dhaka soil showed larger strength due to bonding effect. As the Cam-clay model does not consider the effect of bonding, predicted results became smaller than the observed test results.

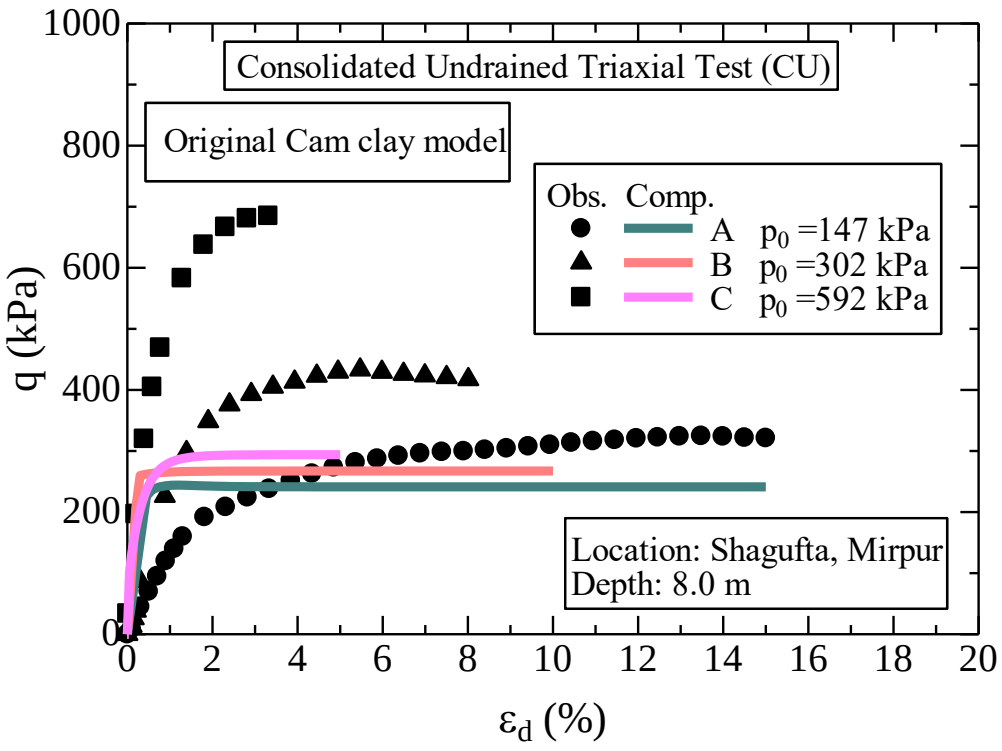

Figure 4.35 Observed and predicted stress-strain relation of Shagufta sample.

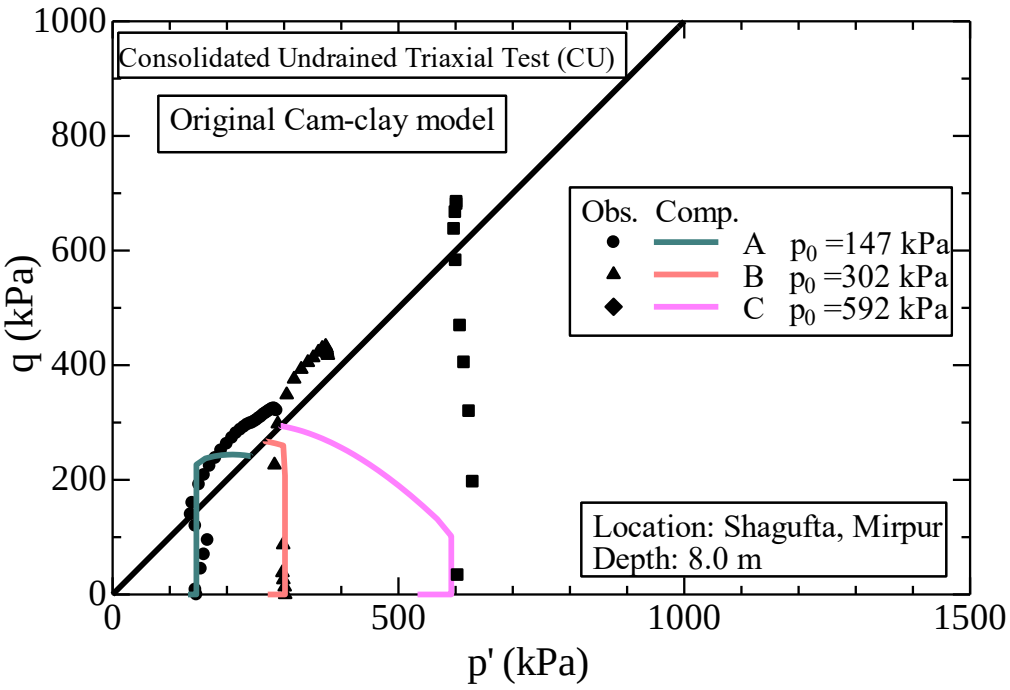

Figure 4.36 Observed and predicted effective stress path in CU triaxial test.

Figure 4.37 shows the predicted stress-strain relation using the modified Cam-clay model. It was observed that for specimen A, predicted results can successfully capture the peak stress, although the stiffness does fit with the observed results. In case of specimen B and C, the modified Cam-clay model was failed to predict the peak strength. Figure 4.38 shows the effective stress path plot of all the specimen.

Figure 4.39 (a) and (b) shows the simulated results using Original Cam-clay model and Modified Cam-clay model respectively. It was observed that both the simulated results does not fit well with the tested results as the subloading t_{ij} model as shown in Figure 4.32.

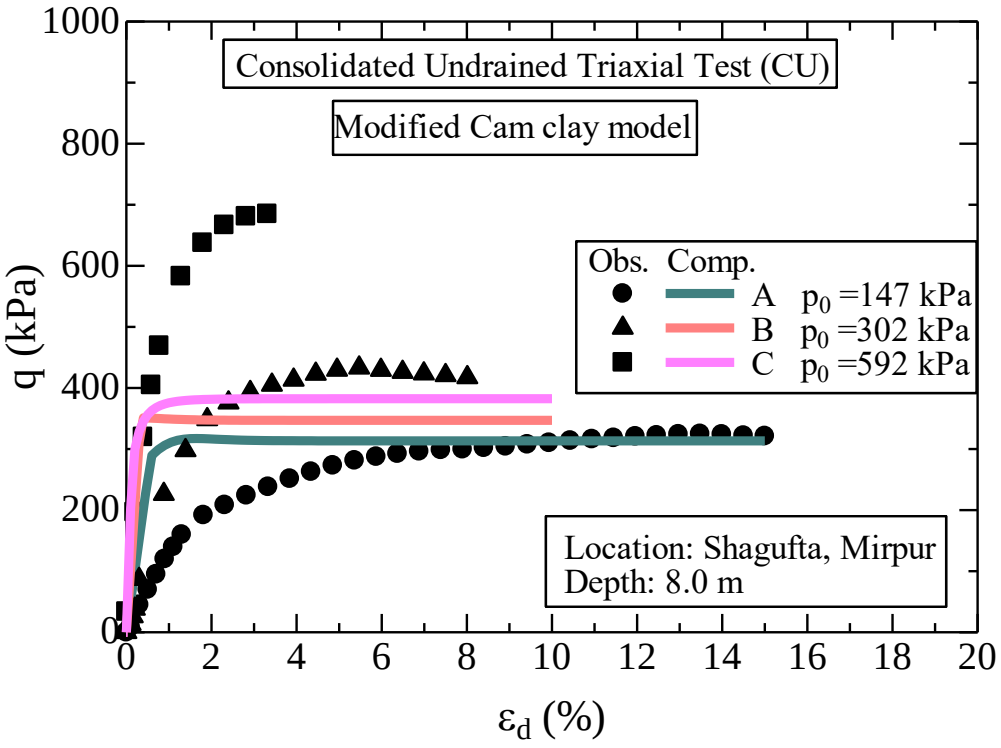

Figure 4.37 Observed and predicted stress-strain relation at undrained condition.

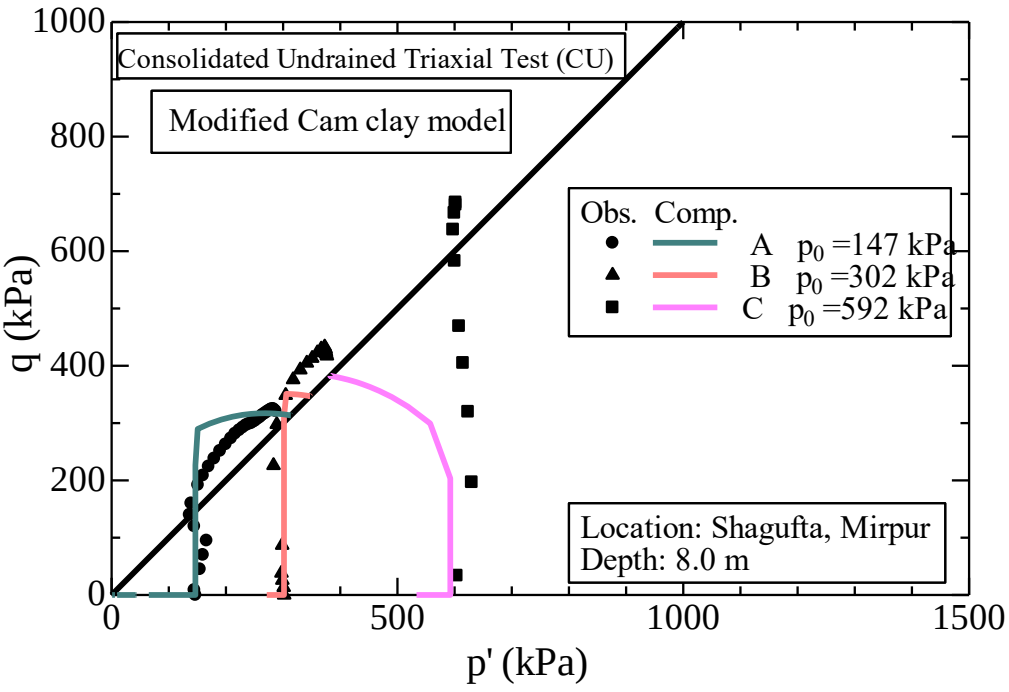

Figure 4.38 Observed and predicted effective stress path in CU triaxial compression test.

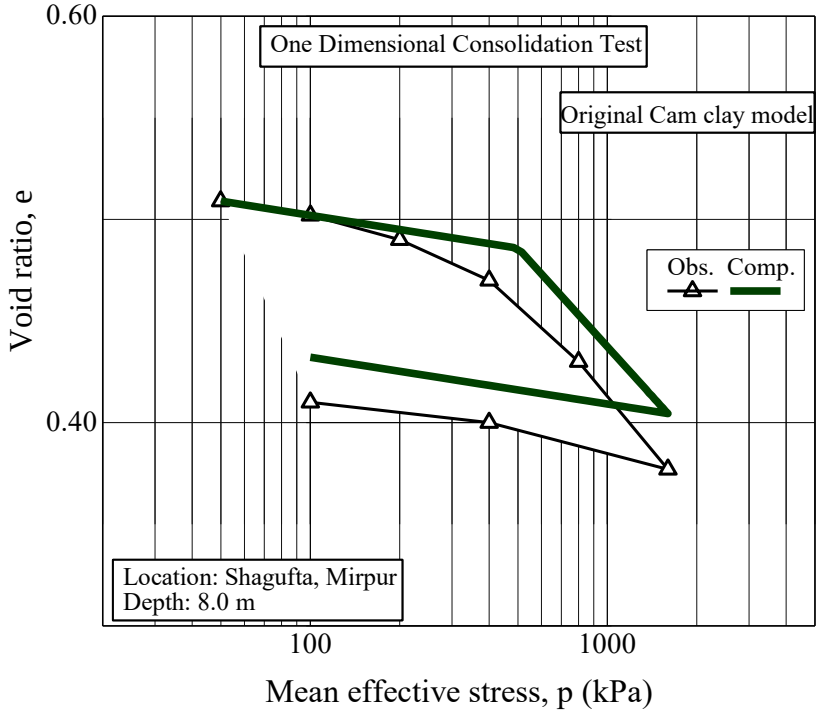

(a)

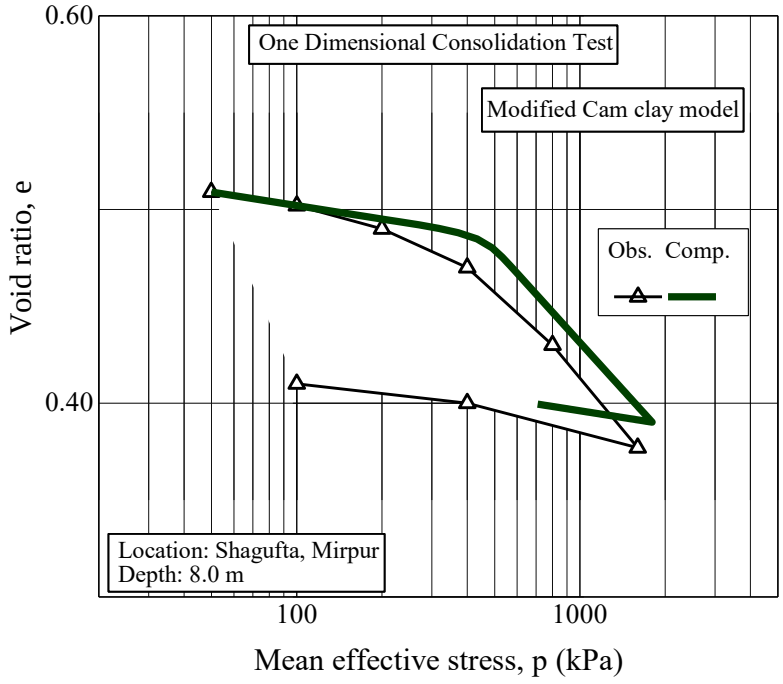

(b)

Figure 4.39 Observed and Predicted $e - lnp$ relationship of Shagufta sample (a) Cam-clay model (b) Modified Cam-clay model.

4.4.3.3 Simulations at Extension Condition

Figure 4.40 shows the predicted results of deviatoric stress and strain at triaxial extension conditions under same effective mean principal stress as the compression condition. From the plot it was found that the deviatoric stress at extension condition is less than that of the compression condition. Figure 4.41 shows the predicted plots of the effective stress paths at extension conditions compared with the observed and predicted results at compression condition.

Thus with the help of Subloading t_{ij} model, realistic results at undrained condition can be captured under both compression and extension condition that cannot be achieved by the Cam-clay model.

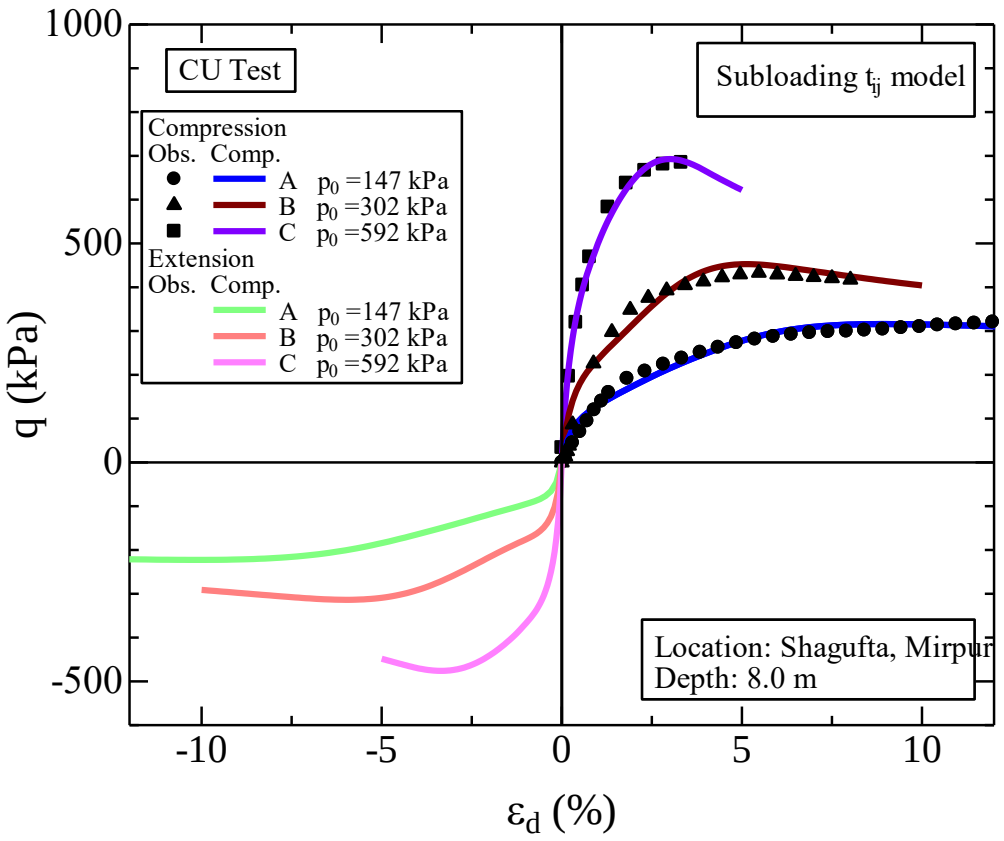

Figure 4.40 Predicted results at extension condition in CU Triaxial simulation.

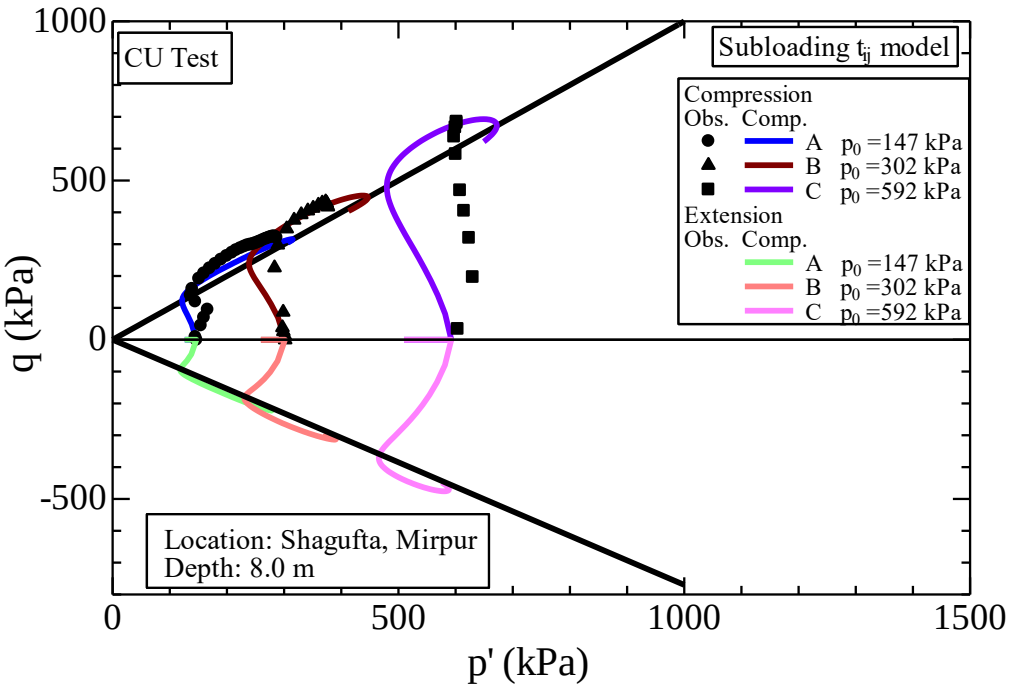

Figure 4.41 Observed and predicted effective stress path in CU triaxial compression and extension test.

4.4.3.4 Simulations of other locations

Figure 4.42 shows that the simulated $e - lnp$ relation fits well with observed results of Baridhara sample using the parameters listed in Table 4.6. From the parameters obtained, it was observed that the value of bonding parameter is 30 which indicates strong influence of bonding during undrained condition. The density parameter was obtained as 300 which is less than the parameters of other samples of different locations. This due to the higher void ratio (0.66) of the sample as compared to the other samples.

In figure 4.43 and figure 4.44, predicted results using Subloading t_{ij} model is plotted with the observed stress-strain results and effective stress paths from undrained triaxial test. It was observed that the predicted results fits well with observed stress-strain plots and effective stress plots satisfactorily like the other locations.

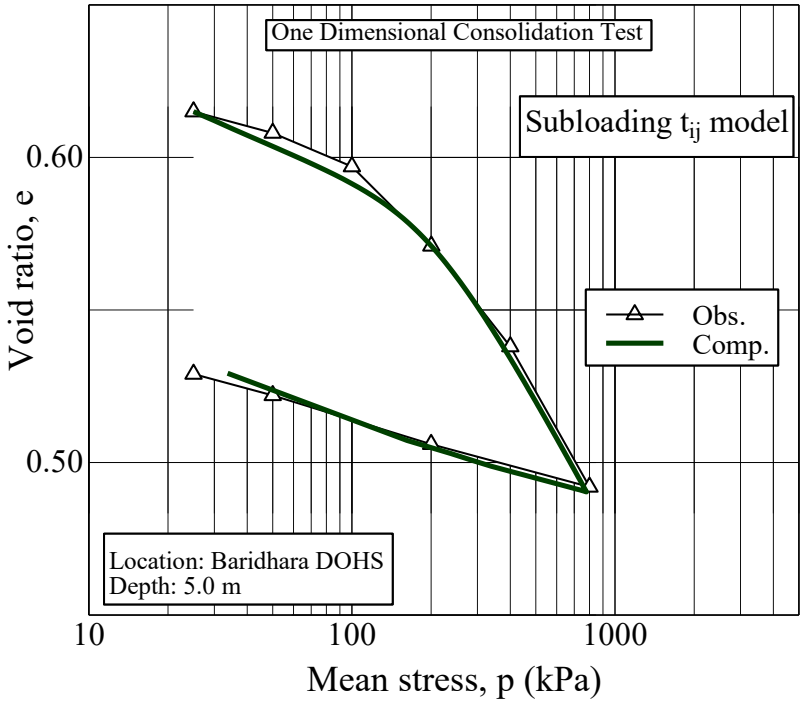

Figure 4.42 Observed and Predicted $e - lnp$ relationship of Baridhara sample.

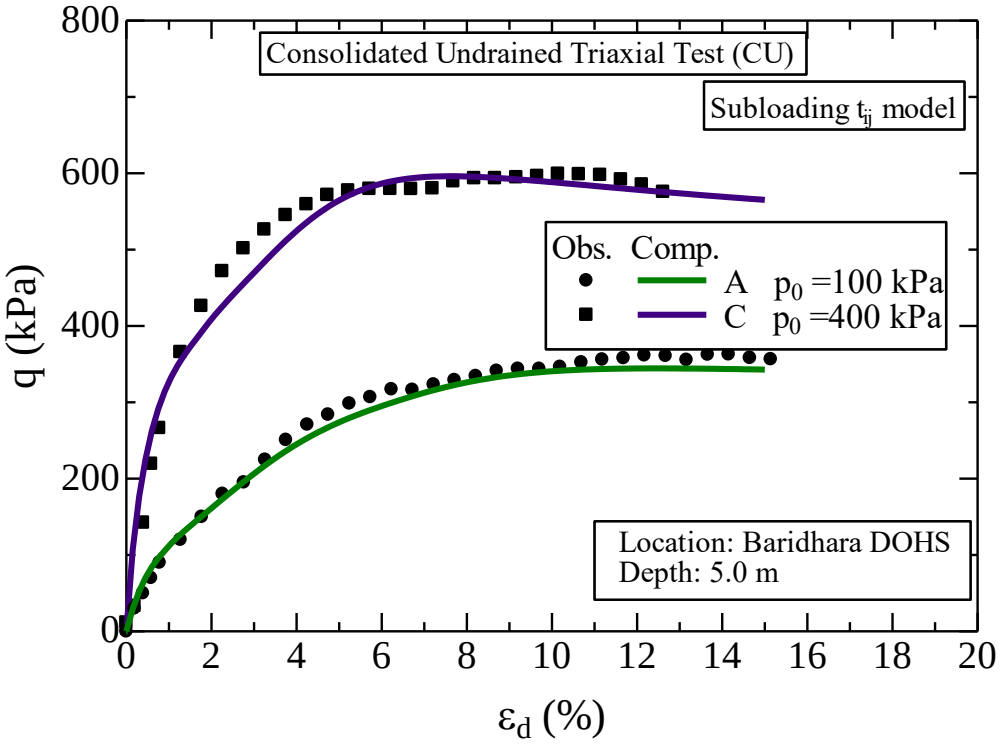

Figure 4.43 Observed and predicted stress-strain relation of Baridhara soil under CU triaxial compression test.

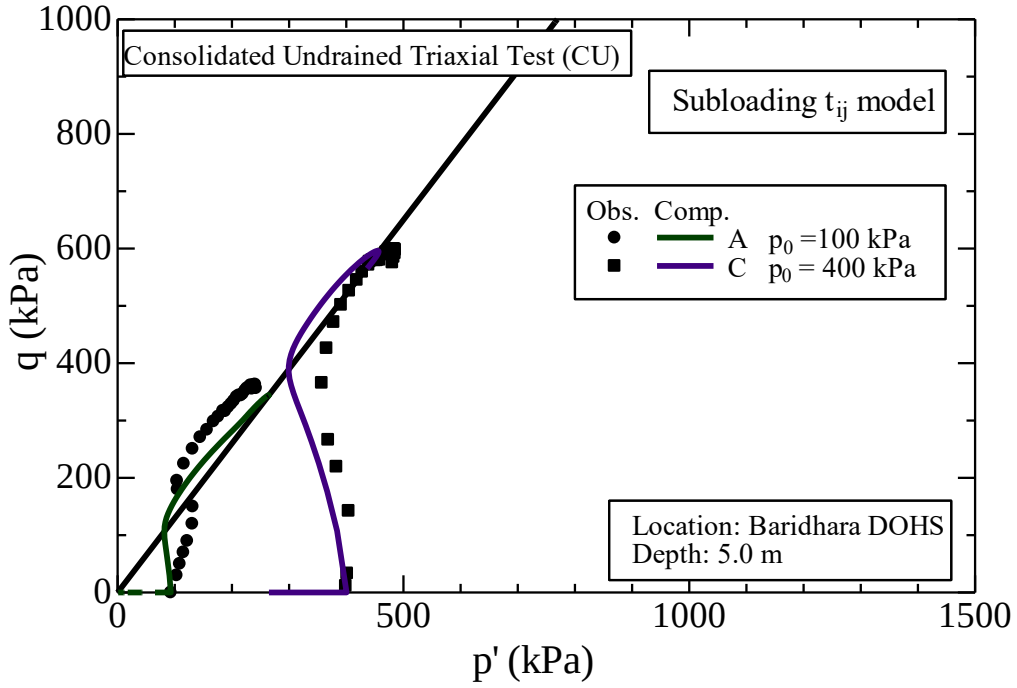

Figure 4.44 Observed and predicted effective stress path in CU triaxial compression test.

Figure 4.45 and Figure 4.46 shows the predicted stress-strain relation and effective stress path plots using the original Cam-clay model. Material parameters obtained from the consolidation and triaxial test as listed in Table 4.6 are used for the simulation. It was observed that the observed deviator stress results are larger than the predicted results. Also, the stiffness is found unrealistic when compared with the observed results.

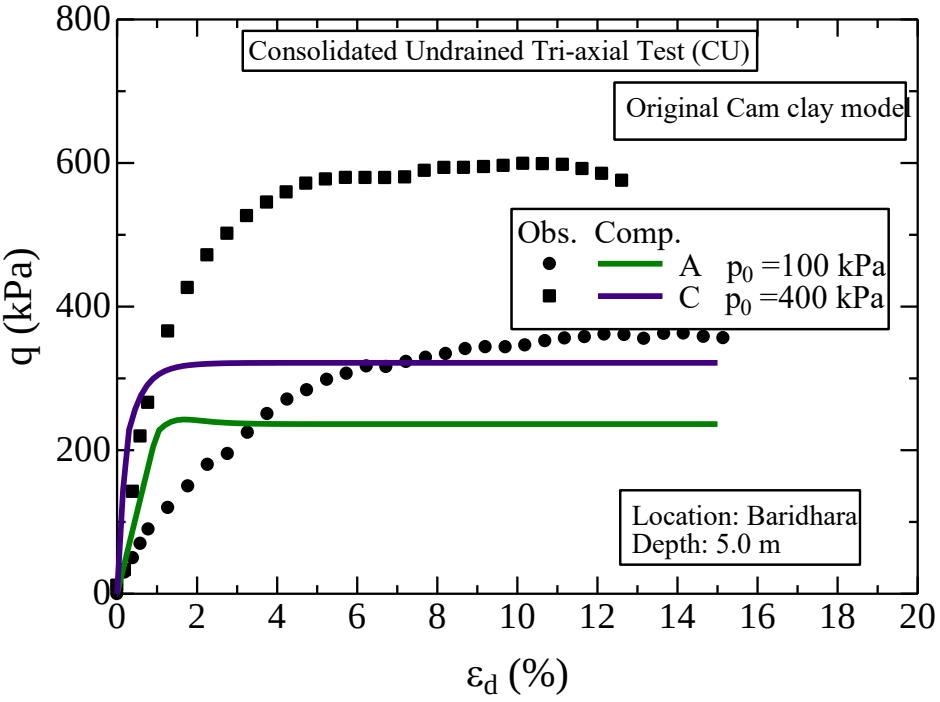

Figure 4.45 Observed and predicted stress-strain relation of Baridhara soil under CD triaxial test.

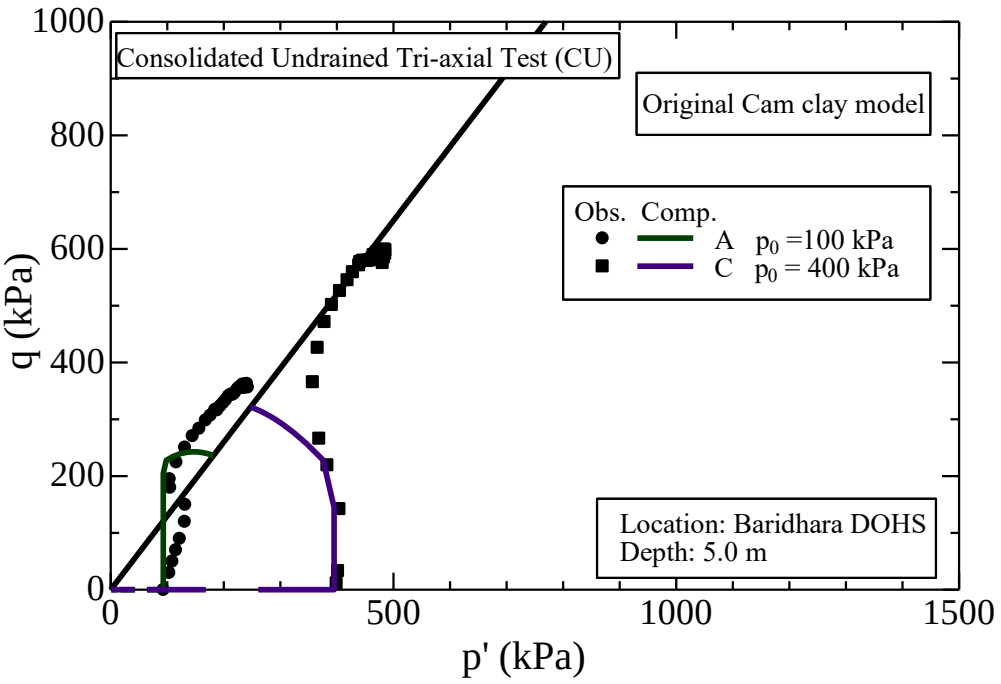

Figure 4.46 Observed and predicted effective stress path in CU triaxial compression test.

Figure 4.47 shows the predicted stress-strain relation using the Modified Cam-clay model. It is observed that for both the specimen A and B, predicted result cannot capture the peak stress also, the stiffness does not fit with the observed results. Figure 4.48 shows the effective stress path plot of all the specimen.

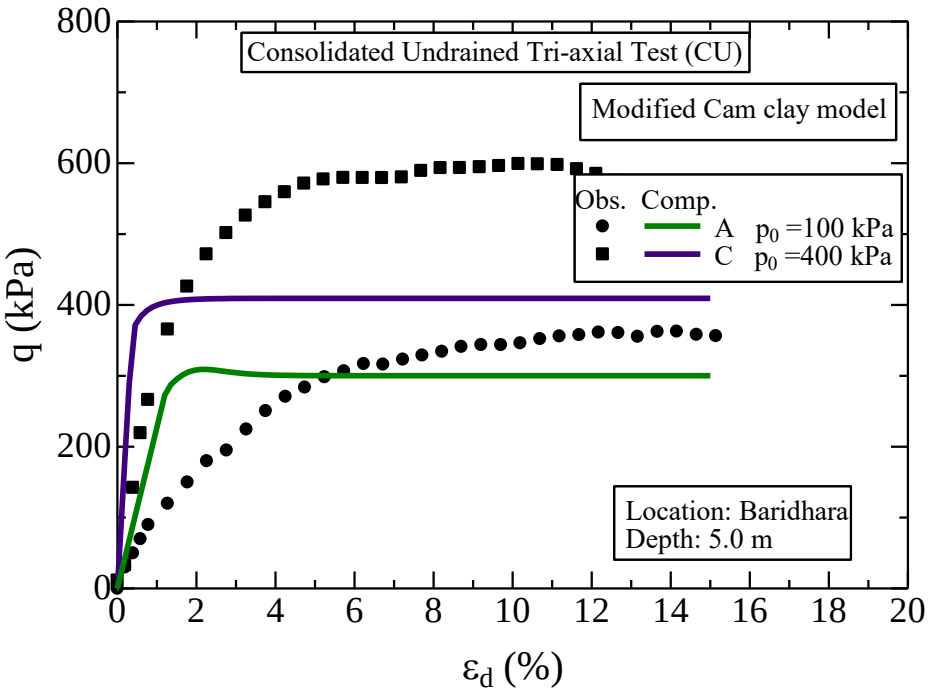

Figure 4.47 Observed and predicted stress-strain relation at undrained condition.

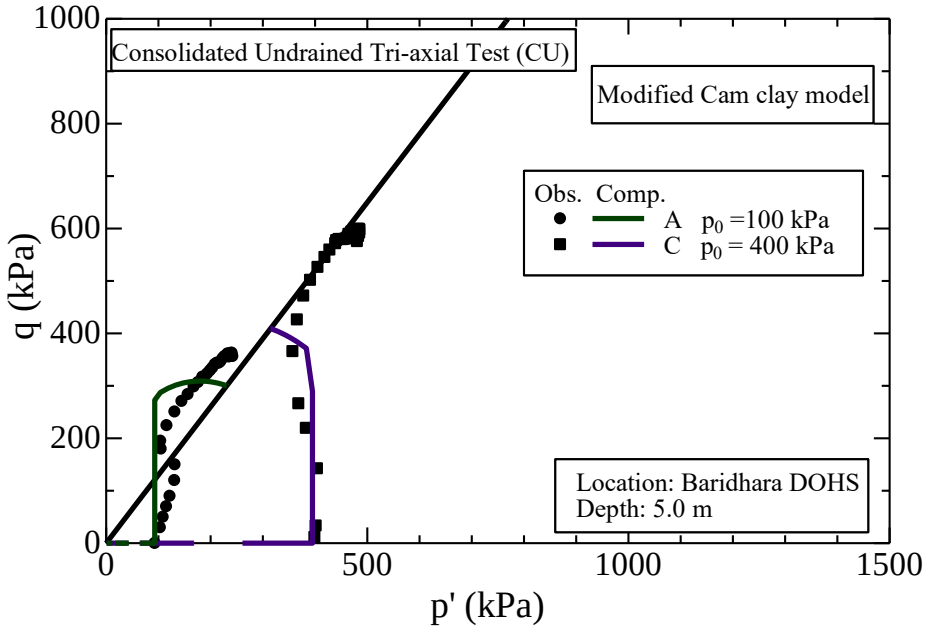

Figure 4.48 Observed and predicted effective stress path at undrained condition.

Figure 4.65 (a) and (b) shows the simulated results using Original Cam-clay model and Modified Cam-clay model respectively. It is observed that both the simulated results does not fit well with the tested results as the subloading t_{ij} model as shown in Figure 4.18.

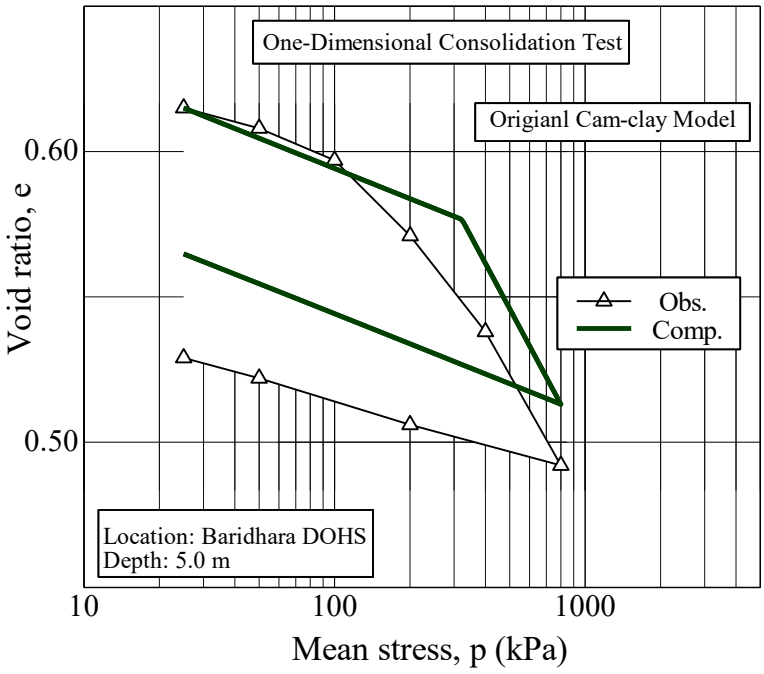

(a)

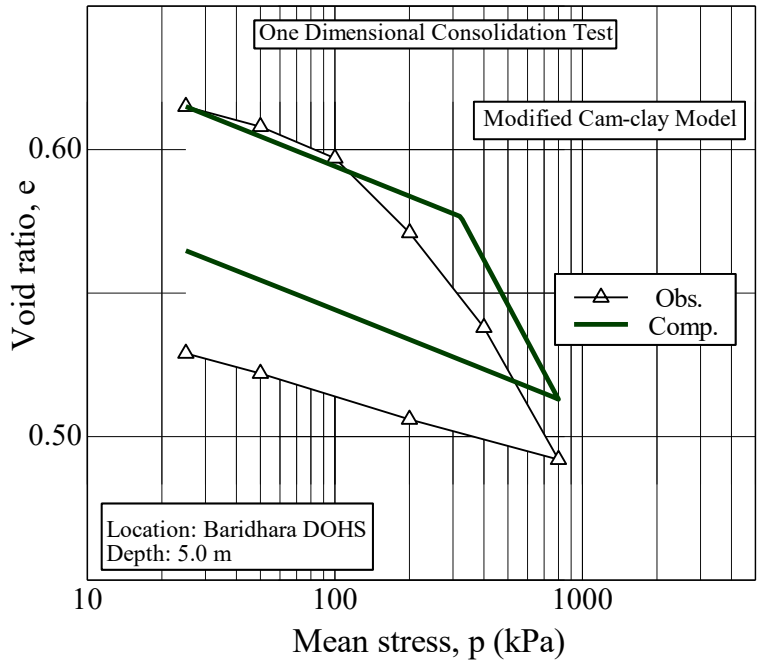

(b)

Figure 4.49 Observed and Predicted $e - lnp$ relationship of Baridhara sample (a) Original Cam-clay model (b) Modified Cam-clay model.

4.5 Influence of Various Parameters of Subloading t_{ij} model

In the subloading t_{ij} model, to take account the influence of density of over-consolidated soil and combined influence of density and bonding, additional parameters were used as shown in the previous sections of this chapter. The influence of this factors will be discussed with necessary simulations in this chapter.

4.5.1 Influence of Density and Bonding Parameters

In Figure 4.50, influence density variable is shown for one dimensional consolidation behavior. When compared to the observed results, it is found that with increasing the value of a, simulated results more approaches to the tested results. As a trial first value is taken a=100 while bonding parameters, b and ω are taken as zero. For the value 300 it is nearly close the observed value. Finally it is found that, for value a=700 simulated result can capture the real behavior of soil collected from Shewrapra, Rokeya Sarani location.

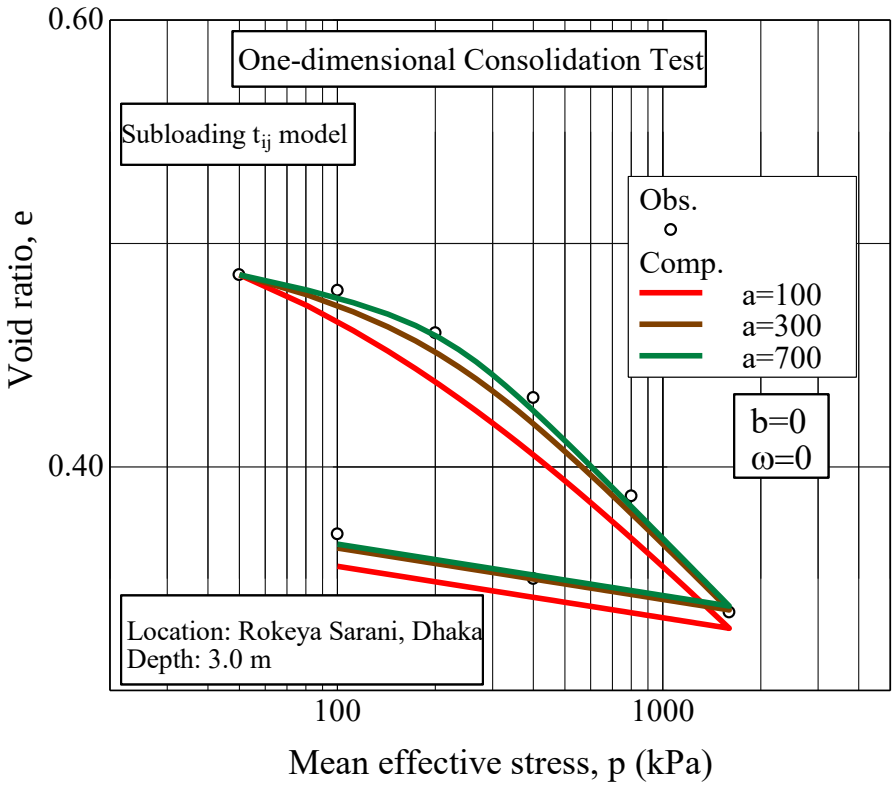

Figure 4.50 Observed and Predicted $e - lnp$ relationship with varying a.

Figure 4.51, shows the influence bonding variable for Shewrapara sample. When compared to the observed results, it is found that with the increase of the value of ω,

predicted change of void ratio is smaller than the observed results. For value ω=0.1, b=10 and a=700, predicted result can well capture the real soil behavior.

Figure 4.52, shows the influence another bonding variable, b for one dimensional consolidation behavior of Shewrapara sample. When compared to the observed results, it is found that with increasing the value of bonding variables ω and b simulated $e - lnp$ relationship become stiffer than the tested results.

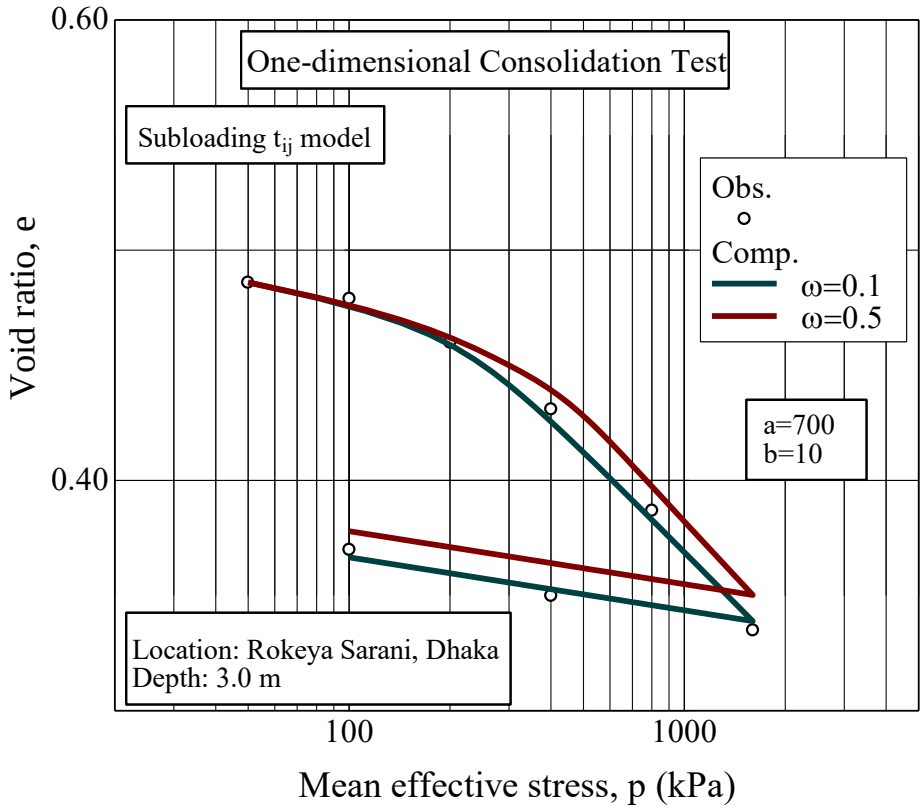

Figure 4.51 Figure Observed and Predicted $e - lnp$ relationship with varying ω.

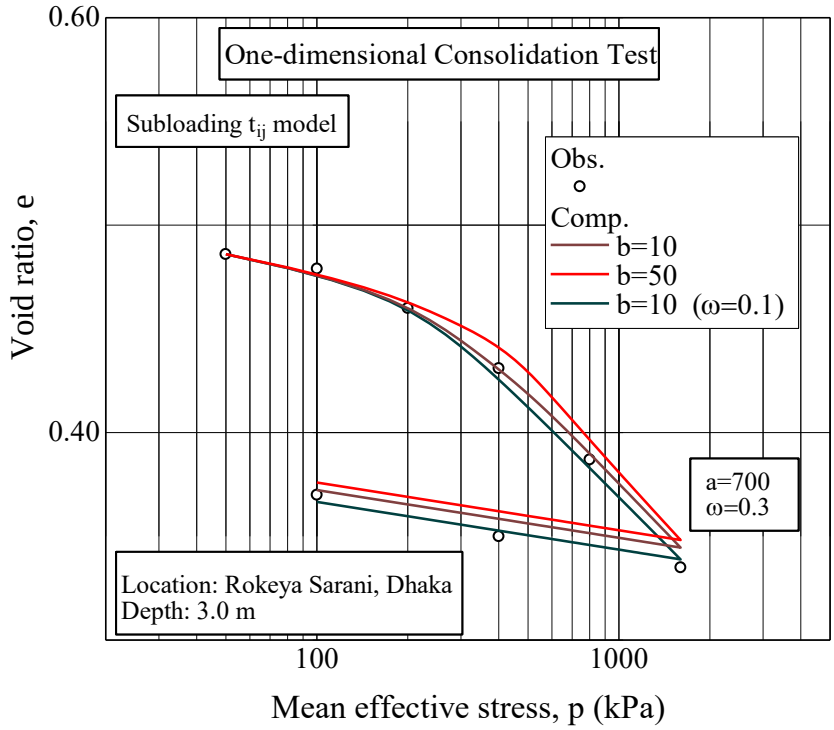

Figure 4.52 Observed and Predicted $e - lnp$ relationship with varying b.

To observe the effect of varying bonding value in undrained condition, sample collected from Baridhara DOHS as shown in section 4.4 is considered. In Figure 4.53, it was observed that, in undrained condition influence of bonding is strong. When the value of ω is taken as 0.6, the peak value rises near to 1000 kPa. For the value ω= 0.3, the simulated result was found to be satisfactory with the observed results. Figure 4.54 shows the simulated and observed stress path plots for the same soil with varying ω. It is found that, with increasing ω, simulated results approaches more to the observed results. However this cannot be accepted as it shows unusual peak stress and stiffness.

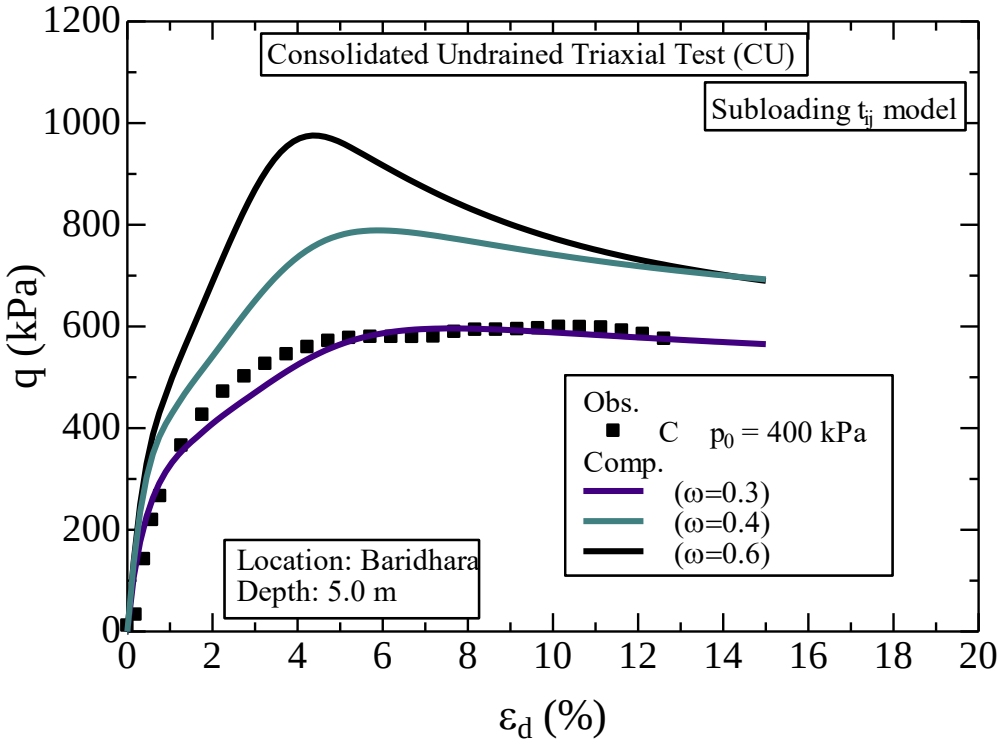

Figure 4.53 Observed and predicted stress-strain relation at undrained condition with varying ω.

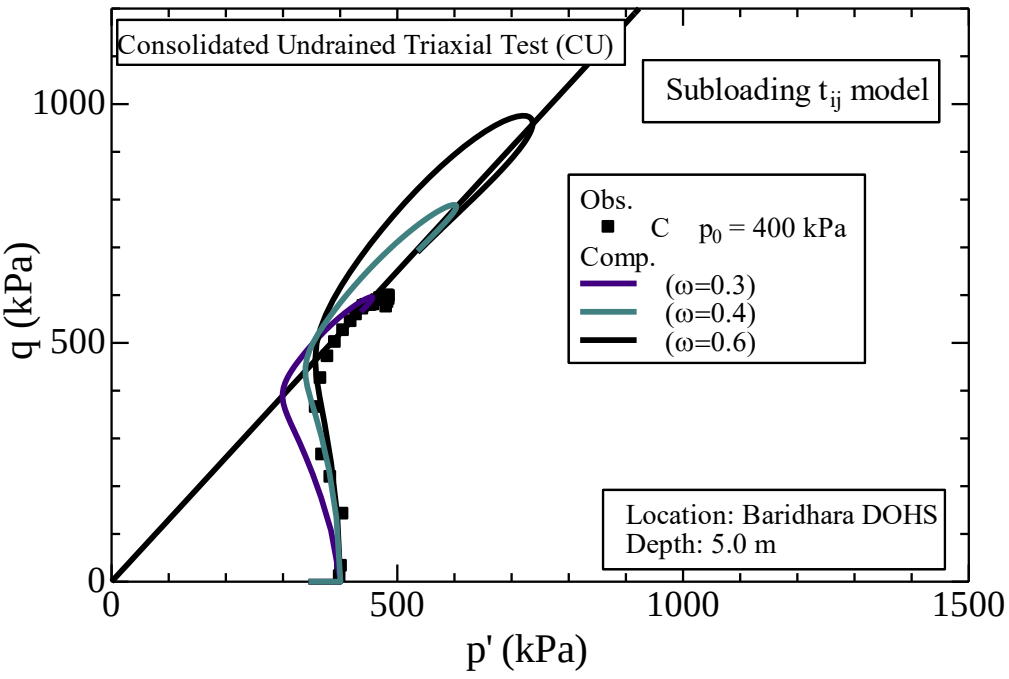

Figure 4.54 Observed and predicted effective stress path in CU triaxial compression test with varying ω.

The influence of bonding parameter, ω on soil behavior at drained condition, sample collected from Shewrapa, Rokeya Sarani is considered. Figure 4.55 shows the effect of ω on specimen A at overconsolidated condition. It is observed that with value ω=0, volumetric strain is predicted larger than the tested results. Also, the peak strength is not captured accurately. For value ω=0.3, the simulated result is found to captured the observed soil behavior including peak strength and volumetric dilation accurately. For value ω=0.5, the peak strength and volumetric dilation is found estimated larger than the tested results. However, in all conditions the stresses meet the critical stress line at the end.

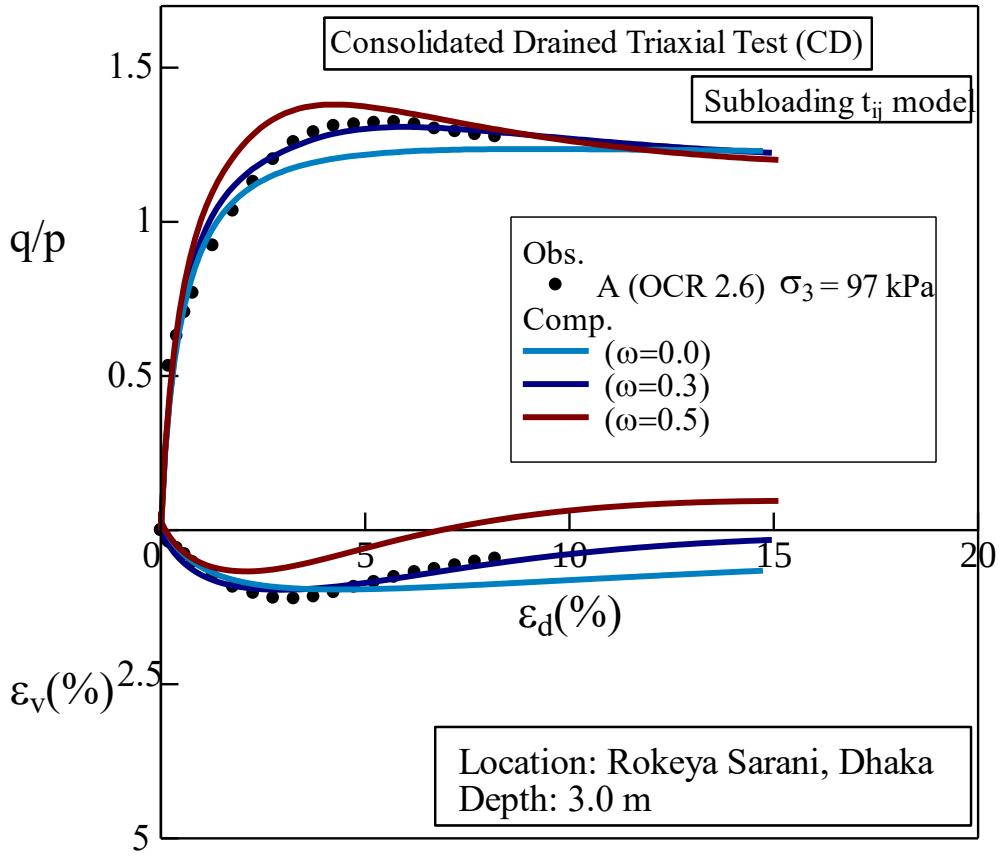

Figure 4.55 Observed and predicted stress-strain relation under CD triaxial test with varying ω.

4.5.2 Influence of Shape Function, β

In this section influence of shape function β will be discussed. In Figure 4.56, the influence of shape function on a normally consolidated soil is shown. It was observed that, at β=1.2 the simulated results do not fit well with the tested results. Initial stiffness was found less than the observed result whereas the volumetric strain was found overestimated. At a larger value of β (1.9), it was observed that the stiffness was found larger than the observed results. Also the volumetric strain was underestimated than the observed result. At β=1.5, simulated results were found to capture the soil behavior accurately.

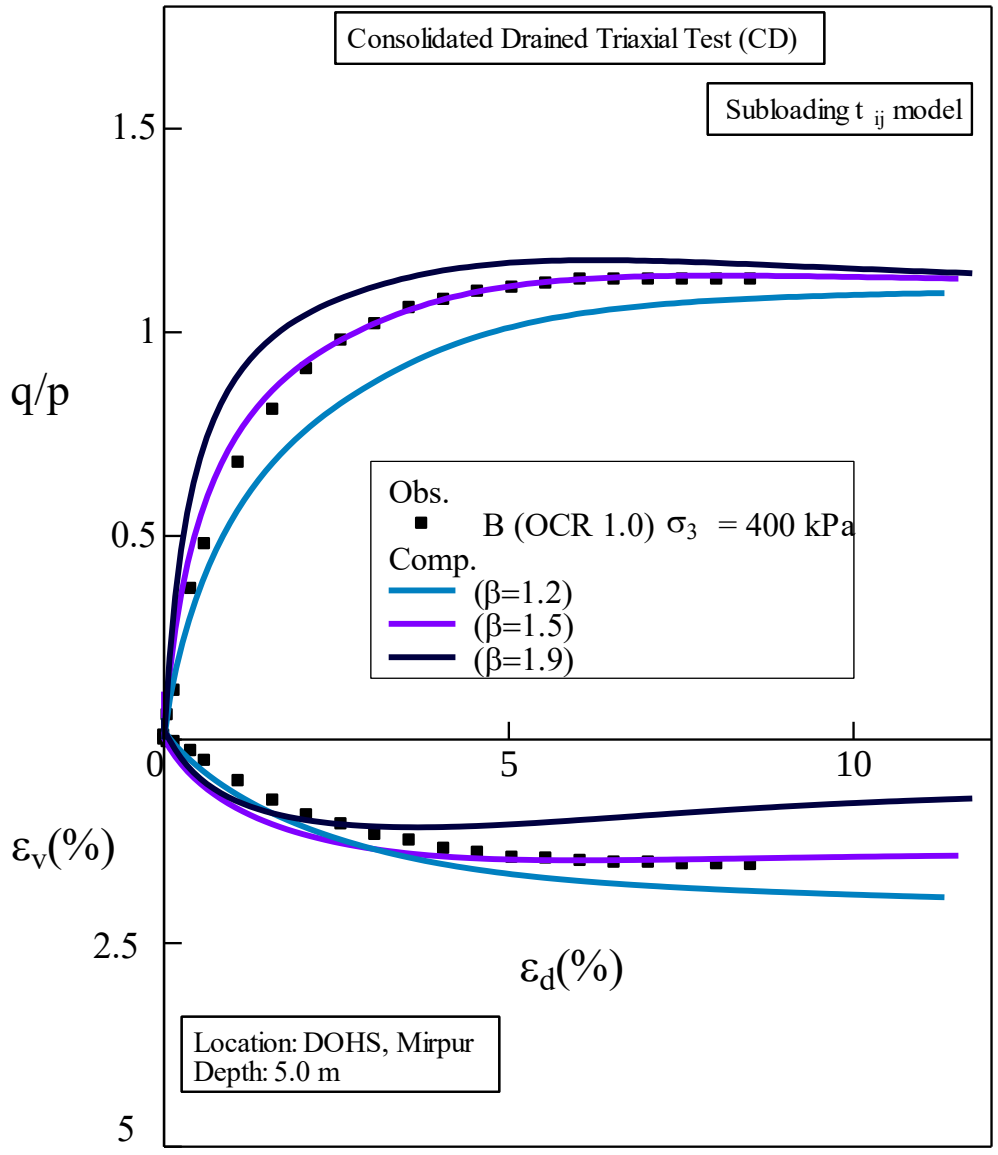

Figure 4.56 Observed and predicted stress-strain relation under CD triaxial test with varying β.

To observe the effect of varying β value in undrained condition, sample collected from Baridhara DOHS as shown in section 4.7 is considered. In Figure 4.57, strong influence of shape function factor is observed in undrained condition. At a larger value β=1.9, the peak value rises near to 800 kPa. At β=1.5, simulated results are found to capture the soil behavior accurately. For a lower value of β=1.1, the estimated results are much lower than the observed results. Figure 4.58 shows the effective stress plots. It was found that, with increasing β, simulated results more approaches to the observed results. However this cannot be accepted as it shows unusual peak stress and stiffness.

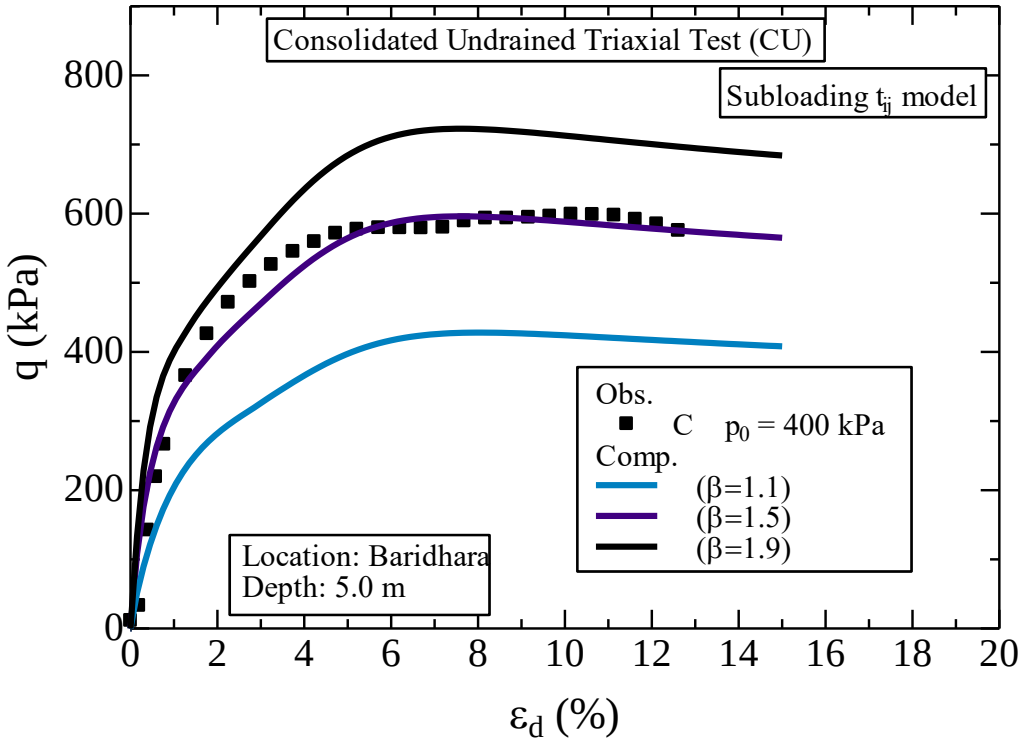

Figure 4.57 Observed and predicted stress-strain relation at undrained condition with varying β.

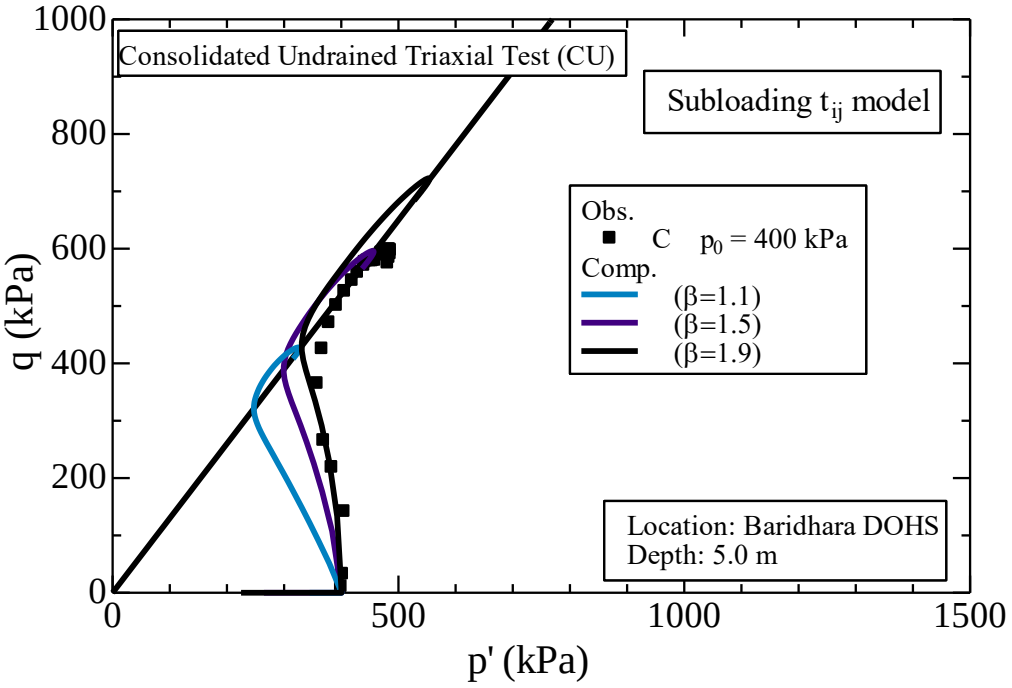

Figure 4.58 Observed and predicted effective stress path in CU triaxial compression test with varying β.

4.6 Summary of the Parameters

Table 4.25 represents the summary of parameters obtained from the test and simulations. Among the parameters, compression index, λ, swelling index, κ, void ratio at atmospheric pressure, N, initial void ratio, e_o and critical stress ratio, Rcs are common for both Cam-clay and Subloading t_{ij} models. In addition to the parameters required for Cam-clay model, Subloading t_{ij} required density parameter a to consider the effect of over-consolidaiton and bonding parameter, b for influence of bonding.

Table 4.7 Summary of parameters obtained from simulation of Subloading t_{ij} model for Dhaka clay.

Location	Drained/ Undrained	Parameters							
		λ	κ	N	e_o	R_{cs}	a	b	Remarks
Gazipur	Drained	0.07	0.015	0.6	0.556	2.8	480	10	True simulation by Subloading t_{ij} model
Shagufta, Mirpur	Undrained	0.07	0.01	0.6	0.53	2.5	450	45	
Shewrapara, Rokeya Sarani	Drained	0.065	0.01	0.52	0.504	3	380	15	
DOHS, Mirpur	Drained	0.057	0.013	0.63	0.606	2.8	400	10	
Savar	Drained	0.06	0.012	0.63	0.62	3	480	10	
Baridhara DOHS	Undrained	0.07	0.015	0.66	0.63	3.3	300	30	

Chapter Five
CONCLUSIONS AND RECOMMENDATIONS FOR FUTURE STUDY

5.1 General

The objectives of this research were to determine the parameters of Cam-clay and Subloading t_{ij} model, and their performance in describing the stress-strain properties of Dhaka clay. Drained and undrained triaxial tests were conducted to evaluate the model parameters. One-dimensional consolidation tests were also conducted to determine the compression and swelling characteristics of Dhaka clay at various locations. The findings of the study have been summarized in this Chapter. Thereafter, conclusions are made based on the findings. Finally, recommendations for future studies are made which beyond the present study.

5.2 Summary of Findings

The main findings of the study were as follows:

(a) The initial void ratio of samples collected from Gazipur, Shagufta and Shewrapara was 0.556, 0.53 and 0.506 respectively. It indicates that the samples are heavily packed, in general leaving, smaller spaces for the voids. Again samples collected from DOHS Mirpur, Savar, DOHS Baridhara has an initial void ratio of 0.606, 0.62 and 0.63 respectively, and indicate relatively higher void ratio and much pore spaces.

(b) From the one dimensional consolidation test the compression index λ was found in the range 0.07 to 0.057 and swelling index κ lies in the range 0.01 to 0.015. These values are low and indicate that soils are of low compressibility and have low swelling potential. Due to bonding effect these soils take higher strength causing less change in the void ratio.

(c) The triaxial compression test were conducted both in drained and undrained conditions. The principal critical stress ratios found to vary, ranging from 2.8 to 3.0 for the samples collected from Gazipur, Shewrapara, Savar and Mirpur DOHS. For the samples collected from Shagufta and Baridhara, the stress ratio was found to be 2.5 and 3.3 respectively. In general, samples with higher void ratio results in a

higher critical stress ratio and a lower void ratio results a lower critical stress ratio. For samples collected from Shagufta with the void ratio 0.53 results a critical stress ratio of 2.5. On the other hand, the sample collected from Baridhara DOHS with the void ratio of 0.63 results a stress ratio of 3.3.

(d) To obtain the density and bonding parameters, one dimensional consolidation properties were simulated with trial value *a* and *b*. From the present study the range of density parameter, ω was found as low as 300 and as higher as 480. It was observed that in general samples with higher stiffness required a higher value of density parameter to fit the simulated result with the observed result.

(e) The effect of bonding parameter on drained and undrained conditions was found with variety. At drained condition, the bonding parameter, b was found in the range 10 to 15. At undrained condition, it was found in the range 30 to 45. It can be concluded that at undrained condition the effect of bonding is larger which require a higher value of bonding parameter.

(f) The stress dilatancy relation at various stress conditions can be described by the Subloading t_{ij} model uniquely as discussed in Section 4.3.3.4. On the Contrary Cam-clay model cannot describe the stress dilatancy relation uniquely at various stress condition as discussed in the same section. Moreover, original Cam-clay model shows a unrealistic linear stress dilatancy relationship. It can be concluded, in case of stress dilatancy relation, Subloading t_{ij} model performed well than the both original and modified Cam-clay model.

(g) Both drained and undrained simulations were done under compression and tension at various stress path to observe the performance of the models. Subloading t_{ij} model was found to describe the behavior of all the samples satisfactorily with consistency at all the stress conditions.

(h) The performance of Cam-clay model was found to have inconsistency. At the normally consolidated stage, original Cam-clay model showed less stiffness than the observed results. Modified Cam-clay model was found to capture stress-strain behavior satisfactorily at normally consolidated stage. At over consolidated stage, both original and Modified Cam-clay model showed higher stiffness than the observed results. However, it reached the critical stress line satisfactorily. In all the

cases, it was observed that both Cam-clay and Modified Cam-clay models volumetric strain is overestimated the observed results.

(i) At undrained condition, Cam-clay model was found to predict a lower strength as compared to the observed values. Modified Cam-clay model predicted a higher strength than that predicted by Cam-clay model but lower than the observed results. Thus, It can be concluded at undrained condition, both original and modified Cam-clay model used to provide lower strength.

(j) In results to effect of density parameter, bonding parameter and shape function it was observed that the peak strength along with the initial stiffness increased with the increase of density, bonding and shape function. Also, predicted volumetric strain was found lower than the observed values for higher values of the parameters. On the other hand, at a lower than the observe value of bonding and shape function parameter, it was observed that the simulated results showed lower stiffness than the observed values. Also, the volumetric strain was over predicted than the observed result.

(k) Thus, based on the above discussion it can be concluded that for Dhaka clay collected from all six locations, Subloading t_{ij} model performed with better accuracy than the both Cam-clay and Modified Cam-clay model at all the stress conditions.

5.3 Conclusions

From this study, following conclusions can be made:

(a) The parameters of the Cam-clay and Subloading t_{ij} models are determined at drained and undrained condtions. Compression and swelling indexes are obtained from One-dimensional consolidation test and critical stress ratios are obtained from triaxial compression tests.

(b) Stress-dilatancy relation of Cam-clay and original Cam-clay model are not unique at different stress conditions and stress paths. Moreover, original Cam-clay model showed a linear stress-dilatancy relation which is not practical. On the other hand stress-dilatancy relationship evaluated by Subloading t_{ij} model is unique and consistent at various stress conditions and stress paths.

(c) It is observed that, Subloading t_{ij} model can well predict the stress-strain behavior of Dhaka clay at different stress conditons. On the other hand both Cam-clay and Modified Cam-clay model cannot predict the Dhaka clay behavior at various test conditions.

5.4 Recommendations for Future Studies

The recommendations for future studies are given as following:

(a) In this study, extension tests were not conducted due to the limitations of the equipment. Only simulated results are presented for extension conditions. In future, researches can be performed extension test to observe the performance of the Subloading t_{ij} model accurately.

(b) In this study, triaxial tests were conducted at effective confining pressures only. Other effective stress path test like constant effective mean principal stress, constant effective major principal stress and constant stress ratio test can be conducted and can observe the model performance.

(c) Unsaturated soil behavior was not included in this study. Hence future study can be done to observe the model performance at unsaturated condition.

(d) Other factors like time dependent behavior, temperature effect was not included in the present study. Hence future study can be done to observe the soil behavior at these conditions.

(e) This study did not consider the seismic features of Dhaka clay. Hence, a future research can be done on behavior of the soil under earthquake loading.

REFERENCES

Akai, K. and Tamura, T. (1978): Numerical analysis of multidimensional consolidation accompanied with elastoplastic constitutive equation. Proceedings of JSCE 269:95–104 (in Japanese).

Alonso, E. E., Gens, A. and Josa, A. A. (1990): A constitutive model for partially saturated soils. Geotechnique 40 (3): 405–430.

Anandarajah, A. (1994). Discrete-element method for simulating behavior of cohesive soil. *Journal of Geotechnical Engineering*, *120*(9), 1593-1613.

Asaoka, A (2003): Consolidation of clay and compaction of sand—An elastoplastic description. Proceedings of 12th Asian Regional Conference on Soil Mechanics and Geotechnical Engineering, Singapore, 2:1157–195.

Asaoka, A., Nakano, M., Noda, T., & Kaneda, K. (2000). Delayed compression/consolidation of natural clay due to degradation of soil structure. Soils and Foundations, 40(3), 75-85.

Asaoka, A., Nakano, M. and Noda, T. (1994): Soil-water coupled behavior of saturated clay near/at critical state. Soils and Foundations 34 (1): 91–105.

Azam, F., Islam, M. S., & Shahin, H. M. (2016). STUDY ON TUNNELING FOR UNDERGROUND METRO RAIL SYSTEM IN DHAKA CITY. *INTERNATIONAL JOURNAL OF GEOMATE*, *11*(20), 1776-1783.

Baldi, G., Hueckel, T., Piano, A. and Pellegrini, R. (1991): Developments in modeling of thermo-hydro-geomechanical behavior of Boom clay and clay-based buffer materials. Report ER 13365, Commission of the European Communities, Nuclear Science and Technology.

Belokas, G., & Kavvadas, M. (2010). An anisotropic model for structured soils: Part i: Theory. *Computers and Geotechnics*, *37*(6), 737-747.

Bishop, A. W. (1959): The principle of effective stress. Teknisk Ukeblad 39:859–863. Bjerrum, L. (1967): Engineering geology of Norwegian normally consolidated marine clays as related to settlements of buildings. Geotechnique 17 (2): 81–118.

Bolton, M. D. and Lau, C. K. (1993). Vertical bearing capacity factors for circular and strip footings on Mohr–Coulomb soil. Canadian Geotechnical Journal 30 (6): 1024–1033.

Brinkgreve, R. B. (2005). Selection of soil models and parameters for geotechnical engineering application. In Soil constitutive models: Evaluation, selection, and calibration (pp. 69-98).

Burland, J. B. (1990). On the compressibility and shear strength of natural clays. *Géotechnique*, *40*(3), 329-378.

Chowdhury, E. Q. and Nakai, T. (1998): Consequence of the tij concept and a new modeling approach. Computers and Geotechnics 23 (3): 131–164.

Hashiguchi, K. (1989). Subloading surface model in unconventional plasticity. *International Journal of Solids and Structures*, *25*(8), 917-945.

Hashiguchi, K. (1980): Constitutive equation of elastoplastic materials with elastoplastic transition. Journal of Applied Mechanics, ASME 102 (2): 266–272. (2009): Elastoplasticity theory. In Lecture notes in applied and computational mechanics. New York: Springer, 42.

Hashiguchi, K. and Ueno, M. (1977): Elastoplastic constitutive laws for granular materials, constitutive equations for soils. Proceedings of Specialty Session 9, 9th International Conference on Soil Mechanics and Foundation Engineering,Tokyo, 73–82.

Henkel, D. J. (1960): The relationship between effective stresses and water content in saturated clays. Geotechnique 10 (2): 41–45.

Hicher, P. Y. and Shao, J. F. (2008): Constitutive modeling of soils and rocks (English version). New York: Wiley

Hicher, P. Y., & Shao, J. F. (2002). Elastoplasticity of soils and rocks. Models of behavior of soils and rocks,1.

Hossain, A.T.M.S., and TOLL, D.G. 2006: Geomechanicl aspects of some tropical clay soils from Dhaka, Bangladesh. Engineering Geology for Tomorrow's Cities, Special publication 22, Book CD-Rom published by Geological Society of London, U.K. ISBN: 978-1-86239-290-8.

Hossain, A. T. (2001). *The engineering behaviour of the tropical clay soils of Dhaka, Bangladesh* (Doctoral dissertation, Durham University).

Islam, M. R. (2014): SPH simulations on failure of a breakwater mound due to tsunami scour under experimental conditions (Doctoral dissertation). Retrieved from file:///D:/OneDrive%20%20Military%20Institute%20of%20Science%20and%20Technology%20(MIST)/1.Thesis_MSc/mohammed_russedul_islam-thesis.pdf

Islam, M. S., Shahin, H. M., Banik, S., & Azam, F. (2013). Elasto-plastic constitutive model parameters and their application to bearing capacity estimation for Dhaka sub-soil. *Journal of Civil Engineering, The Institution of Engineers, Bangladesh, Vo. CE, 42*, 171-188.

Islam, M. S., Siddique, A. and Muqtadir, A. (2004). "Mechanical properties of soft organic Dhaka clay". Journal of Civil Engineering (IEB), 32(2); 143-161

Lade, P. V. (2005). Overview of constitutive models for soils. In *Soil constitutive models: Evaluation, selection, and calibration*(pp. 1-34).

Leroueil, S., & Vaughan, P. R. (1990). The general and congruent effects of structure in natural soils and weak rocks. *Géotechnique, 40*(3), 467-488.

Matsuoka, H. (1974): Stress–strain relationship of sand based on the mobilized plane. Soils and Foundations 14 (2): 47–61.

Matsuoka, H. and Nakai, T. (1974): Stress-deformation and strength characteristics of soil under three different principal stresses. Proceedings of JSCE 232:59–70.

Meyerhof, G. G. (1963): Some recent research on the bearing capacity of foundations. Canadian Geotechnical Journal 1 (1): 16–26.

Mitchell, J. K. and Soga, K. (2005): Fundamentals of soil behavior, 3rd ed. New York: Wiley.

Mitchel, J. K. (1976). The properties of cement stabilized soil." residential workshop on material and methods for low cost road, rail and reclamationworks.

Monsur H. (1995)-An Introduction to The Quaternary Geology of Bangladesh-City press, Dhaka-1000.

Murayama, S. (1964): A theoretical consideration on a behavior of sand. Proceedings of IUTAM Symposium on Rheology and Soil Mechanics, Grenoble, 146–159. ——. (1990): Theory of mechanical behavior of soils.Tokyo: Giho-do (in Japanese).

Murayama, S. and Matsuoka, H. (1971): Earth pressure on tunnels in sandy ground. Proceedings of JSCE 187:95–108 (in Japanese).

Puzrin, A. (2012). *Constitutive modelling in geomechanics: introduction*. Springer Science & Business Media.

Teruo, N. (2013). *Constitutive Modeling of Geomaterials: Principles and Applications*. CRC Press.

Nakai, T., Shahin, H. M. Kikumoto, m., Kyokawa, H., Zhang, F. and Farias, M. M. (2011): a simple and unified three-dimensional model to describe various characteristics of soils, Soils and Foundation, 51(6), 1149-1168.

Nakai, T. (2007): Modeling of soil behavior based on tij concept, Proc. Of 13th Asian Regional Conf. on Soil Mech. And Geotechnical Eng.m Keynote Paper, 2, 69-89.

Nakai, T. and Mihara, Y. (1984): A new mechanical quantity for soils and its applicationto elastoplastic constitutive models. Soils and Foundations 24 (2): 82–94.

Nakai, T. and Hinokio, T. (2004): A simple elastoplastic model for normally and overconsolidated soils with unified material parameters. Soils and Foundations 44 (2): 3–70.

Nakai, T., Kyokawa, H., Kikumoto, M. and Zhang, F (2009): Elastoplastic modeling of geomaterials considering the influence and density and bonding. Proceedings of Prediction and Simulation Methods for Geohazard Mitigation, Kyoto, 367–373.

Rahman, M. A., Shahin, H. M., & Nakai, T. (2018). Stress-strain-dilatancy relationships of normally consolidated dhaka clay. *INTERNATIONAL JOURNAL OF GEOMATE*, *15*(51), 188-194.

Roscoe, K. H. & Burland, J. B. (1968) - On thegeneralized stress- strain behavior of wet clay. Heyman and F. A. Leckie (eds.), Engineering Plasticity, Cambridge University Press, pp535-609.

Schofield, A. N. and Wroth, C. P. (1968) - Critical StateSoil Mechanics, McGrow- Hill, London.

Sekiguchi, H. and Ohta, H. (1977): Induced anisotropy and time dependency in clays. Proceedings of Specialty Session 9, 9th International Conference on Soil Mechanics and Foundation Engineering, Tokyo, 229–238.

Sekiguchi, H. and Toriihara, M. (1976): Theory of one-dimensional consolidation of clays with consideration of their rheological properties. Soils and Foundations 16 (1): 27–44.

Shahin, H. M., Nakai, T., Hinokio, M., Kurimoto, T. and Sada, T. (2004): Influence of surface loads and construction sequence on ground response due to tunneling. Soils and Foundations 44 (2): 71–84.

Shahin, H. M., Nakai, T., Hinokio, M. and Yamaguchi, D. (2004): 3D effects on earth pressure and displacements during tunnel excavations. Soils and Foundations 44 (5): 37–49.

Shahin, H. M., Nakai, T., Zhang, F., Kikumoto, M. and Nakahara, E. (2011): Behavior of ground and response of existing foundation due to tunneling. Soils and Foundations 51 (3): 395–409.

Shibata, T. (1960): On the volume changes of normally consolidated clays. Annals of Disaster Prevention Research Institute, Kyoto University,6:128–134 (in Japanese).

Shibata, T. and Karube, D. (1965): Influence of the variation of the intermediate principal stress on the mechanical properties of normally consolidated clays. Proceedings of 6th International Conference on Soil Mechanics and Foundation Engineering, Montreal, 1:359–363.

Soga, K., & O'SULLIVAN, C. A. T. H. E. R. I. N. E. (2010). Modeling of geomaterials behavior. *Soils and foundations*, *50*(6), 861-875.

Uddin, K. (1990), "Compressibility and Shear Strength of Remoulded Dhaka Clay", M. Sc. Engineering thesis, Department of Civil Engineering, Bangladesh University of Engineering and Technology, Dhaka.

Uddin, M. (2017). Method for improving bearing capacity of foundationin reclaimed areas of Dhaka city (MSc Thesis, Bangladesh University of Engineering and Technology). Retrieved from http://lib.buet.ac.bd:8080/xmlui/handle/123456789/4885

Vaughan, P. R., Maccarini, M., & Mokhtar, S. M. (1988). Indexing the engineering properties of residual soil. *Quarterly Journal of Engineering Geology and Hydrogeology*, *21*(1), 69-84.

Wood, D. M., & Gajo, A. (2005). Hierarchical critical state models. In Soil Constitutive Models: Evaluation, Selection, and Calibration (pp. 459-482).

Wood, D. M., (1990): Soil behavior and critical soil mechanics. Cambridge, England: Cambridge University Press.